Development of a portable ECG and electronic stethoscope device for screening cardiovascular disease in rural locations

by

Gérard Hayden Smith

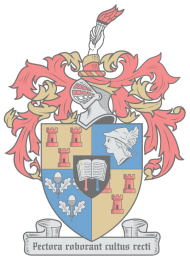

Thesis presented in partial fulfilment of the requirements for the degree of Master of Engineering (Mechatronic) in the Faculty of Engineering at Stellenbosch University

The financial assistance of the National Research Foundation (NRF) towards this research is hereby acknowledged. Opinions expressed and conclusions arrived at, are those of the author and are not necessarily to be attributed to the NRF.

Supervisor: Dr. D.J. van den Heever

Co-supervisor: Mr. W. Swart

March 2018

Declaration

By submitting this thesis electronically, I declare that the entirety of the work contained therein is my own, original work, that I am the sole author thereof (save to the extent explicitly otherwise stated), that reproduction and publication thereof by Stellenbosch University will not infringe any third party rights and that I have not previously in its entirety or in part submitted it for obtaining any qualification.

Date: March 2018

UNIVERSITEIT·STELLENBOSCH·UNIVERSITY
jou kennisvennoot • your knowledge partner

Plagiaatverklaring / Plagiarism *Declaration*

1 Plagiaat is die oorneem en gebruik van die idees, materiaal en ander intellektuele eiendom van ander persone asof dit jou eie werk is.
Plagiarism is the use of ideas, material and other intellectual property of another's work and to present is as my own.

2 Ek erken dat die pleeg van plagiaat 'n strafbare oortreding is aangesien dit 'n vorm van diefstal is.
I agree that plagiarism is a punishable offence because it constitutes theft.

3 Ek verstaan ook dat direkte vertalings plagiaat is.
I also understand that direct translations are plagiarism.

4 Dienooreenkomstig is alle aanhalings en bydraes vanuit enige bron (ingesluit die internet) volledig verwys (erken). Ek erken dat die woordelikse aanhaal van teks sonder aanhalingstekens (selfs al word die bron volledig erken) plagiaat is.
Accordingly all quotations and contributions from any source whatsoever (including the internet) have been cited fully. I understand that the reproduction of text without quotation marks (even when the source is cited) is plagiarism.

5 Ek verklaar dat die werk in hierdie skryfstuk vervat, behalwe waar anders aangedui, my eie oorspronklike werk is en dat ek dit nie vantevore in die geheel of gedeeltelik ingehandig het vir bepunting in hierdie module/werkstuk of 'n ander module/werkstuk nie.
I declare that the work contained in this assignment, except where otherwise stated, is my original work and that I have not previously (in its entirety or in part) submitted it for grading in this module/assignment or another module/assignment.

17050510 **Studentenommer / *Student number***	**Handtekening / *Signature***
GH SMITH **Voorletters en van / *Initials and surname***	20/02/2018 **Datum / *Date***

Abstract

Development of a portable ECG and electronic stethoscope device for screening cardiovascular disease in rural locations

G.H. Smith

Department of Mechanical and Mechatronic Engineering,
University of Stellenbosch,
Private Bag X1, Matieland 7602, South Africa.

Thesis: MEng (Mechatronic)

March 2018

Cardiovascular disease (CVD) is currently the number one cause of death worldwide, resulting in 17.7 million deaths in 2015 (World Health Organisation, 2017). In South Africa, five people suffer a heart attack every hour, placing CVD as the second deadliest disease in the country, after HIV/AIDS (Pillay-van Wyk *et al.*, 2013). Studies predict that by 2030, CVD will be responsible for more deaths in developing countries than the total combined fatalities of HIV/AIDS, malaria and tuberculosis (Beaglehole and Bonita, 2008). Medical equipment required by cardiologists to diagnose cardiovascular disease is expensive and only available at larger hospitals in major cities within South Africa. This presents a significant challenge for the 35% of South Africans residing in rural areas who require medical attention (The World Bank, 2017). Subsequently, many patients in rural areas live with lingering cardiovascular problems.

This thesis entails the design and development of a point-of-care device capable of screening for cardiovascular disease in rural locations in Africa. The device consists of an electrocardiogram (ECG) and electronic stethoscope capable of recording electrical bio-signals and heart sounds, respectively. The ECG consists of a reduced lead set that includes limb leads avL, avR, avF, I, II, III and precordial leads V2 and V4. The data recorded using the ECG can be used to autonomously identify patients with potential cardiovascular disease using machine learning techniques. Furthermore, the potential for reconstructing a full 12 lead ECG recording from a reduced lead set using machine learning is

also investigated.

Data acquired from the Physikalisch-Technische Bundesanstalt (PTB) online database was used to train the machine learning models. A deep pattern recognition neural network (DPRNN) was used to diagnose patients with normal or abnormal cardiac function. Additionally, a focus time-delay neural network (FTDNN) was used to reconstruct precordial leads V1, V3, V5 and V6 from the reduced lead set. The machine learning models were tested on 70 subjects recorded using the device in a clinical study conducted at Tygerberg Hospital. The classification method utilised first order features consisting of ECG amplitudes, intervals and segments, second order features derived from wavelet entropy and Shannon's energy, as well as unsupervised features generated using stacked denoising autoencoders. The classification model, tested in the clinical trial, produced an accuracy, sensitivity, specificity and area under the curve (AUC) of 85%, 83%, 87% and 0.85, respectively. The ECG lead reconstruction produced acceptable root-mean-square error (RMSE) values of 181 to 266 μV, and excellent Pearson r correlation values of 0.91 - 0.95, for the reconstructed precordial leads. All correlation values were statistically significant at $p \ll 0.01$. The results obtained in this study compare favourably with an initial retrospective study as well as prior studies done in the research field. This evidence supports the possibility of deploying a low-cost portable device capable of referring patients with potential cardiac abnormalities, in rural locations, to hospitals for further examination.

Uittreksel

Ontwikkeling van 'n draagbare EKG en elektroniese stetoskoop toestel vir die ondersoek van kardiovaskulêre siekte vir afgeleë liggings

("Development of a portable ECG and electronic stethoscope device for screening cardiovascular disease in rural locations")

G.H. Smith

Departement Meganiese en Megatroniese Ingenieurswese,
Universiteit van Stellenbosch,
Privaatsak X1, Matieland 7602, Suid Afrika.

Tesis: MIng (Megatronies)

Maart 2018

Kardiovaskulêre siekte (KVS) is huidiglik die voorstaande oorsaak van lewensverlies wêreldwyd, en het 17.7 miljoen lewens geëis in 2015 (World Health Organisation, 2017). In Suid-Afrika lei vyf mense aan 'n hartaanval elke uur, wat beteken dat KVS die tweende mees dodelike siekte in die land is, naas HIV/VIGS (Pillay-van Wyk *et al.*, 2013). Studies voorspel dat KVS teen 2030 vir meer afsterwings verantwoordelik sal wees in ontwikkelende lande as die totale afsterwings van HIV/VIGS, malaria en tuberkulose saam (Beaglehole en Bonita, 2008). Die mediese toerusting wat benodig word deur kardioloë om kardiovaskulêre siektes te diagnoseer is duur en slegs beskikbaar by groter hospitale in hoof stede binne Suid-Afrika. Dit lei tot 'n beduidende uitdaging vir die 35% van die Suid-Afrikaanse bevolking wat in afgeleë areas bly en mediese hulp moet bekom (The World Bank, 2017). Gevolglik is daar menige pasiënte in afgeleë nedersettings wat lei aan voortdurende kardiovaskulêre kwale.

Hierdie tesis onderneem die ontwerp van 'n punt-van-behandeling toestel wat in staat is om ondersoek in te stel vir kardiovaskulêre siektes in afgeleë liggings oor Afrika. Die toestel bestaan uit 'n elektrokardiogram (EKG) en elektroniese stetoskoop wat in staat is om elektriese bio-seine en hart klanke afsonderlik op te neem. Die EKG bestaan uit 'n verminderde probe terminaal stel wat die ledemaat probe terminale avL, avR, avF, I, II, III en voorhartversterkingsprobe terminale V2 en V4 bevat. Die data wat deur die EKG opgeneem word,

kan gebruik word vir outomatiese identifisering van pasiënte wat potensieel lei aan kardiovaskulêre kwale deur middel van masjienleer tegnieke. Verder, word die potensiaal om 'n vol 12 terminaal EKG opname te herbou vanuit 'n verminderde terminaal stel deur middel van masjienleer ook ondersoek.

Data wat verkry is vanaf die Physikalisch-Technische Bundesanstalt (PTB) aanlyn databasis was gebruik vir opleiding van die masjienleer modelle. 'n Diep patroon herkenning neurale netwerk (DPHNN) was gebruik om pasiënte te diagnoseer met normale of abnormale hart funksie. Daar is ook 'n bykomende fokus tyd vertraagde neurale netwerk (FTVNN) gebruik vir die herkonstruksie van die voorhartversterkingsprobe terminale V1, V3, V5 en V6 vanuit die verminderde stel probe terminale. Die masjienleer modelle was getoets op 70 opnames wat deur die ontwerpte toestel opgeneem is gedurende 'n kliniese studie by Tygerberg hospitaal. Die klassifikasie metode maak gebruik van eerste orde kenmerke, bestaande uit EKG amplitudes, intervalle en segmente, wat afgelei is vanaf golfvorm (wavelet) entropie en Shannon energie, asook sonder toesig gegenereerde kenmerke wat deur middel van gestapelde geraas kansellasie outokodeerders gegenereer word. Dis klassifikasie model wat getoets is in die kliniese toets het 'n akkuraatheid, sensitiwiteit, spesifisiteit en area onder kurwe van 85%, 83%, 87% en 0.85 afsonderlik gehad. Die EKG probe terminaal herkonstruksie het gelei tot aanvaarbare wortel van die gemiddelde kwadraat foute met waardes vanaf 181 tot 266 μV, en uitstekende Pearson r korrelasie waardes van 0.91 - 0.95, vir die geherkostruksieerde voorhartversterkingsprobe terminale. Alle korrelasie waardes was statisties van belang met $p \ll 0.01$. Die resultate wat verkry was in hierdie studie vergelyk gunstig met die oorspronklike retrospektiewe studie asook voorafgaande studies wat in die navorsingsveld onderneem is. Hierdie bewyse ondersteun die moontlikheid van 'n draagbare, lae koste toestel wat in staat is om pasiënte vanuit afgeleë nedersettings met potensiële hart abnormaliteite te verwys na 'n hospitaal vir verdere ondersoek.

Acknowledgements

First and foremost I would like to thank God, for the gifts and talents You have blessed me with undeservedly, Philippians 4:13. I would also like to express my sincere gratitude to the following people and organisations for the respective roles they played in the last two years of my master's project:

- The National Research Foundation for providing financial assistance for this master's project.
- Mr. P. Spyres, thank you so much for your unbelievable generosity in donating hundreds of ECG electrodes that were used throughout the project.
- Prof. W. Karlen thank you for agreeing to supervise me during my exchange semester abroad at ETH Zurich. I learnt a great deal during the time spent in your research group and it was truly a once in a lifetime opportunity.
- Prof. A. Doubell, Dr. H. Weich and Dr. G. Titus for their respective contributions towards making the clinical trial at Tygerberg Hospital possible.
- Dr. Dawie van den Heever and Mr. Wayne Swart, thank you for providing such an interesting and challenging topic. The project allowed me to learn a great deal about a wide variety of fields as well as grow academically. I also would like to thank you both for not only investing in me as a student but also as a person.
- Gayleigh and Michael Smith, thank you for the personal and financial sacrifices that you have made for me throughout my student career and for your constant love and support. Brendan Smith, thank you for all the help, support and great memories during the years we lived together. Without my family, none of this would ever have been possible.
- Jolene Brooks, for the continuous love and unwavering support throughout this project. Words cannot express my appreciation for all that you do.

Dedications

To the many South Africans currently living with cardiovascular disease, as well as to those who have lost loved ones due to this chronic disease.

Contents

List of Figures

List of Tables

Nomenclature

Abbreviations

ACK	Acknowledge
ADC	Analogue to Digital Converter
AE	Autoencoder
AIDS	Acquired Immunodeficiency Syndrome
ANN	Artificial Neural Network
AUC	Area Under the Curve
AV	Atrioventricular
BBB	Bundle Branch Block
BERG	Biomedical Engineering Research Group
CI	Confidence Interval
CM	Cardiomyopathy
CPU	Central Processing Unit
CS	Chip Select
CVD	Cardiovascular Disease
DPRNN	Deep Pattern Recognition Neural Network
DR	Dysrhythmia
DRDY	Data Ready
DSI	Display Serial Interface
ECG	Electrocardiogram
FFT	Fast Fourier Transform
FIR	Finite Impulse Response
FN	False Negative
FP	False Positive
ESD	Electrostatic Discharge
FTDNN	Focused Time-Delay Neural Network
GND	Ground
GPIO	General Purpose Input Output
GUI	Graphical User Interface
HC	Healthy Control

HIV	Human Immunodeficiency Virus
HT	Hypertrophy
I2C	Inter-Integrated Circuit
ICA	Independent Component Analysis
IEC	International Electrotechnical Commission
KNN	K-Nearest Neighbours
LA	Left Arm
LBBB	Left Branch Bundle Block
LCD	Liquid Crystal Display
LL	Left Leg
LS-SVM	Least Squares Support Vector Machine
LTMIL	Latent Topic Multiple Instance Learning
MI	Myocardial Infarction
MISO	Master-in Slave-out
ML	Mason-Likar
MOSI	Master-out Slave-in
MSB	Most Significant Bit
MSE	Mean Squared Error
NACK	Not Acknowledged
NCD	Non-communicable Disease
NLO	Non-linear Optimisation
PAC	Premature Atria Contraction
PC	Personal Computer
PCB	Printed Circuit Board
PCG	Precordialcardiogram
PCI	Percutaneous Coronary Intervention
PTB	Pysikalisch-Technische Bundensanstalt
RA	Right Arm
RBBB	Right Bundle Branch Block
RL	Right Leg
RLD	Right Leg Drive
RMSE	Root Mean Squared Error
RMSS	Republic of South Africa Military Standards Steering
ROC	Receiver Operating Characteristic
RPi	Raspberry Pi
SA	Sinoatrial
SCL	Signal Clock
SCLK	Signal Clock

S-DA	Stepwise Discriminant Analysis
SDA	Signal Address
SDAE	Stacked Denoising Autoencoder
SNR	Signal to Noise Ratio
SOF	Statistical Overlap Factor
SPI	Serial Peripheral Interface
SPL	Sound Pressure Level
SPS	Samples Per Second
SS	Slave Select
SVM	Support Vector Machine
TN	True Negative
TNR	True Negative Rate
TP	True Positive
TPR	True Positive Rate
t-SNE	t-Distributed Stochastic Neighbour Embedding
USB	Universal Serial Bus
VCG	Vectorcardiogram
VCM	Common Mode Voltage
VHD	Valvular Heart Disease
VNIP	Variation Not Indicating Pathology
WCT	Wilson Central Terminal
WHO	World Health Organisation

Constants

$j = \sqrt{-1}$

Symbols

A_N	Amplifier gain	[−]
a	Neural network activations	[−]
avR	Augmented limb lead vR	[V]
avL	Augmented limb lead vL	[V]
avF	Augmented limb lead vF	[V]
b	Translations	[−]
C	Capacitor values	[F]
C_w	Wavelet coefficients	[−]
c	Dilations	[−]
d	Tapped delay	[−]

E_k	Relative Energy	[−]
Er	Error function	[−]
E_{Total}	Total Wavelet energy	[−]
er	Neural network backpropogation error term	[−]
f_p	Pole frequency	[Hz]
f_c	Corner frequency	[Hz]
f	Selected operating frequency	[Hz]
G	High-pass filter	[−]
G_0	Low frequency gain	[−]
G_f	Gain at the selected operating frequency	[−]
g	Activation function	[−]
H	Low-pass filter	[−]
H_0	Null hypothesis	[−]
H_1	Alternative hypothesis	[−]
h_θ	Hypothesis function	[−]
I	Limb lead I	[V]
I_c	Maximum current consumption	[A]
I_{ECG}	Current consumed by the ECG frontend	[A]
II	Limb lead II	[V]
III	Limb lead III	[V]
I_{Total}	Total current	[A]
I_{LCD}	Current consumed by the LCD touchscreen	[A]
I_{RPi}	Current consumed by the Raspberry Pi	[A]
I_{Out}	Microphone output current	[A]
I_{Steth}	Current consumed by the electronic stethoscope	[A]
J	Cost function	[−]
k	Current scale	[−]
LA	Voltage recorded at the left arm	[V]
LL	Voltage recorded at the left leg	[V]
l	Discrete time step	[−]
N	Total samples	[−]
R	Resistor values	[Ω]
RA	Voltage recorded at the right arm	[V]
R_{ADC}	Analogue to Digital Converter resolution	[V]
$RMSE$	Root mean squared error	[−]
r	Pearson correlation	[−]

$S1$	First heart sound	[−]
$S2$	Second heart sound	[−]
$S3$	Third heart sound	[−]
$S4$	Fourth heart sound	[−]
S	Wavelet scale	[−]
SW	Search window	[−]
s	Input signal	[−]
s_{norm}	Normalised signal	[−]
t	Time step	[s]
V_n	Precordial lead n	[V]
V'_n	Precordial lead n with reference to the right leg	[V]
V_{Steth}	Electronic stethoscope voltage	[V]
V_{Raw}	Raw recorded voltage	[V]
V_{Range}	Analogue to Digital voltage recording range	[V]
V_{ECG}	ECG voltage	[V]
V_{Reff}	ECG frontend reference voltage	[V]
V_{Gain}	Voltage gain	[V]
V_{Out}	Microphone output voltage	[V]
V_{CC}	Supply voltage	[V]
V_{OP}	Maximum operating voltage	[V]
V_B	Bias voltage	[−]
x	Input to neural network	[−]
y	Original lead	[−]
$\hat{y}$	Reconstructed lead	[−]
W	Wavelet transform	[−]
WCT	Wilson central terminal	[V]
WE	Wavelet Entropy	[−]
α	Type 1 error rate	[−]
$\Delta\Theta$	Correction term	[−]
γ	ECG wave significance threshold	[−]
δ	Neural network individual correction term	[−]
δ_S	Difference between the true positives in class 1 and 2.	[−]
ε	ECG wave detection threshold	[−]
η	Discordance	[−]
Θ	Weighting vector	[−]
θ	Weighting factor	[−]

μ	Signal mean	[−]
ξ	ECG wave onset and offset threshold	[−]
π_1	True positives in class 1	[−]
π_2	True positives in class 2	[−]
σ	Signal standard deviation	[−]
Ψ	Fourier transformed wavelet prototype	[−]
ψ	Wavelet prototype	[−]
ω	Sampling frequency	[rad/s]

Chapter 1

Introduction

The World Health Organisation (WHO) identified non-communicable diseases (NCDs), collectively, as the most significant challenge to modern healthcare in the 21st century. This is due to the potential for NCDs to inflict long-term human suffering as well as crippling socio-economic development. Of all the NCDs, none is more deadly than cardiovascular disease (CVD), resulting in 17.7 million deaths in 2015, the highest cause of death worldwide. Statistics revealed that 75% of all deaths caused by CVDs in 2015 occurred in developing countries (World Health Organisation, 2017). The WHO initiated the development of a Global NCDs Action Plan which alludes to the importance of addressing the increase in CVDs by ensuring the widespread availability of affordable medical technology, in both private and public medical facilities. This project aims to address this challenge by developing a point of care device capable of screening cardiovascular disease in rural areas.

1.1 Background

Cardiovascular disease is an umbrella term used to reference diseases that affect the heart or surrounding blood vessels. Examples of some of the many CVDs include myocardial infarction (MI), heart failure, branch bundle block (BBB), valvular heart disease (VHD), cardiomyopathy (CM), arrhythmia, myocarditis (MC), dysrhythmia (DR) and stroke. The underlying cause and symptoms of CVDs differ across the various individual diseases. Traditionally, cardiologists diagnose CVD in a clinical environment using recordings obtained from the gold standard 12 lead ECG and may include supporting results gathered from stethoscope auscultation. Additional advanced methods include the echocardiogram and cardiac MRI. The patient's medical history, current symptoms, blood pressure, age and lifestyle habits also contribute to providing a complete diagnosis.

In 2007, research into screening for abnormal heart sounds and murmurs was initiated by Visagie (2007), within the Stellenbosch Biomedical Research Group (BERG). This resulted in the creation of an "auscultation jacket" prototype seen in Figure 1.1, which is capable of recording heart sounds and ECG data from patients. An artificial neural network (ANN) was trained using heart sounds acquired using the "auscultation jacket" from 17 healthy patients and 14 patients suffering from valve-related heart disease. The output of the ANN indicated the diagnosis of the patient.

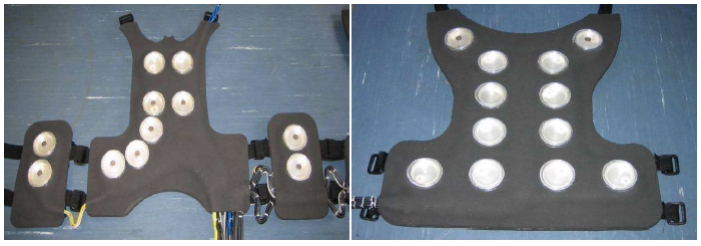

Figure 1.1: Auscultation jacket prototype (Visagie, 2007).

In 2010, an additional project was initiated by Botha (2010), which led to the development of the Precordialcardiogram (PCG) device seen in Figure 1.2. This device aimed at addressing the major pitfalls in the "auscultation jacket's" design. The number of electronic stethoscopes and built-in ECG electrodes used by the PCG device was significantly reduced in comparison with that of the previous generation "auscultation jacket", with the overall design simplified. This would allow for the operation of the device by a nurse rather than a doctor or specialist practitioner. In this study, 62 patients were examined using the PCG device. The study population included 28 patients suffering from cardiovascular disease and 34 healthy patients. The recorded heart sounds were used to autonomously classify patients as either healthy or unhealthy using an ANN classification system, similar to research done by Visagie (2007).

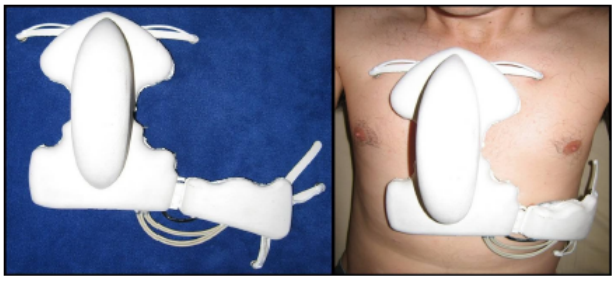

Figure 1.2: Precordialcardiogram prototype device (Botha, 2010).

The present study entails the design and development of a portable electrocardiogram (ECG) and electronic stethoscope system. The device will be completely portable and is intended to be operated by trained nurses in rural locations, at the point of care, to identify and patients with potential cardiovascular disease. These identified patients will be referred to local hospitals for further examinations. The device will record both the heart's electrical biosignals and auscultation, with more research effort focused on the ECG data as a means for diagnosis. A reduced ECG lead set will be recorded and input into a classification neural network to make a diagnosis. The possibility of reconstructing absent leads is also investigated. This would allow the generation of the standard 12 lead ECG printout familiar to general practitioners and cardiologists, from a reduced lead set. The electronic stethoscope allows the recording, playback and visualisation of heart sounds. The device is capable of transmitting ECG and electronic stethoscope recordings, as well as patient information to specialists, wirelessly, using Bluetooth or Wi-Fi technology.

1.2 Motivation

In South Africa, five people suffer from heart attacks every hour with 215 daily fatalities due to heart disease and strokes. This places CVD as the second deadliest disease in South Africa (after HIV/AIDS) and more fatal than cancer (Pillay-van Wyk *et al.*, 2013). Prior studies indicate that by 2030, CVD will be responsible for more deaths in developing countries than the total combined fatalities of HIV/AIDS, malaria and tuberculosis (Beaglehole and Bonita, 2008).

Medical equipment and devices (such as the 12 lead ECG, echocardiograms and cardiac MRI) required by cardiologists to diagnose cardiovascular disease are expensive and only available at larger hospitals in major cities within South Africa. This presents a significant challenge for the 35% of South Africans residing in rural areas who require medical attention (The World Bank, 2017). It is not always possible for rural patients to travel vast distances to visit a doctor, or specialist, such as a cardiologist, as the average rural household survives on less than R630 per month (Daniels *et al.*, 2013). This results in many patients in rural areas living with lingering cardiovascular problems and not receiving proper medical attention, which may ultimately lead to death.

Currently, ECG lead placements are performed by trained medical technicians in hospitals, who specialise in these placements. The desired outcome would be to empower nurses, or trained individuals, in rural communities with a point-of-care medical device capable of automated CVD screening. This relies on the ability to simplify the current ECG procedure by minimising complicated lead positions or stethoscope placements. Research into automated diagnosis using both ECG and electronic stethoscopes recordings has increased in recent

years with many specialists searching for elementary methods to accurately screen for cardiovascular disease. Lead reconstruction is of particular interest as it simplifies the lead placements procedure while still generating the full 12 lead ECG recording. The successful implementations of such technology could extend further than rural applications and ultimately revolutionising the way cardiovascular screening is performed in hospitals and clinical environments, as well as significantly simplify outpatient care.

1.3 Aims

The aims that underpin the purpose of the project are listed as the following:

1. The research and development of a low-cost portable device to evaluate and screen patients with potential cardiovascular diseases in rural locations. The patients identified as having potential cardiovascular disease would ideally be referred to major hospitals for further evaluation by specialists.

2. Test the feasibility of the system by taking recordings of healthy and unhealthy subjects identified by trained cardiologists and comparing the results with previous studies.

1.4 Objectives

The development of a portable ECG and electronic stethoscope system can be divided into the following project objectives:

1. Develop a fully functional prototype that can record the heart's electrical signals and heart sounds.

2. The device should be portable and able to be used in rural locations.

3. The cost of the device should be cheaper than currently existing technology.

4. Recorded signals should be plotted graphically and stored locally on the device.

5. The device should contain wireless data sharing capabilities so that records may be sent to healthcare specialists for analysis.

6. The development of machine learning algorithms to diagnose a patient as either healthy or potentially having cardiac disease, as well as an investigation into the potential for 12 lead ECG reconstruction from a reduced lead set.

1.5 Thesis Outline

This thesis document will consist of the following chapters and topics:

Chapter Two: A literature review will begin by presenting information pertaining to the functioning of the heart, the human circulatory system, the production of heart signals (electric and auscultation) as well as the methods used to process these signals. Currently available technology, prior research done on the subject matter as well as current approaches such as ECG lead reduction techniques and patient classification are also discussed.

Chapter Three: This chapter discusses the hardware and software design of the complete ECG and electronic stethoscope system. All the individual components required to build the prototype device are explained in detail as well as the manner in which these components interact. The function and design of the graphical user interface, as well as its integration with the prototype device, is also discussed.

Chapter Four: This chapter describes the research methodology of the project. The database retrospective study is introduced followed by the clinical study, which includes details on population size, the research protocol and the materials used in the study. Statistical analysis methods used to quantify the results are also described.

Chapter Five: This chapter provides a background to machine learning and artificial neural networks. The relevant algorithms and models used in ECG classification and lead reconstruction are explained in detail.

Chapter Six: The results from both the retrospective and clinical study are analysed using statistical methods found in literature and presented in this chapter.

Chapter Seven: A discussion of the results obtained in both the retrospective and clinical study is provided. The key findings are compared with prior studies completed in the research field.

Chapter Eight: The conclusion summarises the work completed with reference to the project's objectives. Noteworthy limitations, as well as future recommendations, are discussed.

Chapter 2

Literature Review

2.1 The Cardiovascular System

The cardiovascular system is an organ system consisting of the heart, blood and blood vessels. The system is responsible for the circulation of blood containing nutrients, oxygen, carbon dioxide, hormones and blood cells to and from the cells of the body. This enables the body to sustain life by supplying nourishment, fighting disease and foreign particles, regulating temperature and pH levels as well as ensuring that homoeostasis is maintained (Marieb, 2015).

2.1.1 The Heart

The heart is situated within the thoracic cavity (Figure 2.1 (Marieb, 2015)), between the lungs and is protected by the sternum and rib-cage.

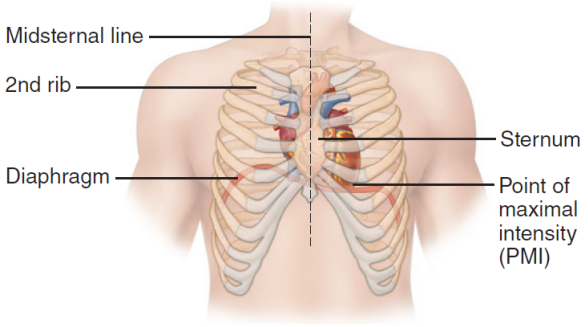

Figure 2.1: Position of the heart in relation to the ribcage (Marieb, 2015).

The wall of the heart consists of three layers, namely the outer epicardium, the middle myocardium and the inner endocardium. The myocardium is composed of cardiac tissue and is the layer responsible for contractions due to stimulation. The heart is divided into four chambers: two superior atria and

two inferior ventricles (Figure 2.2). Blood is received initially in the atria under low pressure via the veins and is not involved in the pumping process. The walls of the ventricles are much thicker and are responsible for discharging the blood from the heart into circulation. Contraction of the ventricles results in blood being propelled into circulation (Marieb, 2015).

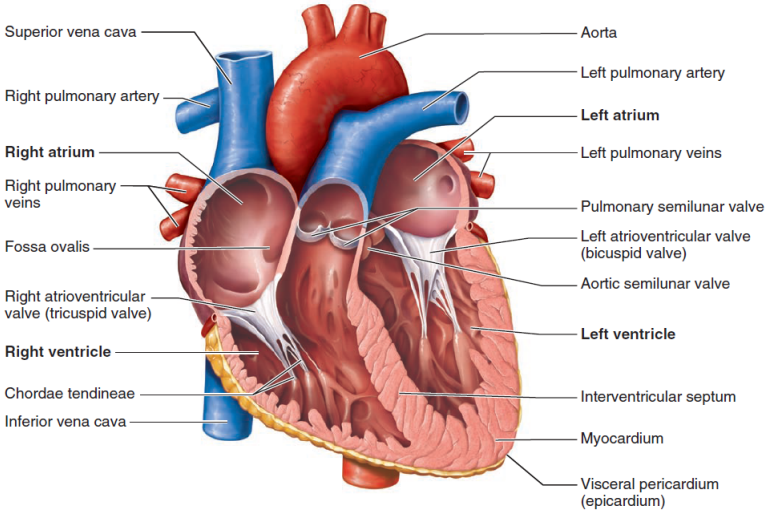

Figure 2.2: Anatomy of the human heart (Marieb, 2015).

The heart contains four valves, namely two atrioventricular (AV) valves and two semilunar valves, which respond to pressure changes in the heart and ensures the flow of blood in only one direction. The AV valves are situated between the atrial and ventricular chambers on either side of the heart. The left AV valve is referred to as the bicuspid, or mitral valve, as it consists of two flaps of endocardium. The right AV valve is referred to as the tricuspid valve and has three flaps of endocardium. The AV valves are anchored to the walls of the ventricles by white tendonous cords known as the chordae tendinae. The semilunar valves are situated between the ventricles and the two large arteries that transport blood away from the heart known as the aorta and the pulmonary artery. The individual semilunar valves are identified as either the pulmonary or the aortic semilunar valve (Marieb, 2015).

2.1.2 The Circulatory System

The heart is separated into a left side and right side, along the septum and operates as a double pump. The right side supplies blood to the pulmonary circuit and the left half services the systemic circuit (Figure 2.3) (Marieb, 2015). The pulmonary circuit receives oxygen-deficient blood from veins via the superior and inferior venae cavae and pumps it out through the pulmonary artery towards the lungs. Once in the lungs, carbon dioxide is released and exchanged

for oxygen. The oxygen-enriched blood travels from the lungs to the left side of the heart via the pulmonary veins, where it is pumped out through the aorta and forms part of the systemic circuit (Marieb, 2015).

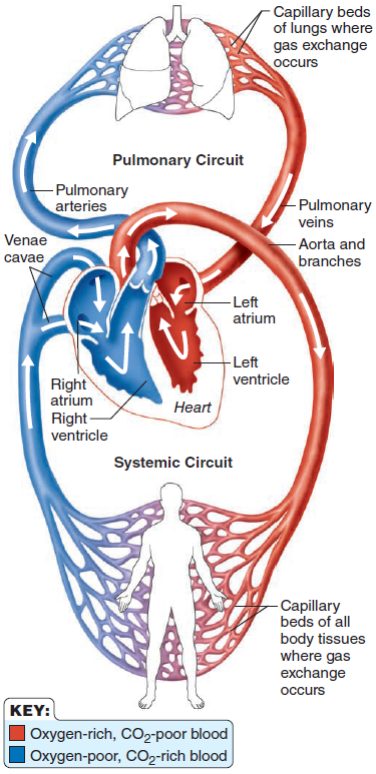

Figure 2.3: Circulatory system divided into the pulmonary and systemic circuits (Marieb, 2015).

2.1.3 The Cardiac Cycle

A cardiac cycle is divided into two phases experienced by any chamber of the heart, namely the systole (contraction) and the diastole (dilation). During systole, blood is pumped into the adjacent heart chamber or artery; whereas during diastole the heart chamber relaxes and fills with blood (Marieb, 2015). The cardiac cycle is initiated by atrial systole where blood flows from the atria into the ventricles. The endocardium flaps of the AV valve hang limply in the ventricles under diastole. The intra-ventricular pressure rises as the ventricles fill with blood, forcing the valve flaps upward where the chordae tendineae keep the flaps in position, sealing the chamber and preventing blood returning to the atria. The atrial systole, with a duration of approximately 100 ms, is followed by ventricular systole and atrial diastole, with a duration of 275 ms and 700 ms, respectively (Visagie, 2007; Marieb, 2015).

During ventricular systole, and corresponding atrial diastole, a build-up of inter-ventricular pressure results in blood being pumped out of the heart which forces the leaflets of the semilunar valve open and flat against the walls of the arteries. Blood leaving the heart through the arteries causes the inter-ventricular pressure to decrease below the pressure in the arteries. Blood attempts to flow back towards the heart, shutting the semilunar valves, preventing blood returning to the ventricular chambers which are now under diastole. This concludes one cardiac cycle with an approximate time of 800 ms, and the next cardiac cycle will begin upon the next atrial systole (Visagie, 2007; Marieb, 2015).

2.2 Electrocardiography

Electrocardiography is a branch of medical technology found in the offices of general practitioners, local clinics as well as hospitals. Investigations into the phenomena of electrical impulses within living organisms, conducted in the early 18th century led to the discovery that nerve and muscle tissue are triggered by electrical stimuli. Thereafter, it was discovered that the heart produces low voltage signals that may be measured using electrodes. These findings initiated the development of the initial technology that would serve as the cornerstone of electrocardiography. With the turn of the 20th-century, medical experts and scientists stressed the medical relevance and importance of ECGs and worked to produce a protocol for the procedure of taking ECG recordings. Decades of research and technological innovation culminated in the creation of a device of paramount importance to the field of cardiology (Geselowitz, 2015).

2.2.1 The ECG Biosignal

Since the heart consists of cardiac muscle, it beats completely involuntarily and is not consciously controlled by the brain. Stimuli sent from the cardiac centre in the brain, via the spinal cord and along the vagal nerve, arrive at a local nerve centre known as the sinus node or sinoatrial (SA) node (Figure 2.4). The rhythmic beating of the heart is controlled by special cells known as pacemaker cells that reside in the SA node (Zinke-Allmang, 2008). Impulses sent from the SA node travel to the AV node Figure (2.5), which is located at the bottom of the right atrium, near the tricuspid valve. The AV-node operates in a similar manner to the SA-node, with the difference being the AV-node's slower rate of depolarisation. The slower depolarisation rate results in a 0.1-0.2 second delay in the nerve impulse reaching the cells of the ventricular muscle. This delay provides enough time for the atria to empty into the ventricles before the blood is pumped from the heart into circulation. Once the AV-node is triggered, the electric impulse leaves through the AV-bundle and splits into

two major branches, the right bundle branch along the right side of the heart and the left bundle branch along the left side of the heart after crossing over the inter-ventricular septum. The impulses reach the Purkinje fibres, which are the muscle cells of the heart responsible for the contraction, and are the final destination of the nerve impulse (Zinke-Allmang, 2008). Once the ventricles have repolarised, the cardiac cycle is repeated.

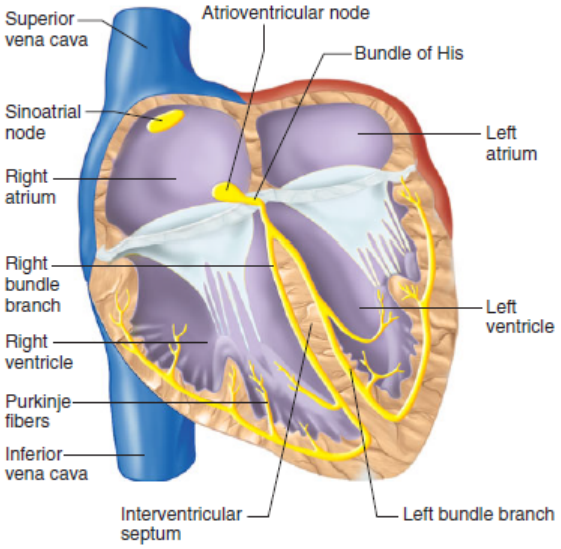

Figure 2.4: Anatomy responsible for the stimulation and propagation of electrical activity within the heart (Barret *et al.*, 2012).

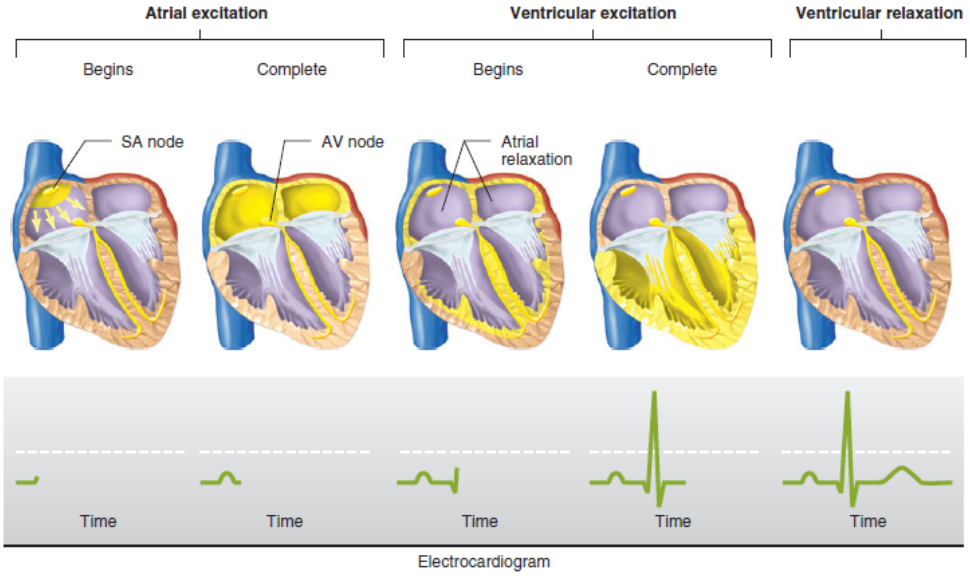

Figure 2.5: Sequence of the electrical activity within the heart (Barret *et al.*, 2012).

2.2.2 The 12 Lead Electrocardiogram

The electrocardiogram (ECG) is a medical diagnosis and observation tool for time-resolved measurements of the electric activity of the cardiac muscle and is the current clinical gold standard. The method was first developed by Willem Einthoven in 1906, in which he developed a method to monitor a human's heart beating within the chest cavity (Zinke-Allmang, 2008). The current 12-lead ECG is recorded by attaching the lead-wires to the ten adhesive electrodes placed across the chest and limbs (Figure 2.6). The right leg (RL) electrode is not used in diagnosis but acts as the reference electrode and is used in the "right leg drive" (RLD) circuit. A RLD circuit is often used with biopotential differential amplifiers to reduce common mode voltage and improve stability (Winter and Webster, 1983).

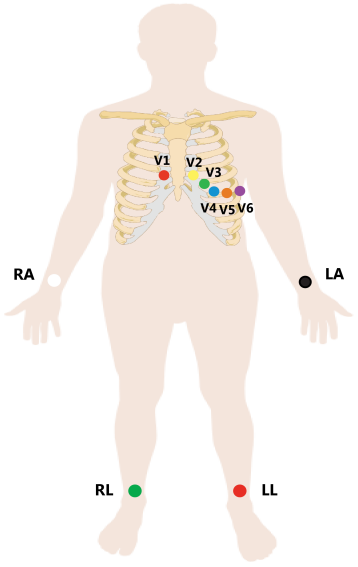

Figure 2.6: Placement of a the standard 12 lead ECG electrodes.

The first ECG leads were introduced by Einthoven who derived leads I, II and III using the left arm (LA), right arm (RA) and left leg (LL) limb electrodes, represented as:

$$I = LA - RA \tag{2.1}$$

$$II = LL - RA \tag{2.2}$$

$$III = LL - LA \tag{2.3}$$

His work was followed by Goldberger, who successfully derived the augmented leads aVR, aVL and aVF from the limb leads, using the following equations:

$$\begin{aligned} avR &= RA - 0.5 \times (LA + LL) \\ &= -0.5 \times (I + II) \end{aligned} \tag{2.4}$$

$$\begin{aligned} avL &= RA - 0.5 \times (LA + LL) \\ &= 0.5 \times (I - III) \end{aligned} \tag{2.5}$$

$$\begin{aligned} avF &= RA - 0.5 \times (LA + LL) \\ &= 0.5 \times (II + III) \end{aligned} \tag{2.6}$$

A graphical illustration of the limb leads (I-III) and the augmented leads (avR, avL and avF) is depicted in Figure 2.7.

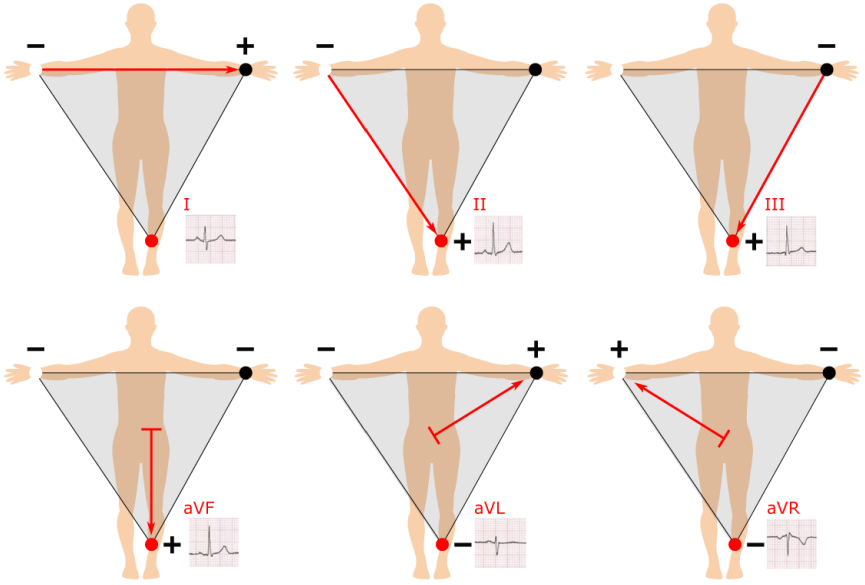

Figure 2.7: Illustration of the Einthoven triangle (Cables and Sensors, 2011) which requires the use of 4 limb electrodes, where the right leg is the reference. Each of the limb leads (I-III) are recorded at the positive pole location with respect to the negative pole location, specific to that particular limb lead. The augmented leads (avR, avL and avF) are recorded in the direction from the theoretical WCT to the positive pole. The pole locations correspond to the various limb electrodes, whereas the WCT is a derived theoretical location without a corresponding electrode.

Wilson *et al.* (1934) derived the precordial leads V1-V6, by the introduction of the "Wilson central terminal" (WCT), which is the average of the limb leads electrode potentials and is calculated as:

$$WCT = \frac{1}{3} \times (LL + RA + LF) \tag{2.7}$$

The precordial leads (V1-V6) are recorded in the direction from the central terminal to either one of the six precordial electrode positions, represented as:

$$V_n = V'_n - WCT \tag{2.8}$$

where V_n is the precordial lead voltage ($n = 1, ..., 6$) and V'_n is the voltage recorded at the n_{th} precordial electrode position (Figure 2.6) with reference to RL. The directions of the 12 lead ECG are represented as vectors in Figure 2.8. The limb leads and the augmented leads record the heart's electrical activity in the frontal plane, whereas leads V1 to V6 record electrical activity in the transverse plane emanating outward from the central terminal.

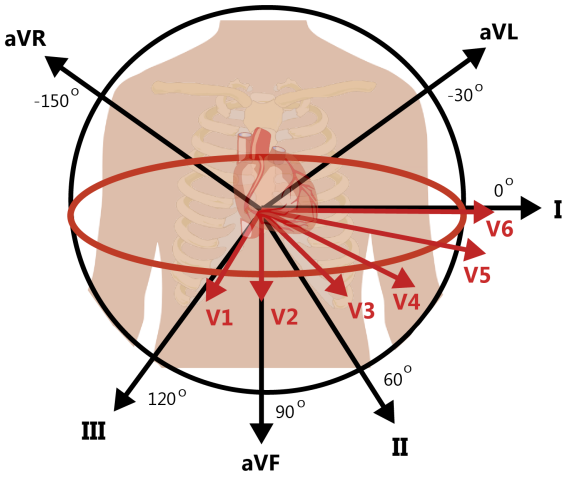

Figure 2.8: Hexaxial illustration of all 12 ECG leads. The leads in the frontal plane are represented as black vectors and the leads in the transversal plane represented in black.

The different lead vectors provide information pertaining to the direction and magnitude of the heart's electrical activity focusing on different regions of the heart (Table 2.1). This provides a coherent snapshot of the heart's current condition, as viewed from different angles and regions.

Table 2.1: The views of the heart provided by the 12 lead ECG.

Leads	Regions of the heart
II, III, avF	Inferior
I, avL, V5, V6	Lateral
V1, V2	Septal
V3, V4	Anterior

2.3 Heart Auscultation and Heart Sounds

Auscultation is the medical procedure in which a doctor uses a stethoscope to listen to sounds within the body. Heart auscultation refers specifically to the analysis of sounds produced by the heart and blood circulation through the valves and the circulatory system (Reed *et al.*, 2004). To this day, heart auscultation remains a fundamental tool and primary method for identifying potential underlying pathology related to cardiovascular disease (Visagie, 2007). When performing heart auscultation on a patient, there are specific positions on the thorax that a physician places the stethoscope. Figure 2.9 illustrates the various heart auscultation positions relative to the heart valves.

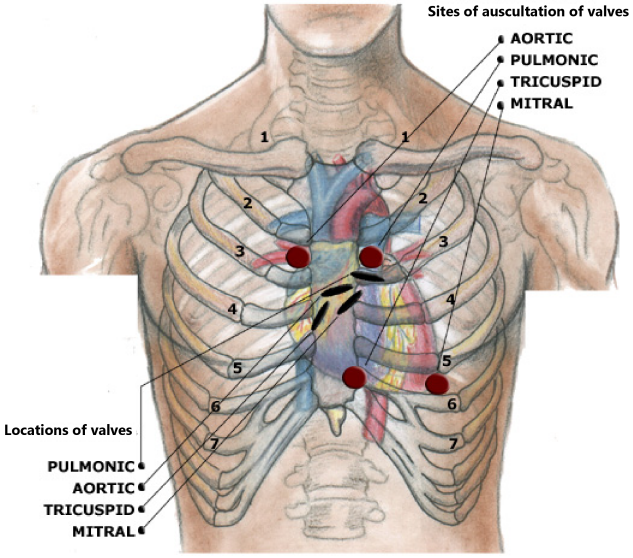

Figure 2.9: The heart auscultation positions that correspond to the various heart valves (Stethographics, 2007).

The aortic valve, located between the left ventricle and aorta, is audible at the second intercostal space, situated to the right of the sternum between the second and third rib. The pulmonary valve, located between the right ventricle and the pulmonary artery, is audible in the second intercostal space, to the left of the sternum. The tricuspid valve, located between the right atrium and right ventricle, is audible at the fifth intercostal space to the left of the sternum, between the fifth and sixth ribs. The mitral valve that divides the left atrium and ventricle is audible left of the sternum in the fifth intercostal space (Visagie, 2007).

Phonocardiograms are used to illustrate recorded heart signals graphically (Figure 2.10). The heart signals are divided into four characteristic sounds (Rangayyan and Reddy, 2002) referred to as S1 to S4. The most well-known

sounds, S1 and S2, are most commonly referred to as the "lubb-dupp" sound, in which "lubb" and "dupp" refers to S1 and S2, respectively. Originally it was believed that S1 was solely the result of the closure of the mitral and tricuspid valves, and S2 solely the result of the aortic and pulmonary valves. However, additional theories indicate that the vibration of the entire cardiovascular system, initiated by pressure gradients, as well as turbulent blood-flow, could contribute to generation of heart sounds S1 and S2 (Rangayyan and Reddy, 2002; Visagie, 2007).

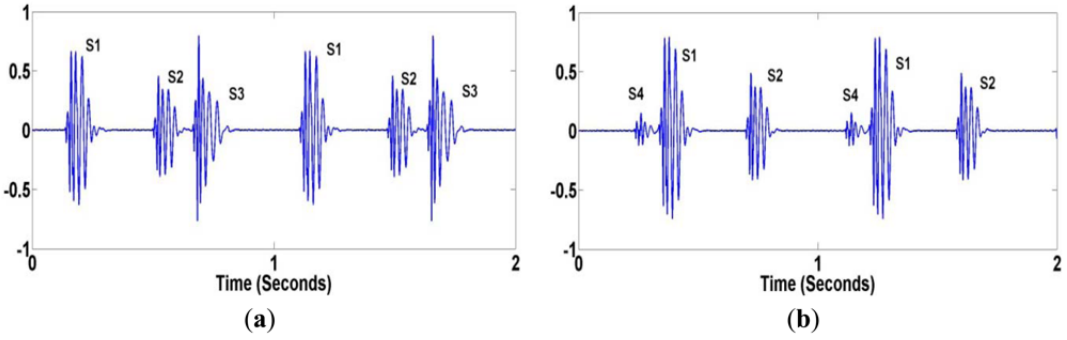

Figure 2.10: Phonocardiogram recording (Sa-ngasoongsong *et al.*, 2012): (a) The standard heart sounds S1 and S2, followed by the additional S3 heart sound. (b) A recording indicating the presence of the additional heart sound S4 with respect to the standard heart sounds S1 and S2.

A third heart sound, S3, is occasionally heard due to the abrupt termination of the phase in the cardiac cycle responsible for blood rapidly filling the ventricles from the atria. The sound is characterised by a low-pitch sound audible at the heart's apex (Munro and Edwards, 1990) and is common in healthy young adults and athletes. The S3 heart sound may disappear before middle age, with its presence in older patients indicating impaired ventricular function.

The fourth heart sound S4 is an additional heart sound that occurs during a late diastole, before S1. It is a low-pitch sound audible at the apex of the heart. The S4 occurs in normal patients but tends to become prominent during the atrial systole of patients with ischaemic heart disease and hypertension (Munro and Edwards, 1990). The S3 and S4 heart sounds may be detected in healthy patients with a sufficiently slow heart rate, however, as the heart rate increases the two heart sounds tend to overlap (Visagie, 2007).

2.4 Existing Technology

2.4.1 Electrocardiograms

Since the creation of the first instance of the ECG by Einthoven in the late 18th century the device has evolved and improved with contributions by various scientists until it was introduced into healthcare facilities in the 1960's (Barill and Inc, 2012). The first three lead ECG was introduced over a 100 years ago and continues to be used today. A three lead ECG may contain either three or four ECG electrodes, providing leads I, II and III (from electrodes at RA, LL and LL), with a possible fourth reference electrode RL. A three lead ECG is still commonplace in various applications such as emergency departments, medical procedures, long duration monitoring and telemetry (Barill and Inc, 2012).

However, in the 1990's, additional research revealed that the three lead ECG was not sensitive enough to identify various ischemic cardiovascular diseases. This led to the expansion of the three lead ECG to the five lead ECG, with the addition of lead V1 resulting in four extremity leads and one precordial lead. While the three lead systems were still in use, most of the new ECG devices allowed for an optional five lead system. The use of the five lead system increased the accuracy of identifying ischemic cardiovascular disease and was also beneficial in dysrhythmia monitoring (Barill and Inc, 2012). The reason for this increased sensitivity was due to lead V1 providing additional views of the heart, correlating to the sternum as well as a partial right side view. Finally, the addition of precordial ECG leads V2 to V6 culminated with the 12 lead ECG (Figure 2.11), which is the current non-invasive clinical gold standard.

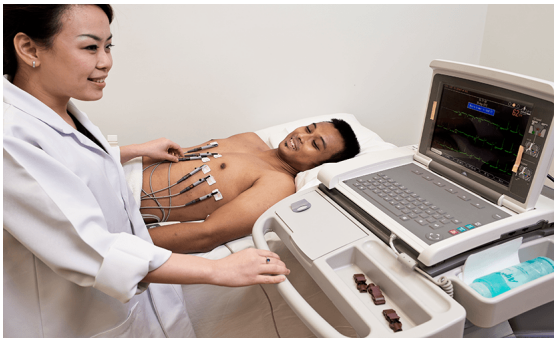

Figure 2.11: An example of a 12 lead ECG with precordial leads V1-V6 visible on the subjects chest (Sunway, 2017).

The 12 lead's additional precordial leads allow for the detection of a wider range of CVD and abnormalities. This is achieved by including the additional leads that focus on the anterior sections of the heart as well as the already

included lateral, septal and inferior regions already available in the five lead ECG. However, due to the manner in which the limb leads are derived as well as the close positional proximity of the precordial leads, many of the ECG leads reproduce similar information (Dawson *et al.*, 2009). This has led healthcare specialists and researchers to question the necessity for all 12 leads, resulting in a renewed focus into simpler ECG lead placement systems and methods.

A normal ECG recording, regardless of the number of leads, only provides a short duration snapshot of the heart's current condition. Some pathologies may not appear during a routine ECG test and require longer recording times. In the event of long duration ECG monitoring, a patient is given a portable device known as a Holter monitor (Figure 2.12) which is used to record ECG data from 24 hours, up to two weeks, while the individual partakes in their daily routine. The number of leads ranges between three and eight, varying between Holter models and manufacturers. After the recording period, the data is uploaded to a computer which automatically analyses the signals using specialised software. The software identifies rhythmic information as well as sections of interest within the recordings that should be studied by a technician who prepares a report for a specialist. The Holter monitor may be used on patients who have experienced a heart attack, patients on new medication or patients with rhythmic problems such as atrial fibrillation, multi-focal atrial tachycardia, paroxysmal suprevaentrical tachycardia, bradycardia and ventricular tachycardia (Chen, 2016).

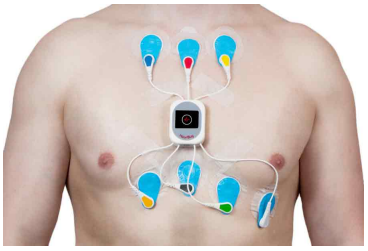

Figure 2.12: An example of a seven lead wire Holter monitor.

2.4.2 Electronic Stethoscopes

Since the inception of the first acoustic stethoscope, the technology used in auscultation has remained relatively unchanged. Years later, the introduction of the electronic stethoscope (Figure 2.13) provides physicians with greater control and flexibility over the volume and frequency bandwidth of stethoscope recordings. The use of the electronic stethoscope ensures that recordings may be stored, plotted graphically as well as shared with professionals which resulted in the emergence of a new field of computer-aided auscultation. This

has generated an increased interest in the use of recorded heart sounds in the automatic diagnosis of cardiovascular diseases (Leng *et al.*, 2015).

Figure 2.13: Electronic stethoscopes (Thinklabs, 2003; Littmann, 2017): Examples of state of the art electronic stethoscopes by Littmann (a) and Thinklabs (b) .

The procedure of acquiring electronic auscultations occur in three main stages, namely the data acquisition, pre-processing and signal processing stages. In the data acquisition stage, the electronic stethoscope records the heart signals which are converted to electronic signals. Popular transducers used in electronic stethoscopes consist of small electret microphones, piezoelectric crystals or capacitive-based microphones. Electret microphones are the simpler solution but are more prone to environmental noise. The microphone is placed inside the chestpiece of a standard stethoscope and records the fluctuations in sound pressure created by the stethoscope diaphragm, converting the sound waves into electrical signals. Piezo-electric transducers operate using a different principle to that of the electret microphone. The stethoscope diaphragm deforms the piezo-electric crystal that generates an electric charge resulting in the conversion of a heart sound into an electric signal. A challenge with using this type of sensor is the presence of signal distortion due to the operation of the transducer with central frequencies close to the piezoelectric element's resonant frequency (Assous *et al.*, 2007). This may alter the tone of the recorded heart sound. An additional transducer used in electronic stethoscopes is the capacitive sensor modelled on the micro-electro-mechanical system (MEMS) technology. Sound is recorded when the change in acoustic pressure displaces the diaphragm in phase with the source, altering the nominal capacitance value of the MEMS sensor (Leng *et al.*, 2015).

Acquired signals are pre-processed by filtering to remove noise. The heart sounds may be corrupted by various sources of noise which include internal noise such as respiratory and digestive noise, external ambient noise which may be picked up by the microphone, as well as 50 Hz electrical mains noise.

In many cases the heart sound bandwidth overlaps the frequency range of these sources of noise, making filtering extremely challenging. This resulted in the development of advanced filtering techniques which operate in the time domain as well as the transform domain. Once the heart sounds are filtered, the beats are segmented by dividing the data into S1 (systole) and S2 (diastole) segments. The segmented data may be used to extract features which are used to classify heart sounds used in assisted diagnosis in the signal processing stage (Leng *et al.*, 2015).

2.4.3 Hybrid Electronic Stethoscope and ECG Devices

2.4.3.1 Rijuven CardioSleeve

The CardioSleeve is a stethoscope add-on device capable of recording heart sounds as well as three lead ECG signals. In order to record heart sounds the device is attached to any standard stethoscope by detaching the chestpiece of the standard stethoscope from its tubing and inserting the CardioSleeve between the chestpiece and the tubing (Figure 2.14a). The device contains two dry electrodes which can be aligned in various orientations on the chest in order to measure three ECG leads. The heart sounds and ECG signals are transmitted using Bluetooth to any mobile, or desktop device, where the signals may be viewed, recorded and analysed (Figure 2.14b). The acquired signals are analysed using cloud-based computing and provides diagnosis support to the user by predicting the patient's current condition (Rijuven, 2016).

Figure 2.14: CardioSleeve (Rijuven, 2016): (a) The hybrid stethoscope ECG device with the mobile application (b) indicating a simultaneous ECG and heart auscultation recording.

2.4.3.2 Eko Duo

The Echo Duo (Figure 2.15a) is a compact, hand-held device consisting of a single lead ECG and digital stethoscope. The Duo provides simultaneous recordings of the single lead ECG and heart sound which is streamed to a mobile device or PC using Bluetooth 4.0, for viewing purposes (Figure 2.15b). The ECG data is recorded at 500 Hz and contains a 0.01 high-pass and 50 Hz mains filter. The heart sounds are recorded at 4000 Hz and contains ambient noise reduction. The device contains a 3.5 mm audio jack that allows the user to listen to the heart sounds in real-time using headphones. The device has a built-in rechargeable battery which allows for nine hours of continuous use (Eko, 2017).

Figure 2.15: Eko Duo (Eko, 2017): The hybrid stethoscope ECG device (a) with corresponding sensors and mobile application (b).

2.5 Previous Research

A summary of previous research within the department as well as in related fields associated with the subject matter is presented in this section. Finally, a comparison between previous research and this study is drawn.

2.5.1 Screening for Abnormal Heart Sounds and Murmurs

Research into screening for abnormal heart sounds and murmurs was initiated by Visagie (2007) within the Stellenbosch Biomedical Research Group (BERG). This led to the creation of the "auscultation jacket" device which consisted of a neck piece, front piece and back piece. The device was embedded with 21 electronic stethoscopes, responsible for recording both the heart

and lung sounds, and included a standard 12-lead ECG. The electronic stethoscopes were implemented using Panasonic WM-61B black electret condenser microphones which converted sound waves into electrical signals. Each stethoscope was connected to the computer via USB and recorded using software on the computer. The microphones had a frequency range of 20 - 20000 Hz and the recorded signals were sampled at 2000 Hz with 16-bit resolution. In locations in which ECG electrodes overlapped with auscultation points, stethoscope and electrode combinations were used to record both heart sounds and electrical activity simultaneously. The various ECG electrodes and electronic stethoscope placements are illustrated in Figure 2.16.

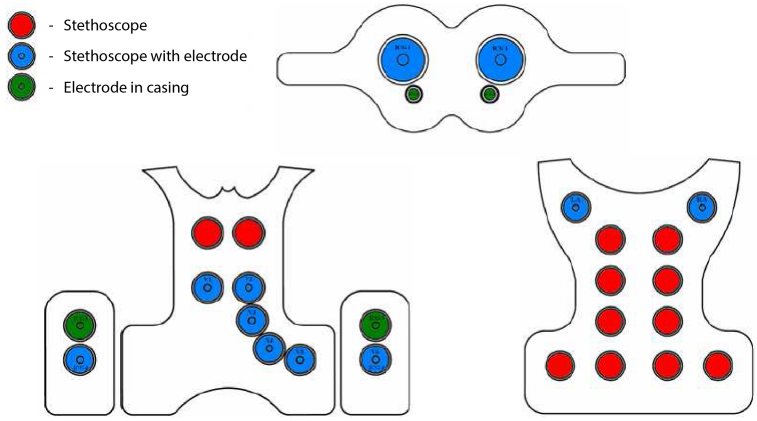

Figure 2.16: Final positions of the electrodes and stethoscopes in the front, neck and back piece of the ausculation jacket (Visagie, 2007).

During the testing procedure, patients fitted with the jacket were asked to lay on their backs on an examination bed and were recorded while breathing normally, holding their breath at the end of expiration as well as holding their breath at the end of inspiration. This allowed for the splitting of the different heart sounds (S1 and S2) resulting in improved data analysis. Throughout the study, 31 patients were examined of which 14 patients suffering from cardiovascular disease and 17 healthy patients were recorded using the "auscultation jacket". Once the raw data was obtained it was filtered to remove any noise and artefacts. The heart sounds were filtered by a bandpass filter with a bandwidth of 25 - 700 Hz and then further filtered using the wavelet threshold method. The ECG signals were low-pass filtered using a 4th order Butterworth filter with a selected cut-off frequency corresponding to 40 Hz in order to remove any 50 Hz electrical noise. Once the signals were filtered, four cardiac cycles of heart sounds were extracted by using a beat detection algorithm that identifies the QRS peaks in the ECG signals. This allowed for the proper synchronisation of the beginning of the four cardiac cycles. The four cycles were divided into features that would be potentially used to train

the neural network's classification system to distinguish between normal and abnormal heart sounds and murmurs. These features were later reduced during the feature selection process with the help of the dimensionality reduction technique known as "statistical overlap factor". This reduced the total features that would be used to train, validate and test the neural network, from 70 features down to three. The neural network consisted of two hidden layers with 10 neurons and five neurons respectively. The sigmoid function was selected as the activation function. The input layer consisted of three neurons and the output layer contained one neuron. The network was trained using the backpropagation algorithm that made use of an adaptive learning rate. Regularisation was utilised to ensure that over-fitting does not occur. The results of the classification system produced a sensitivity of 76.2%, specificity of 90.3% and an overall accuracy of 84.6% when classifying between normal and abnormal heart sounds and murmurs. Over and above the full 12-lead ECG, an additional external three lead ECG was later required to identify the beginning of heart sound S1, which resulted in an inefficient design as two ECG recordings were required. Additionally, the study did not explore the use of the ECG recordings in the patient classification process.

The physical size and dimensions of the "auscultation jacket" was not adjustable. The device was designed for the male South African population and was modelled on anthropometric data obtained from the RSA Military Standards Steering Committee (RMSS), which made use of data acquired from the 50th percentile. This can be seen as a limiting factor in the design as the stethoscope and ECG electrodes require precision placement for woman and men of all body types. The most notable pitfall in the design of the "auscultation jacket" was experienced during respiration. When the patient's chest expanded and contracted, the stethoscopes and ECG electrodes shifted relative to the surface of the body. This led to unreliable recording as well as artefacts and noise entering the signals. The large number of stethoscopes and ECG electrodes resulted in numerous wires and increased the weight of the jacket significantly. Patients suffering from valvular heart disease (VHD) were extremely weak which presented an additional challenge in fitting these patients with the auscultation jacket.

2.5.2 Autonomous Auscultation of the Human Heart

A study involving the autonomous auscultation of the human heart was conducted by Botha (2010) and expanded on the previous work done by Visagie (2007). The objective of the study was to use a new prototype, the Precordialcardiogram (PCG) device (Figure 2.17), to record the patient data within a clinical environment.

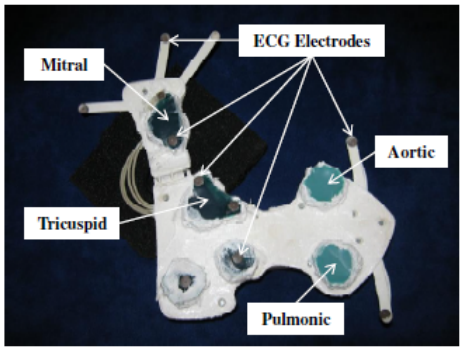

Figure 2.17: Layout of the ECG electrodes and electronic stethoscopes (mitral, tricuspid, pulmonic and aortic) used in the Precordialcardiogram device.

The PCG device was used in combination with auscultation software capable of autonomously screening patients for various cardiovascular disease. The new device attempted to address some of the major pitfalls of the previous generation "auscultation jacket". Similar to Visagie (2007), the PCG utilised multiple sensors to record patients heart sounds and electrical activity, simultaneously. However, the PCG distinguishes itself from its predecessor by the reduced total number of electronic stethoscopes (from twenty-one to four) and ECG electrodes as well as its compact, simplistic design. The improved design was aimed at allowing the device to be operated by a trained nurse rather than a doctor or specialist practitioner. In this study, 62 patients were examined with the PCG device, of which 28 patients suffering from cardiovascular disease and 34 healthy patients were recorded. The PCG device contains four USB sound-card stethoscopes embedded inside the plastic housing as well as a full 12-lead ECG and is connected to a personal computer (PC) via a USB hub. The PC powers the PCG device and saves the patient's data on the hard drive which is analysed by the auscultation software. The stethoscopes were sampled at a frequency of 8 kHz with a 16-bit resolution (Koekemoer and Scheffer, 2008). In order to allow for some variation in adult chest dimensions, the lateral section of the PCG could hinge separately to the body of the device (Koekemoer and Scheffer, 2008).

Once data was collected, the study followed similar steps to that of Visagie (2007), in which the data was filtered to remove noise and artefacts, followed by beat segmentation, feature extraction and classification using neural networks. During the filtering process, additional active noise cancellation was utilised to reduce environmental noise in the sound recordings. This was achieved by using a second microphone which records ambient sounds and then inverts the signal. The stethoscope signal and the inverted ambient environment recording are summed together resulting in the attenuation of environmental noise. A wavelet filter method and low pass filter were also implemented to filter the

heart sounds and ECG signals respectively, followed by segmentation using a beat detection algorithm similar to that of Visagie (2007).

The results of the classification system produced a sensitivity of 82.1%, specificity of 88.2% and an overall accuracy of 85.5% when distinguishing between typical heart diseases and healthy patients. This classification performance is only a slight improvement on the "auscultation jacket", with more available training data. The study struggled to record high-quality electronic stethoscope and ECG signals for obese patients as well as for women. This is due to the fixed design not allowing the electronic stethoscope to make proper contact at the correct auscultation positions and the fixed limb leads could not extend far enough towards the shoulders. This resulted in noisy recordings as the device was manually pressed against the subject. The ECG records were also omitted from the patient classification process. Recommendations included limb lead wires as well as the inclusion of a design feature that would allow the device to mechanically extend to allow for proper contact is achieved between the electronic stethoscopes and the skin.

2.5.3 Reconstruction of the 12 Lead ECG

The 12-lead ECG electrode placement has been considered the gold standard for non-invasive cardiac monitoring, evaluation and diagnosis since its induction, more than a century ago. Misplacement of ECG electrodes due to human error is a common issue in electrocardiography. Small displacements in the precordial electrodes has a more significant influence on the measured ECG signal due to their close proximity to the heart compared to that of the limb leads (Van Oosterom *et al.*, 2000; Rajaganeshan *et al.*, 2008). Deviations in ECG electrode placements from the correct "standard" positions (Kligfield *et al.*, 2007) can also result from errors made by trained medical staff (Herman *et al.*, 1991; McCann *et al.*, 2007; Rudiger *et al.*, 2007; Rajaganeshan *et al.*, 2008). Therefore, a notable drawback is poor reproducibility of the precordial lead placements which results in high variability in the data obtained via ECG recordings (Kania *et al.*, 2014). Kerwin *et al.* (1960) reported that lead placements with an error of less than 1 cm were attained by trained medical staff in merely 50% of cases pertaining to males and 20% of cases pertaining to females. It was discovered that these placement errors were frequently in the range of between 2 cm and 3 cm, with some cases recording errors of up to 6 cm. Bond *et al.* (2012) discussed that incorrect electrode placement contributes to incorrectly diagnosing cardiovascular disease in 17 - 24% of cases completed by either a human or computer-based analysis (Schijvenaars *et al.*, 1997).

Various studies have attempted to reconstruct absent leads from different configurations of reduced lead sets, with varying success (Sejersten *et al.*, 2003;

Drew *et al.*, 2004; Nelwan *et al.*, 2008; Schreck and Fishberg, 2013; Ostertag, 2014; Tsouri and Ostertag, 2014). Initial studies (Dower *et al.*, 1980; Feild *et al.*, 2002; Nelwan *et al.*, 2004) used linear transforms to create a matrix of basis leads consisting of coefficients, known as a "Dower universal transform", used to reconstruct any absent leads using algebraic calculations. This method was a "one-size-fits-all" solution with questionable accuracy due to the derivation of the coefficients relying on biological and environmental factors within populations that are prone to significant variability (Schijvenaars, 2000; Feild *et al.*, 2008). The Simplex non-linear optimisation method was used to construct an additional universal transformation matrix (Schreck *et al.*, 2002; Schreck and Fishberg, 2013) capable of reconstructing missing leads. The base leads used in reconstructing the remaining 12 lead ECG, by virtue of the universal transform matrix, initially included leads I, aVF and V2 (Schreck *et al.*, 2002), with later work focusing on I, II and V2 (Schreck and Fishberg, 2013).

The universal transforms were followed by "population specific transforms" which categorised patients under headings based on their gender, age and disease classification. This strategy resulted in the creation of transforms that were tailored to specific patient sub-populations in an attempt to increase accuracy. Finally, independent component analysis (ICA) was used to generate a third transform, known as "patient specific transform", which reconstructs missing leads from a reduced lead set, tailored to a specific patient (Ostertag, 2014; Tsouri and Ostertag, 2014). This method relies on the availability of all 12 ECG leads which are required to calibrate the transform coefficients, after which leads are removed at a later stage and subsequently reconstructed.

Nelwan *et al.* (2008) made use of a reduced lead system known as the "EASI" ECG whereby five electrodes were placed at simple anatomical locations, found using landmarks on the thorax, to create a derived 12 lead ECG. These landmark positions are based on the Frank lead system in which reconstructs missing leads by utilising the empirically obtained transform coefficients. This method is developed from the heart dipole hypothesis that underlines vectorcardiography. The EASI lead produces three non-orthogonal leads, of which all other leads are reconstructed using algebraic calculations. This is achieved by using linear combinations of the three non-orthogonal leads and the transformation coefficients.

Drew *et al.* (2004) made use of an unconventional five lead wire system. The optimal electrode positions were determined by optimising the root mean squared error between the true leads and the reconstructed leads. The process was repeated for 20 patients using 16 potential locations. This resulted in the use of Mason-Likar electrode placement positions for electrodes RA, LA and LL in which these limb electrodes are relocated onto the thorax. The LL electrode is placed in the 6th intercostal space at the left mid-clavicular line,

which is located just below the standard V4 lead position. A chest electrode is placed in the 4th intercostal space in the middle of the left mid-clavicular line and the left sternal border, close to the standard V3 lead position.

2.5.4 Autonomous Patient Classification using ECG records

The classification of ECG recordings is an integral step in the clinical diagnosis of cardiovascular disease. Traditionally performed by a specialist such as a cardiologist, recent studies have proven that artificial intelligence and machine learning algorithms can be utilised to accurately classify cardiovascular disease from ECG recordings. The autonomous patient classification process is illustrated in Figure 2.18. Initially, the ECG data is recorded and pre-processed, which consists of filtering to remove baseline drift and 50 Hz electrical mains noise. The filtered data progresses to the feature extraction phase in which a set of features is identified from the ECG leads and used to train a classification model in a supervised manner. In supervised classification applications, the classification model is trained with labelled data, which refers to a feature set where the current cardiovascular condition (also referred to as the target classification) for each patient is known. The type, and number, of features that serve as the input to the classifier is the decision of the designer. The feature set should sufficiently describe the data needed to be classified. Once the model is trained it may be used to predict the diagnosis of future patients.

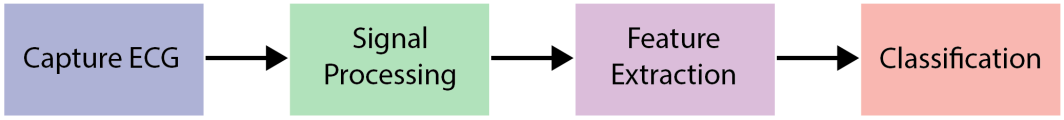

Figure 2.18: A flowchart indicating the steps in the ECG classification process.

First order features can be identified directly from the recorded ECG data such as time intervals between peaks or between successive heartbeats (R-R interval) as well as peak amplitude voltages (Ouyang *et al.*, 1997; Meghriche *et al.*, 2008). Additional second order features can be derived from advanced methods such as spectral entropy (Anuradha and Reddy, 2008), discrete wavelet transforms and Fourier transforms (Dokur and Ölmez, 2001; Sengur and Turkoglu, 2008), to name a few. Prior studies have utilised a wide variety of different machine learning techniques in ECG classification. Examples machine learning techniques include support vector machines (SVMs) (Übeyli, 2007; Chengwei *et al.*, 2007; Asl *et al.*, 2008), fuzzy set theory (Lei *et al.*, 2007) and artificial neural networks (ANNs) (Prasad and Sahambi, 2003; Güler and Übeylı, 2005; Yu and Chen, 2007).

Prior studies by Tripathy *et al.* (2014), Yan *et al.* (2010) and Arif *et al.* (2012), focused on individual heartbeat classification using multi-lead ECG records obtained from the Physikalisch-Technische Bundesanstalt (PTB) online ECG database. Tripathy *et al.* (2014) developed a unique second order metric, referred to as principal component multi-variate multi-scale sample entropy, to classify multi-lead ECGs. The principal component analysis reduces the dimension of the features generated using the multi-variate multi-scale sample entropy approach, which are fed into a least squares support vector machine (LS-SVM) for classification. The LS-SVM was tasked with classifying between healthy controls (HC), cardiomyopathy (CM), dysrhythmia (DR), hypertrophy (HT) and myocardial infarction (MI) classification classes. Yan *et al.* (2010) utilised the SVM classification method to distinguish between HC, CM, HT, bundle branch block (BBB) and valvular heart disease (VHD). The features included first order location, amplitude and interval features, as well as second order features derived from the mean shift algorithm method. The dimension of the features were reduced using generalised discriminant analysis. Arif *et al.* (2012) developed an MI classifier using the K-nearest neighbour (KNN) method. First order time domain features which include the T wave amplitude, as well as Q wave and ST deviation, are inputs to the KNN classifier.

Prior studies performed by Huang and Zhou (2015), Sun *et al.* (2012) and Haraldsson *et al.* (2004), developed models that focused on patient classification using multi-lead ECG records obtained from the PTB online database, or clinical trials. Huang and Zhou (2015) utilised the stepwise discriminant analysis (S-DA) method to classify patients cardiac function as either normal or abnormal, using records obtained from the PTB database. The first order features included the T wave type, time intervals, peak amplitudes and waveform gradients which underwent dimensionality reduction using PCA.

Sun *et al.* (2012) developed the latent topic multiple instance learning (LTMIL) method for automatic detection of myocardial infarction from ECG records within the PTB database. The features selected to be used in the classification process included both first and second order features. The first order features included an average ST length to RR interval ratio, as well as the height to length ratio of each ST segment. The second order features comprised of fitting a polynomial relationship for the ST segment and recording the polynomial coefficients as features, across all 12 leads.

Haraldsson *et al.* (2004) developed a Bayesian inference ANN classifier to detect MI in 12 lead ECG data recorded from 1119 patients, at the emergency department of the University Hospital in Lund, Sweden. The features set included second order features such as coefficients from Hermite basis functions as well as first order features such as amplitude and gradient metrics for the ST-T interval.

2.5.5 Comparison of the Present Study with Previous Research

The current study expands on the prior work presented by Visagie (2007) and Botha (2010). A new portable reduced lead ECG and electronic stethoscope device will be designed and developed with the aim to deploy the device in rural hospitals and clinics that lack the equipment required to diagnose CVD. The device is designed to be operated by personnel without specialist knowledge in cardiology, such as nurses or laymen, to autonomously identify patients with potential cardiovascular disease and refer these patients to hospitals for further evaluations. The initial ECG and auscultation recordings can be wirelessly sent to specialists for analysis. The past devices (auscultation jacket and PCG) were bulky, consisting of a network of cables tethered to computers and power sources and would be restricted to clinical environments. The current hand-held device is battery powered, compact and completely portable, with the potential to be used in clinics or in the field as a point of care and first stage screening tool. The new device was also intended to improve on the pitfalls of the previous designs, capable of quality ECG and electronic stethoscope recordings of both men and woman with all body types.

The use of ECG records during patient classification was not investigated by the previous authors, with its application limited to the beat segmentation process. The current study places more emphasis on the diagnostic capabilities of the ECG data during classification, with the addition of the electronic stethoscope to provide specialists, who may have been absent during the application of the device, with playback and visualisation options. In comparison to prior studies done in the field relating to ECG classification, the current study will leverage the power of deep artificial neural networks as opposed to standard artificial neural networks (ANNs) or other popular classification methods. A deep pattern recognition neural network (DPRNN) will be trained to classify individual beats in a retrospective study and expanded on further to perform patient classification on records acquired using the prototype device in a clinical study.

Prior studies utilised a single type of feature, or a limited feature set, to be fed as the required input into a selected classification model. The current study intends to extract a combination popular first order and second order features from multiple ECG leads, while exploring the possibility of feature generation in an unsupervised manner using stacked denoising autoencoders. The current study also investigates the potential of ECG lead reconstruction using a reduced lead set. Lead reconstruction enables the generation of an interpolated full 12 lead ECG recording when only a reduced lead set is available. Prior lead reconstruction studies made use of various methods to generate matrix transforms which could be applied algebraically to available leads in order to

reconstruct any missing leads. The current study intends to investigate the possibility of training a deep focused-time delay neural network (FTDNN) to learn complex functional relationships between a reduced set of input leads and the absent leads. The trained FTDNN will be fed the reduced lead set as an input and calculate the absent lead as the network output resulting in a full 12 lead ECG.

Chapter 3

Device Design

Chapter three elaborates on the design and development of the portable ECG and electronic stethoscope device (Figure 3.1). The chapter is divided into two sections relating to hardware and software design, in which the individual aspects are discussed in detail.

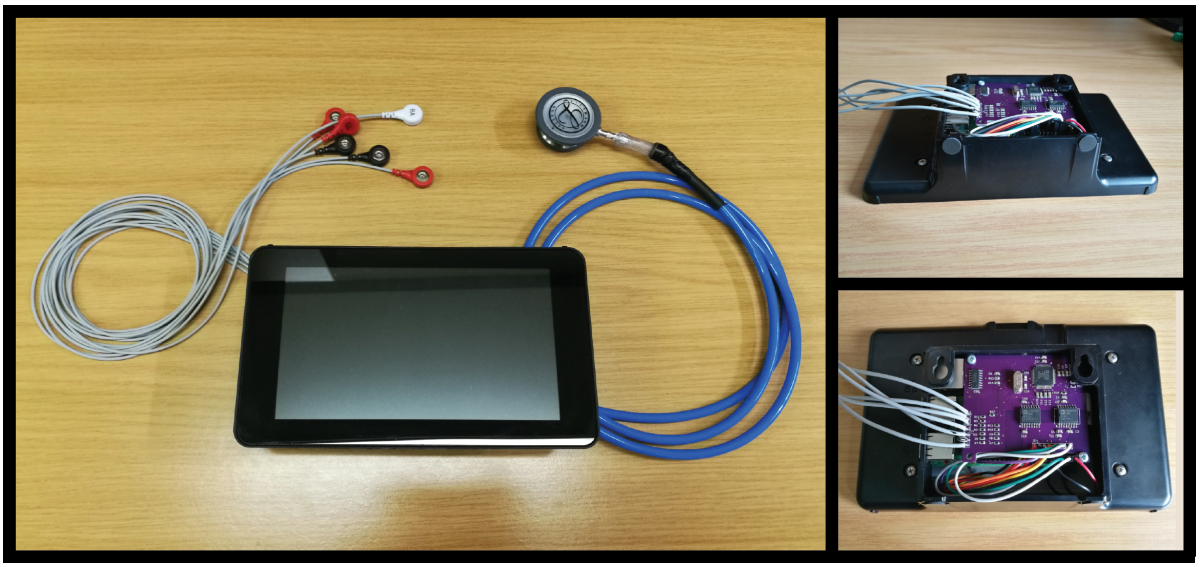

Figure 3.1: Portable ECG and electronic stethoscope device seen from different angles. The electronic stethoscope is detachable and the back of the case is removed to expose the printed circuit board.

3.1 Hardware

The various components utilised within the device are represented in Figure 3.2 and are discussed in greater detail in the subsequent sections.

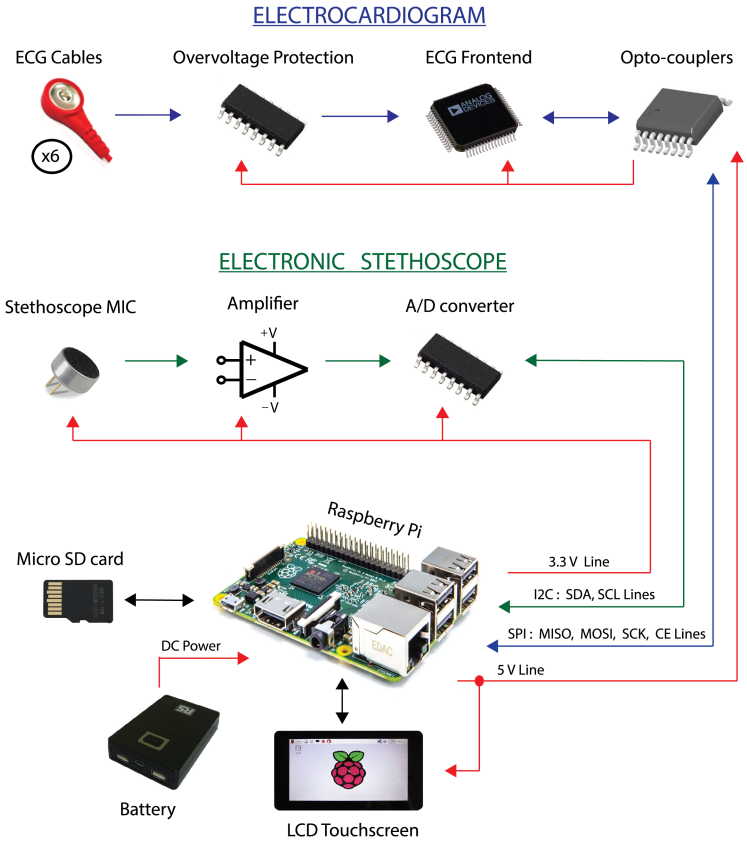

Figure 3.2: Flowchart indicating the interaction between the various hardware and signals required to operate the device.

3.1.1 Raspberry Pi

The present study made use of the Raspberry Pi (RPi) 3 model B (Figure 3.3), which is a powerful, low-cost, single board computer. The RPi is compact in size, housing all its components within a surface area slightly larger than a credit card. The device boots from a Micro SD memory card, which contains the operating system as well as provides file storage capabilities. The RPi is affordable, compact and has low power requirements which makes it an ideal candidate for portable devices. There are an abundance of available "general purpose input output" (GPIO) pins on the RPi, which are required to connect to peripheral devices and sensors. The GPIO pins interface the RPi with the ECG front end, LCD touchscreen and the electronic stethoscope's analog-to-digital converter (ADC). The RPi provides a variety of serial communication protocols, in which Serial Peripheral Interface (SPI) and Inter-Integrated Circuit (I2C) is required to interface with the ECG front-end and electronic stethoscope, respectively. The RPi has a dedicated display serial interface (DSI) port which enables communication with the LCD touchscreen. The powerful quad-core processor ensures that signals may be sampled at a

sufficient clock speed and displayed in real time with relative ease. Furthermore, the Wi-Fi and Bluetooth 4.1 wireless capabilities enables the potential application of the device in telemedicine and cloud-based computing. Finally, the RPi is responsible for compiling the software required to interface with the ECG front-end and electronic stethoscope, displaying the data graphically on the LCD touchscreen as well as storing the records locally on the memory card.

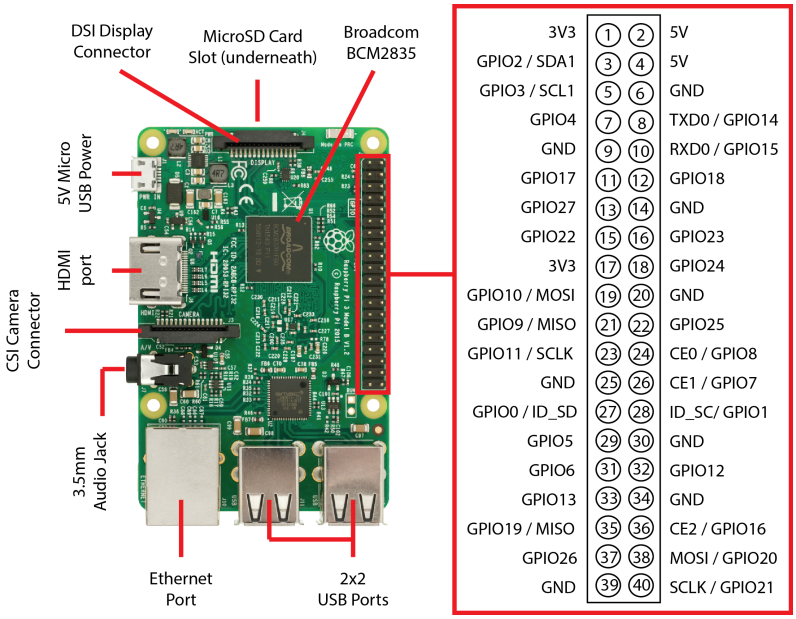

Figure 3.3: Labelled schematic of the Raspberry Pi 3 model B.

3.1.2 LCD Touchscreen

The touchscreen creates a tablet interface, emphasising the portability aspect of the project. The 7-inch touchscreen display has a total dimension of 194 x 110 x 20 mm and a screen resolution of 800 x 480 pixels. The size is ideal for viewing the many available ECG leads while still maintaining a compact design. Only two of the RPi header pins, a 3.3 V voltage supply and ground (GND), are required by the touchscreen (Figure 3.4a). This is advantageous as it frees up more available pins to connect to additional sensors. The use of a touchscreen eliminates the need for additional peripherals such as an external monitor, keyboard and mouse, thereby greatly simplifying the design. The touchscreen case (Figure 3.4b) also protects the RPi and adapter board as well as houses the additional ECG and electronic stethoscope circuitry.

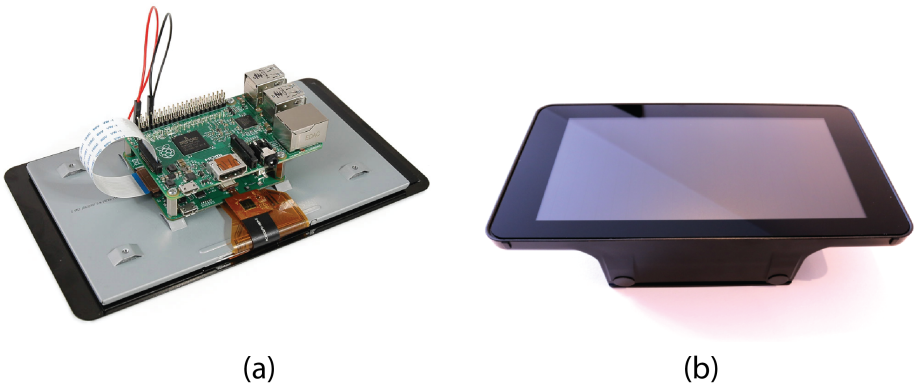

Figure 3.4: LCD touchscreen: (a) Positioned with screen facing downwards, without the protective case. The touchscreen adapter board and the mounted RPi are visible (b) Positioned with the screen facing upwards, resting on the base of the protective case that covers the RPi and adapter board.

3.1.3 Power Consumption

During the design of ECG and electronic stethoscope device, the selection of low-power components was prioritised in a bid to reduce the load placed on the battery and maximising the available hours of use. The voltage and current requirements of the device are broken up into the major components and represented in Table 3.1.

Table 3.1: Portable ECG and electronic stethoscope voltage and current requirements.

Component	Voltage	Current
Raspberry Pi	5 V	500 mA
LCD Touchscreen	3.3 V	455 mA
ECG	5 V	16 mA
Electronic Stethoscope	3.3 V	0.17 mA

During standard testing conditions, the device is operated solely using the touch screen without any USB peripherals. The average total current consumption of the device is calculated as:

$$\begin{aligned} I_{total} &= I_{RPi} + I_{LCD} + I_{ECG} + I_{Steth} \\ &= 500\ mA + 455\ mA + 16\ mA + 0.17\ mA \\ &= 971.17\ mA \end{aligned} \tag{3.1}$$

This project made use of an external 10500 mAh battery pack to power the device. The battery pack provided approximately 11 hours of continuous use.

3.1.4 Electrocardiogram

This section elaborates on the various components used in constructing the ECG section of the device. The printed circuit board (PCB) and major components, illustrated in Figure 3.5, will be discussed in greater detail in the following sections. The corresponding PCB design schematics are illustrated in Appendix A.

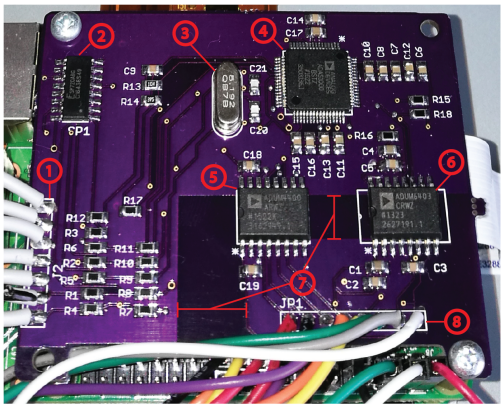

1	ECG LEAD WIRES
2	SP720
3	CRYSTAL OSCILLATOR
4	ADAS1000
5	ADUM4400
6	ADUM6403
7	INSULATION REGION
8	JUMPER WIRES TO RPI

Figure 3.5: ECG printed circuit board with the corresponding circuit components, mounted ontop of the RPi.

3.1.4.1 Electrocardiogram Lead Wires

The ECG device consists of a six lead wire system, of which four leads are limb leads (RA, LA, RL and LL) and the remaining two are precordial leads (V2 and V4). The lead wires have snap connectors that attach to disposable electrodes (Figure 3.6) which are stuck to the body at their respective positions. Most disposable adhesive electrodes make use of highly conductive metals such as silver, or a silver chloride compound, that connects to the ECG lead wires. The electrodes contain a saline-based conductive gel which is in contact with the body and reduces the skin's high resistive properties, resulting in improved signal quality.

Figure 3.6: ECG lead wires and adhesive electrode.

3.1.4.2 Defibrillator, Overvoltage and ESD Protection

ECG devices and other medical equipment that attach to patients in hospitals, or emergency settings, may require protection against defibrillation. In circumstances when defibrillation protection is not required, safety measures to negate over-voltage, or electrostatic discharge (ESD), is recommended. The ADAS1000 ECG front-end does not provide any on-board defribillation protection and therefore requires additional components and circuitry. The recommendations made by the ADAS1000 datasheet (Analog Devices, 2014) with regards to providing the necessary defibrillation, over-voltage and ESD protection are adhered to. The SP720 (Figure 3.7) is a diode array which is applied in parallel with the ECG channels and provides protection to sensitive circuitry connected to the ECG electrodes by clamping any input voltages that exceed the reference value (5 V). The resistors connected to the right leg drive (RLD) circuit ensure a safe termination voltage for an open ECG electrode. In the event that defibrillation is required, the SP720 is able to protect the device against voltage spikes of up to 8 kV when two input pins are connected in parallel to each ECG lead (Littelfuse, 2017). This provides sufficient protection against standard defibrillation voltages between 300 to 1000 V.

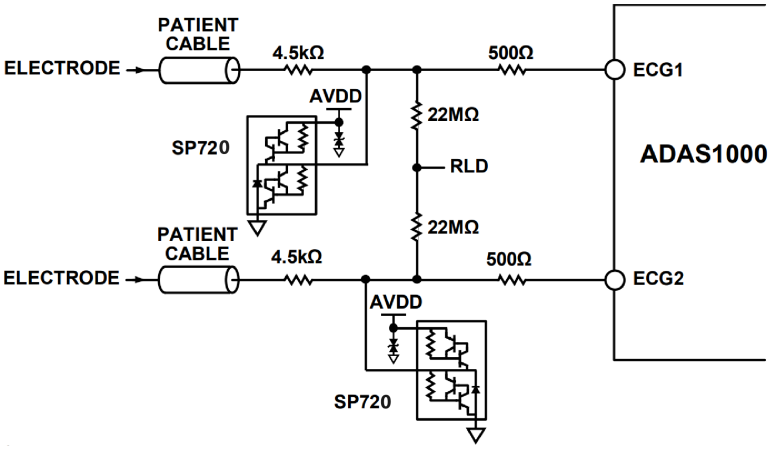

Figure 3.7: Recommended defibrillation protection on ECG channels using diode protection (Analog Devices, 2014).

3.1.4.3 ADAS1000 Analog Front-end

The selected ECG front-end for this study is the ADAS1000 (Analog Devices), capable of recording 5 lead ECG signals with an additional RLD lead. The ADAS1000 is a compact, low power device, designed to produce high-quality readings in portable applications. This significantly simplifies the procedure of recording ECG biosignals as the ADAS1000 outputs the recorded data to the RPi for post-processing via the SPI serial communication protocol. The

ADAS1000 provides inputs for up to six lead wires which include limb leads (RA, LA, LL) a reference right leg drive (RLD) as well as two precordial leads of the user's choice. The two precordial leads used in this project are leads V2 and V4. The simplified flowchart focusing on the ECG functionality of the ADAS1000 is illustrated in Figure 3.8.

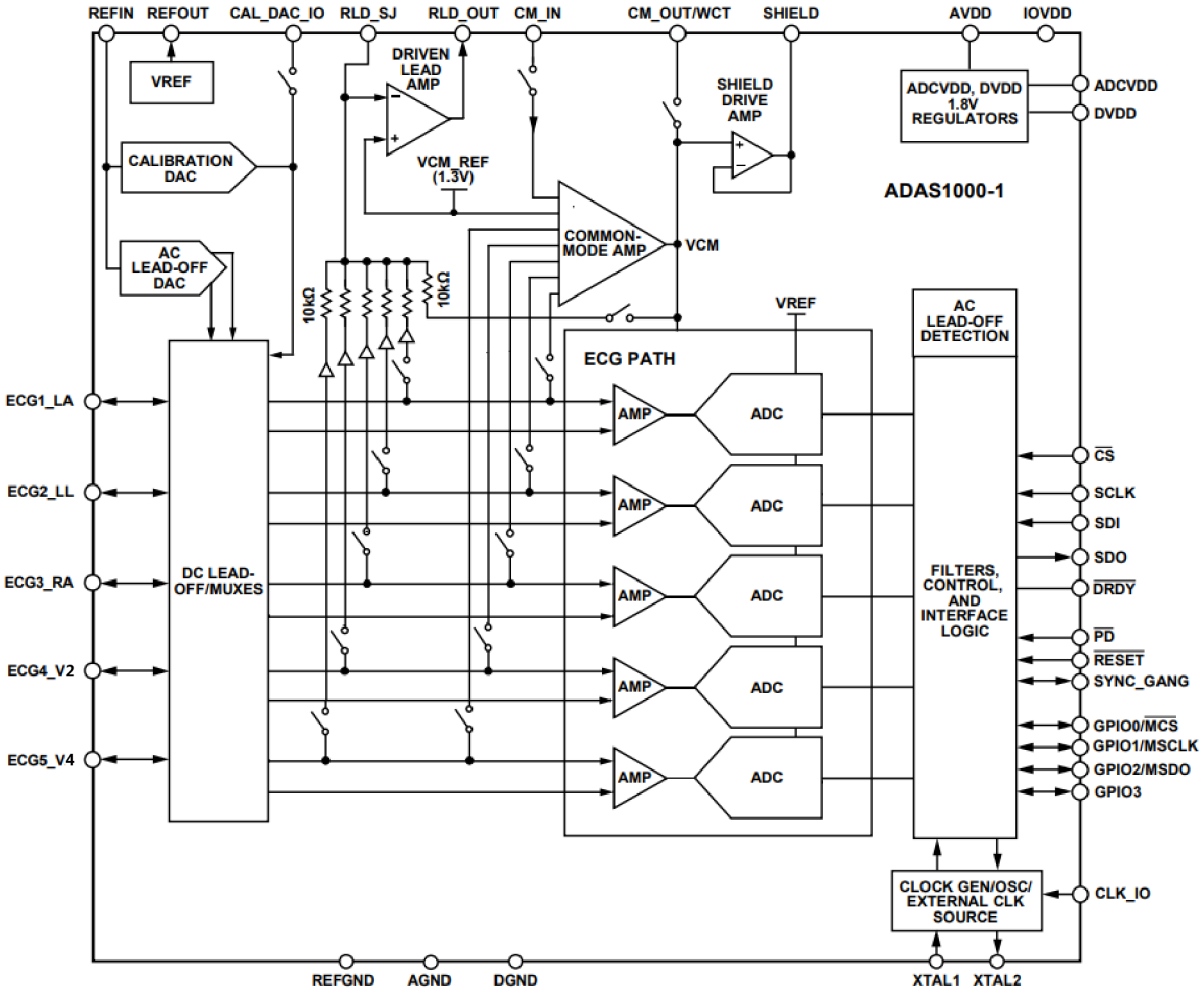

Figure 3.8: ADAS1000 flowchart (Analog Devices, 2014).

The ADAS1000 receives the recorded signals from the ECG lead wires. The output of the RLD circuit is attached to the right leg (RL) lead wire to provide common-mode rejection and improved signal quality. Internal switching provides the user with options in selecting various leads to contribute to the calculation of the RLD circuit as well as to the common mode voltage (VCM). Each of the input ECG channels contains a differential amplifier with a programmable gain, an anti-aliasing filter, additional buffers as well as an ADC. Once the leads are calculated and filtered in the digital domain they are sent to

the RPi using SPI communication which makes use of the chip select (CS), the clock signal (SCLK), data ready (DRDY), "SDI", "SDO", and "RESET" lines.

In a standard 5 lead ECG configuration, the ADAS1000 supplies data for Lead I, II, III and V2 and V4 via SPI serial communication to the RPi. The remaining augmented limb leads (aVR, aVL and avF) are calculated from leads I, II and III. This is done locally in a post-processing step on the RPi using Equations 2.4 - 2.6. The digital lead mode was selected in which leads LA, LL and RA (represented by the closed internal switches in Figure 3.9) contribute to the VCM, thus creating the Wilson central terminal (WCT) required to digitally calculate lead V2 and V4.

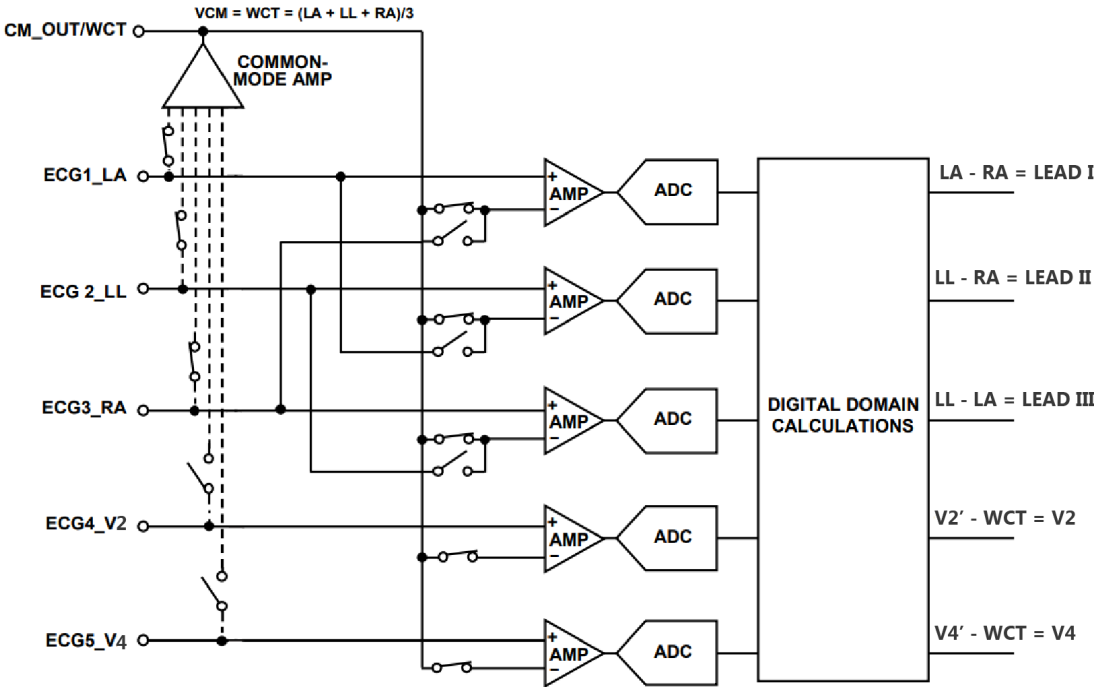

Figure 3.9: Electrode and lead configuration for digital lead mode (Analog Devices, 2014).

The sampling speed of the ADAS1000 in low power mode is 1.024 MHz which can be provided by the internal clock or in this case an external crystal oscillator. The frame rate can be adjusted by tapping off data at a reduced rate, set by the user, which was selected as 2 kHz. This is the slowest available rate on the ADAS1000 and is more than sufficient, with 250 Hz believed to be the minimum acceptable ECG sampling frequency (Abboud and Barnea, 1995). A DC-coupled approach is used by the ADAS1000 in which the RLD ensures that each ECG channel is biased to operate within the front end's dynamic range. This is achieved by driving the electrical average of the electrodes to

1.3 V, maximising each signal's range when using the ADC. The RLD circuit (Figure 3.10) also contributes to improving signal quality by providing common mode rejection and eliminating interference and noise from external mains powered sources in the vicinity of the device. The RLD circuit also provides additional patient safety features in defibrillation and over-voltage protection circuits. The design of the RLD circuit, as well as the external resistor and capacitor and values, are recommended by the ADAS1000 datasheet.

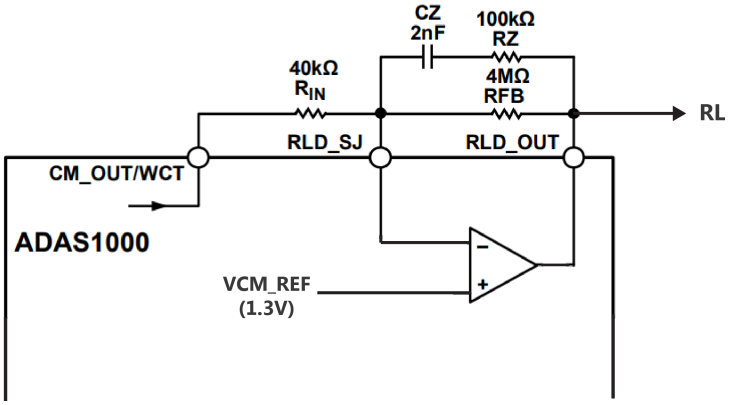

Figure 3.10: External components used in the right leg drive circuit (Analog Devices, 2014).

3.1.4.4 Electrical Isolation and Insulation Layer

The current device is designed to be battery operated, however, there may be occasions where the RPi is to be connected to additional peripherals, such as monitors or printers, which require a mains power supply. Opto-couplers isolate sections of the PCB that are exposed to a high-voltage power supply while simultaneously allowing the transfer of signals to, and from, the isolated region. This allows for electrical separation, or isolation, between the leads attached to patients and high voltage peripherals that may be attached to the RPi. The ADUM4400 and ADUM6403 were used in the optocoupler circuit (Appendix B.1.1 Figure B.1). In addition to the optocoupler circuit, the PCB was manufactured with an insulated region, without copper, which runs under the optocouplers to the boundaries of the PCB. This separates the isolated region from the remainder of the PCB (Appendix B.1.1 Figure B.2) and prevents the flow of potential creepage currents. An in-depth discussion relating to the applied safety measures and overall adherence to ECG safety standards, is presented in Appendix B.

3.1.5 Electronic Stethoscope

This section will elaborate on the various components used in constructing the electronic stethoscope (Figure 3.11). The electronic stethoscope is created using a condenser microphone placed in close proximity to a standard stethoscope chest-piece. The microphone converts the sound waves in the stethoscope chest-piece to electrical signals. The electrical signals are amplified and transmitted to the RPi via the ADS1015 ADC.

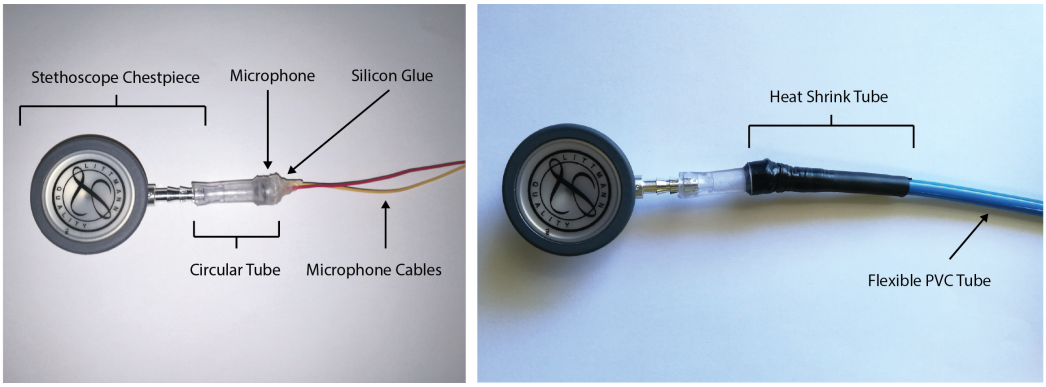

Figure 3.11: Electronic stethoscope prototype: (a) Exposed wire and microphone. (b) Flexible PVC tube protecting the microphone and wires.

3.1.5.1 Electret Condensor Microphone

The electronic stethoscope made use of a Panasonic WM-61A (Figure 3.12) omnidirectional electret condenser microphone which is placed in a plastic tube connected to a standard Littmann chestpiece. The microphone has a signal-to-noise ratio (SNR) of 62 dB and a flat frequency response over the range of 20-20000 Hz.

Figure 3.12: Panasonic WM-61A electret condensor microphone.

3.1.5.2 Microphone Amplifier and Analog to Digital Converter

The signal from the WM-61A is transmitted to an amplifier circuit which amplifies the signal with a bias voltage in the middle between the 3.3 V supply voltage (VCC) and ground. The gain of the signal is limited by the rails of the operational amplifier. Signals close to the supply voltage and ground result in the operational amplifier being driven into saturation, thereby clipping the recorded signal. The MCP6002 single supply, rail to rail operational amplifier allows signals to reach the rail values without clipping, thus increasing the total available voltage swing and possible signal amplification. The amplifier circuit, as well as the component values, are seen in Figure 3.13 with the calculation of the component values explained in Appendix C.

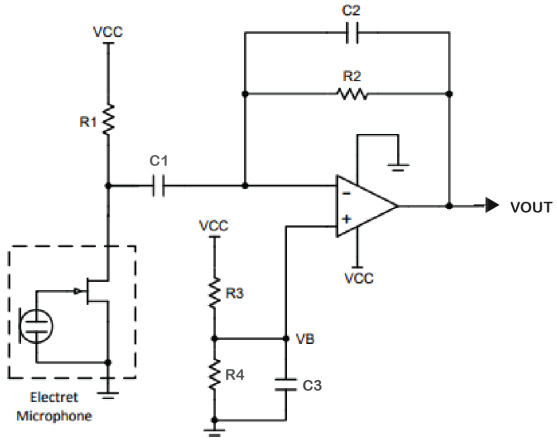

Components	Value
R1	15 kΩ
R2	56 kΩ
R3	100 kΩ
R4	100 kΩ
C1	2.2 μF
C2	15 pF
C3	2.2 μF

Figure 3.13: The microphone and amplifier circuit with corresponding component values.

The signal from the amplifier is sent to the ADS1015 (Figure 3.14) which is a low-power, 12-bit ADC and I2C module. The ADS1015 is interfaced with the RPi using the clock signal (SCL) and the address signal (SDA) required by the I2C protocol. The ADS1015 also requires a 3.3 V power and ground lines, shared by the MCP6002 operational amplifier and WM-61A, that is provided by the RPi.

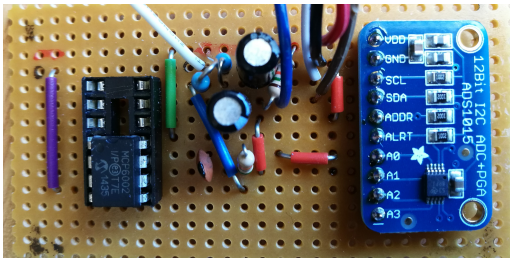

Figure 3.14: Amplifier circuit connected to the ADS1015.

3.2 Software

This section discusses the software development of the portable device. The Graphical User Interface (GUI) was developed using the open-source software Qt, which is a cross-platform application framework, built using the C++ programming language. The software is installed and compiled locally on the memory card of the RPi. The Qt GUI facilitates the input from the user via the touchscreen, the interfacing of the ECG and electronic stethoscope using serial communication as well as the display and storage of recorded data.

3.2.1 Hand-held Prototype GUI

Upon starting the GUI, the user is greeted by the "Getting Started" screen (Figure 3.15), which provides information pertaining to the operation of the device as well as illustrations depicting the ECG lead and auscultation positions.

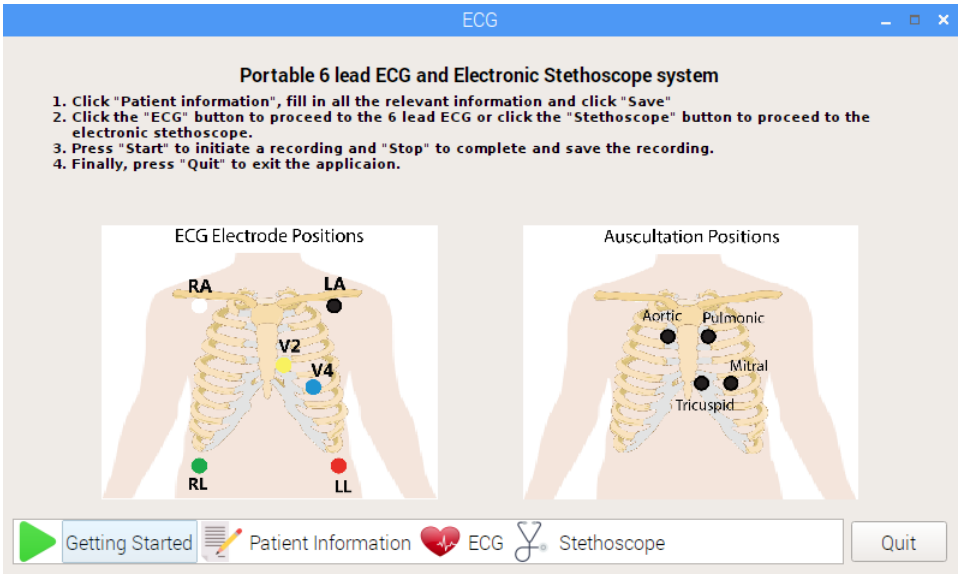

Figure 3.15: Graphical user interface start screen.

In the event that the "Patient Information" button at the bottom of the screen is selected, a tab window will appear (Figure 3.16). The user is able to use the touchscreen to select the appropriate text input and complete the information using a touchscreen keyboard. Once the user has filled in the required information and has clicked "Save" the device will save the patient information to a text file locally on the memory card of the RPi.

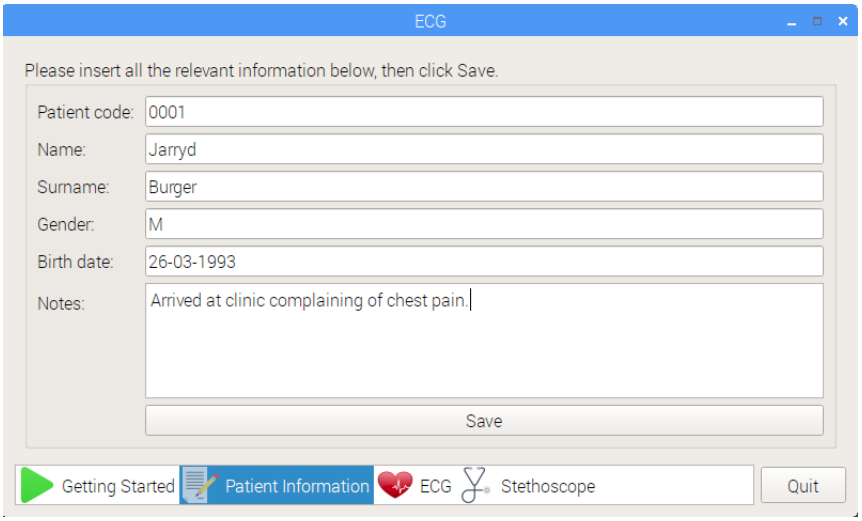

Figure 3.16: Graphical user interface patient information tab.

The user is able to press the "ECG" button at the bottom of the screen, which will load the "ECG" tab window (Figure 3.17). Initially when the tab window opens the graphs displaying the ECG lead data will be empty. Once the leads are placed on the patient and the "Start" button is pressed, the ECG data will begin to record and display on the various graphs. When the "Stop" button is pressed the device will stop recording and the data will save to an additional text file. The same procedure is followed to record, display and save data using the electronic stethoscope (Figure 3.18).

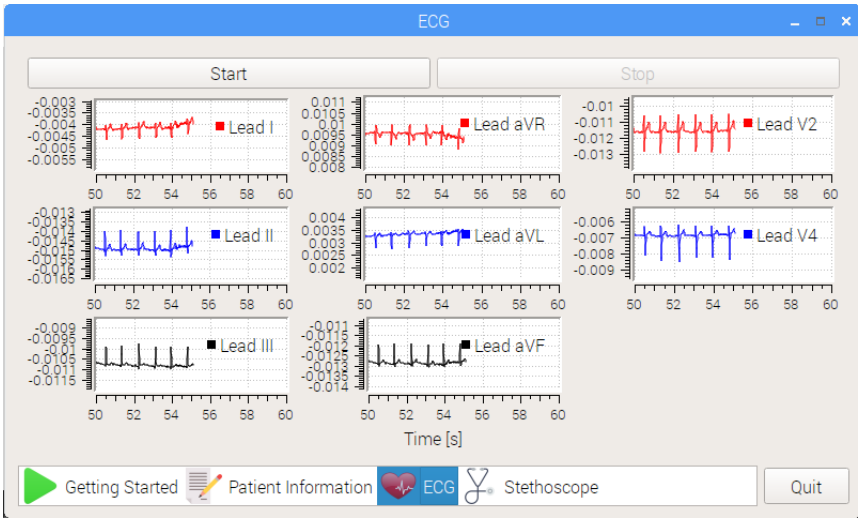

Figure 3.17: Streaming ECG data for the various leads to the graphical user interface.

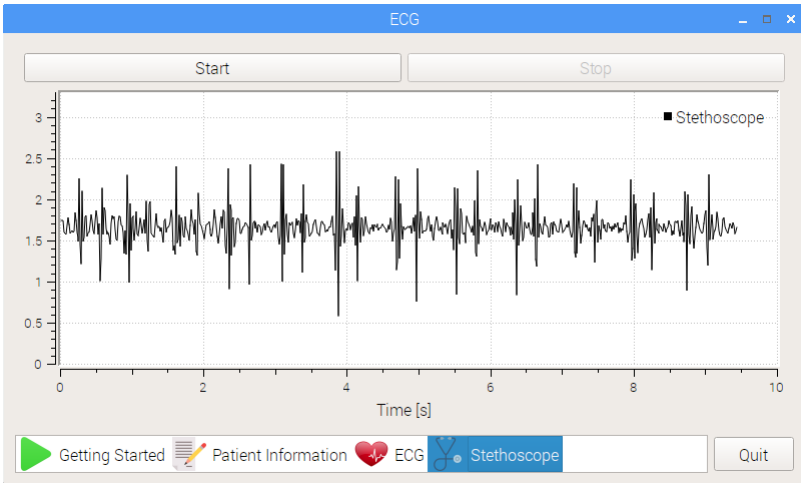

Figure 3.18: Streaming electronic stethoscope data to the graphical user interface.

3.2.2 Interfacing the ADAS1000

The RPi communicates with the ADAS1000 using the SPI interface bus by virtue of the BCM2835 C-code library which simplifies the SPI communication protocol with the help of built-in functions. This is required to configure the necessary register settings as well as read the recorded ECG data outputted, as frames, by the ADAS1000. The SPI protocol bus is explained in detail in Appendix D.1.

In order to start receiving the frames from the ADAS1000, a sequence of write commands has to be sent to initiate the device, set the register values and trigger the streaming of ECG readings. Any write command will consist of 32 bits, in which the first bit is set to 1 to write or 0 to read, the following 7 bits indicates the address of the register in which you wish to communicate with and the remaining 24 bits are the data bits. When writing to a register, the data bits are used to configure the register to the relevant settings and are unused in the event of reading values from a register. Once the registers are initialised, the "FRAMES" register is written to, triggering the ADAS1000 to repeatedly send frames containing ECG data to the Raspberry Pi.

Once the configuration of the ADAS1000 is complete, the RPi reads frames by transmitting a read command to the header register. The RPi receives the frames in a 32-bit format where the register value consists of the first byte, with the remaining bytes consisting of data (Table D.1 in Appendix D.1.2). This allows the user to distinguish between data from the various ECG leads during sampling. Data is read continuously until an additional read or write command is issued. The data ready (DRDY) pin indicates when a frame of data is available to be read. When the pin is low the line is ready and data

commands may be sent. The different addresses as well as the process flowchart required to send and receive data, to and from the ADAS1000, are listed in Table D.2 (Appendix D.1.2) and depicted in and Figure 3.19.

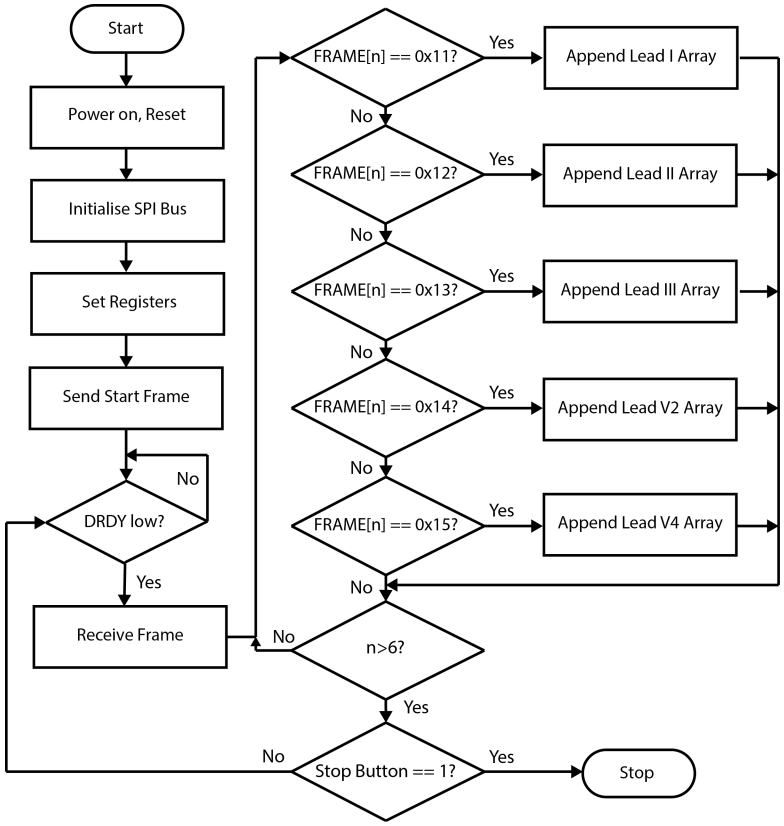

Figure 3.19: Flowchart indicating the process required to interface the RPi and the ADAS1000, using the SPI protocol.

Sampled data is transferred from the ADAS1000 to the RPi with the most significant bit (MSB) first. Therefore, the recorded data is bit-shifted before conversion to the actual voltage (V_{ECG}) occurs, using the equation

$$V_{ECG} = \frac{4 \times V_{Reff} \times V_{Raw}}{V_{Gain} \times (2^{R_{ADC}} - 1)} \tag{3.2}$$

where the raw voltage (V_{Raw}) is the value sent from the ADAS1000, V_{Reff} is the reference voltage range (1.3 V) of the ADAS1000, V_{Gain} is the programmable amplifier gain (set to 1.3) and R_{ADC} is the resolution (24 bit) of the ADC.

3.2.3 Interfacing the ADS1015

The RPi interfaces with the ADS1015 using the I2C serial bus and the BCM2835 library. The function of the I2C bus is explained in greater detail in Ap-

pendix D.2. The settings of the ADS1015 are initialised by writing to the "CONFIG" register. The device was programmed to sample at 3600 samples per second (SPS) with a programmable voltage range of 4.096 V. The values required to programme the ADS1015 as well as the process flowchart used to initialise and communicate with the ADS1015 is displayed in Table D.3 (Appendix D.2.2) and Figure 3.20.

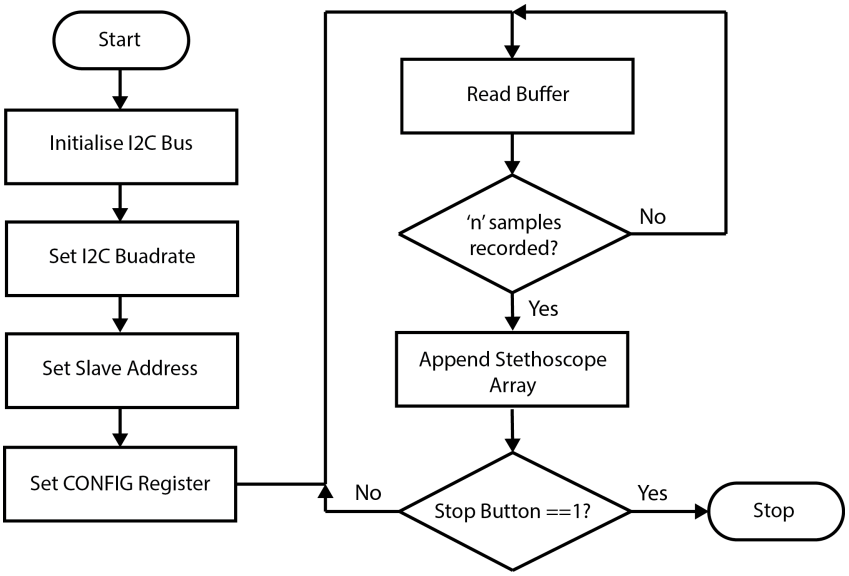

Figure 3.20: Flowchart indicating the process required to interface the RPi and the ADS1015, using the I2C serial protocol.

Sampled data is transferred from the ADS1015 to the RPi with the MSB first. Therefore, the recorded data is bit-shifted before conversion to the actual voltage (V_{Steth}) occurs, using Equation 3.3:

$$V_{Steth} = V_{Raw} \times \frac{V_{Range}}{2^{(R_{ADC}-1)}} \tag{3.3}$$

where the raw voltage (V_{Raw}) is the value sent from the ADC, V_{Range} is the selected programmable voltage range (4.096 V) of the ADS1015 and R_{ADC} is the resolution (12 bit) which is subtracted by 1 due to the signed bit.

3.2.4 Multi-threading

Multi-core processing allows applications to stack their processing requirement across the central processing unit (CPU). Applications are able to multi-task by running several different processes simultaneously. Occasions arise in which parallelism is required within the process itself. This parallelism is achieved by using threading. With the use of multiple cores, an application can assign a different thread to each core, allowing the application to operate in

a concurrent manner. With the use of a Qt application, the GUI is run on the main thread (GUI thread) and a worker thread can be assigned to additional tasks. A single worker thread is initialised during the sampling of either the ECG (Figure 3.21) or the electronic stethoscope. Compelling reasons to use threading includes increased processing speed by using multiple cores, as well the ability to maintain a responsive GUI thread by assigning long lasting processing tasks to worker threads.

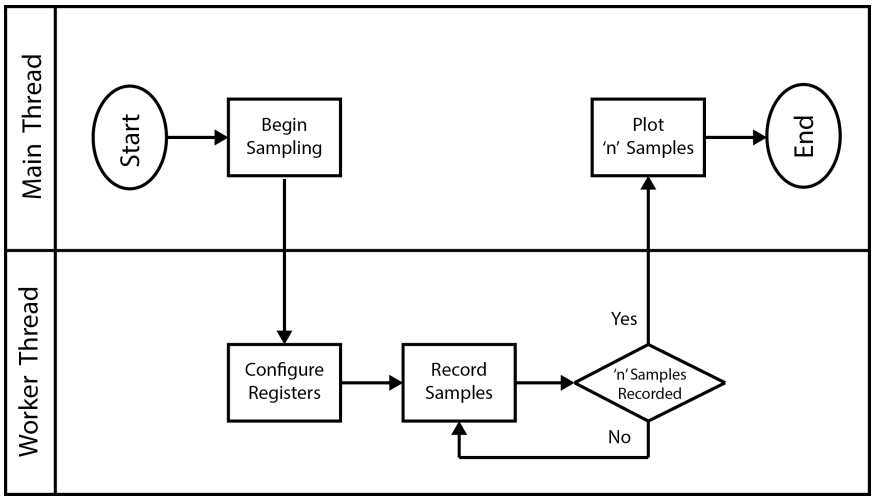

Figure 3.21: Flowchart indicating the communication between the main thread (GUI thread) and the worker thread used in sampling ECG and electronic stethoscope data.

3.2.5 Saving Data

During a recording process using the portable device, three text (".txt") files are saved. The first file contains the patient information, the second contains the ECG data and the third file contains the electronic stethoscope data. The text file contains data for leads I-III, V2 and V4. The augmented leads (avR, avL and avF) are derived in a post-processing step using leads I-III and Equations 2.4 - 2.6.

Chapter 4

Methodology

4.1 Retrospective Study

This section covers the database study in which online ECG records were used to prepare and train the lead reconstruction and classification neural networks, which are subsequently tested using data obtained from a clinical trial.

This study made use of Physiobank's Pysikalisch-Technische Bundensanstalt (PTB) diagnostic ECG database created by the National Metrology Institute of Germany for research and academic purposes. The ECG data was recorded from both healthy individuals and patients with cardiovascular disease at the Department of Cardiology of the University Clinic Benjamin Franklin in Berlin Germany. An ECG prototype recorder was used to take the recordings, with a summary of the specifications listed in Table 4.1.

Table 4.1: The specifications of the ECG prototype device.

PTB ECG Prototype	
Channels	16 channels (14 ECG, 1 respiration, 1 line voltage)
Input Voltage	$\pm$ 16 mv with $\pm$ 300 mv compensated offset voltage
Input Resistance	100 Ω
Resolution	16 bit, 0.5 μV/LSB with 2000 A/D units per mV
Bandwidth	0 - 1 kHz synchronous sampling
Noise	10 μV (pp) max, 3 μV RMS with input short circuit

The PTB database consists of 549 recordings from 290 individuals between the ages of 17 and 87 years, with a mean age of 57.2 years. Of the total 290 individuals recorded, 209 were male and 81 females with a mean age of 55.5 years and 61.6 years, respectively. Each recording consists of a standard 12 lead ECG as well as a Frank 3 lead vectorcardiogram (VCG). However, for this study only the standard 12 lead ECG recordings were analysed (Goldberger *et al.*, 2000). Of the 290 subjects available in the PTB database, 22 contained

unconfirmed ground truths and were subsequently excluded from the study. The resulting population is seen in Table 4.2.

Table 4.2: The diagnostic class of the subjects in the PTB database including the number of corresponding records.

Diagnostic Class	Subjects	Records
Myocardial Infarction	148	368
Cardiomyopathy	18	20
Bundle Branch Block	15	17
Dysrhythmia	14	16
Myocardial Hypertrophy	7	7
Valvular Heart Disease	6	6
Myocarditis	4	4
Miscellaneous	4	4
Healthy Controls	54	80
Total	268	522

4.2 Clinical Study

This section involves gathering additional data acquired during a clinical trial in order to test the trained lead reconstruction and classification methods.

4.2.1 Sample Size Calculation

The sample size calculation is performed in order to determine whether the population size is statistically significant when classifying patients as either healthy or unhealthy. This is achieved by determining the population size required to produce a statistical power goal of 0.9 or greater. After consultation with Prof. Nel at the Stellenbosch University Centre for Statistical Consultation, the subject population size was determined using the McNemar's, two proportion, paired sample, sample size calculation. The null hypothesis and the alternate hypothesis of the form,

$$H_0 : \delta = 0$$
$$H_1 : \delta \neq 0$$

where

$$\delta_S = \pi_1 - \pi_2$$

in which π_1 equates to the number of true positives in the first measurements identified using by the gold standard medical equipment and π_2 equates to the number of true positives recorded in second measurement, identified using

the prototype. The McNemar's test requires the prediction of both δ_S as well as the probability of discordance, denoted as η, which is often referred to as the "nuisance parameter". The McNemar's test was conducted for this study using the software package "Statistica 13", using the parameters and their corresponding selected values displayed in Table 4.3. The required sample size versus the desired power curve is represented in Figure E.1 (Appendix E.1). The required sample size with a corresponding power goal of 0.9 equates to 51 test subjects.

Table 4.3: McNemar's test parameters and their corresponding values.

McNemar's Test	
Parameters	Values
Delta (δ_S)	0.2000
Eta (η)	0.2500
Type 1 error rate alpha (α)	0.0500
Power Goal	0.9000
Actual Power for Required N	0.9022
Required Sample Size (N)	51

4.2.2 Precordial Lead Selection

Many possible combinations of the six different precordial leads are available when performing lead reconstruction. The selected precordial leads are combined with the limb leads to create the reduced lead set recorded by the prototype device in the clinical study. Studies that made use of only a single precordial lead made use of lead V2 as this resulted in the best performance (Feild *et al.*, 2002; Schreck and Fishberg, 2013). This was verified using data from the PTB database by alternating the precordial leads used in the reduced lead set, as the input to the FTDNN, and calculating the resulting RMSE and Pearson r values (Appendix G.1, Table G.1 and G.2). Classification performance supported the use of lead V2, producing the highest overall accuracy and sensitivity of all the precordial leads (Table G.3 and Figure G.1). An additional lead was included to improve the overall reconstruction performance by ensuring that all the areas of the heart are represented by the input leads (Table 2.1). Leads V3 and V4 produced the next best reconstruction results. Although V3 produced better reconstruction overall, in comparison to V4, it is the neighbouring lead of the already selected V2 lead, providing a similar performance for leads within its vicinity. Lead V4 produced better lead reconstruction results for leads V5 and V6 due to its proximity. With regards to practical ECG lead placement, a technician is required to first locate V4 before placing V3, therefore the selection of lead V3 would not take steps towards simplifying the already complex lead placement process. With regards to classification, V4 produced slightly lower overall performance in comparison

with the remaining precordial leads. However, lead V4 produced the highest specificity score, complementing the highest overall accuracy and sensitivity achieved by V2.

4.2.3 Experimental Setup

During the clinical trial, ECG data was recorded using both the portable device as well as the gold standard 12 lead ECG. The control device provided a means for comparison between the reconstructed leads and the actual recorded leads. The Norav PC-ECG, model 1200HR, was used as the control device during the clinical study (Figure 4.1a). The PC-ECG is connected to the patient using a 12 lead cable (Figure 4.1b) as well as to a laptop via a USB cable. The device is powered through the USB port of the laptop. The ECG data is sampled at 500 Hz and displayed and stored on the laptop (Figure 4.1c). The portable device (Figure 4.2a) was connected to the patient using the six lead wire system (Figure 4.2b). The device was operated using the touchscreen, allowing the user to record the patient information and display the graphs for the various ECG leads in real-time (Figure 4.2c). The recorded data was saved locally on the Micro SD memory card of the RPi as text files. The device was powered via the RPi micro-USB port using an external battery pack.

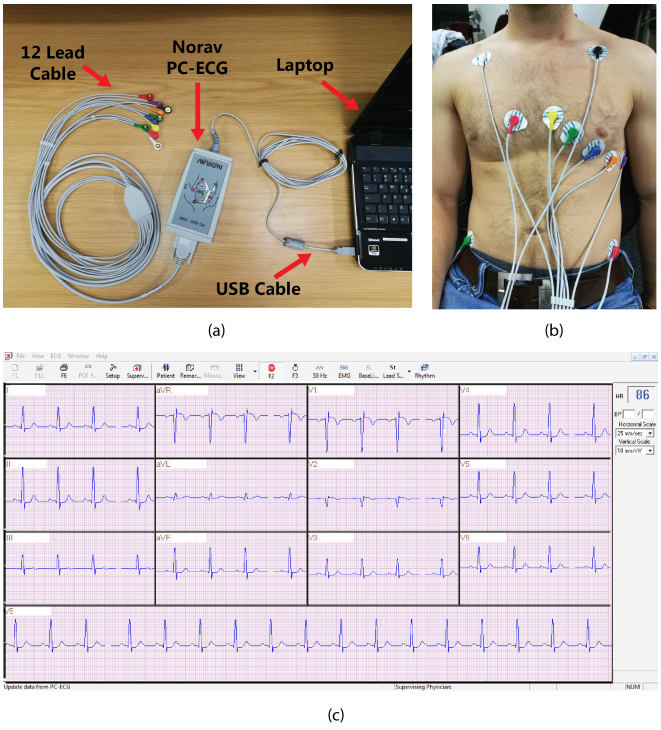

Figure 4.1: Gold standard 12 lead ECG control apparatus: (a) The Norav PC-ECG connected to a laptop computer via USB cable. (b) The 12 lead ECG placement on a test subject. (c) The laptop software displaying the 12 lead ECG recording.

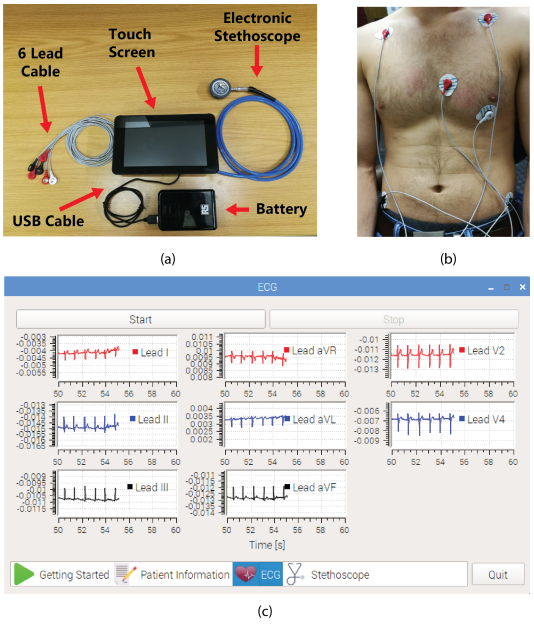

Figure 4.2: The developed prototype test apparatus: (a) The portable ECG and electronic stethoscope prototype. (b) The reduced 6 lead wire placement on a test subject lead ECG placement on a test subject. (c) The programmed GUI displaying the recorded ECG leads.

4.2.4 Protocol

The study population included patients, 18 years and older, presenting to Tygerberg Hospital's Coronary Care Unit, Cardiac Outpatients Department and F1 Medical Emergency Unit. These patients regularly undergo 12 lead ECG tests before, and after, a clinical assessment. Therefore, the study does not place additional strain on the workforce and patient flow within the hospital. During each test session, ECG signals were recorded by both the gold standard 12-Lead ECG device, used as the control, as well as the portable reduced lead prototype device. The subjects were asked to lay down on an assessment bed in a relaxed position until the recording procedure is complete. This helps to prevent low frequency muscle potentials and motion artefacts from degrading the quality of the recorded ECG signals. First the full 12 lead ECG is recorded by the control device. A trained medical technician or medical doctor placed the 10 disposable electrodes onto the subject in the relevant positions. The limb electrodes (LA, RA, RL and LL) are placed at the lower end of the arms and legs, close to bone to avoid muscle potentials. Alternatively, if access to the patient's limbs are limited, the LA, RA and LL, RL electrodes can be relocated to the shoulders and hips, respectively. The more complex precordial lead placements are summarised in Table 4.4. The portable handheld prototype device records the ECG in the same manner as the previously mentioned gold standard 12 lead ECG, with the exception being the number

of precordial leads that are required. The device only required precordial leads V2 and V4 as well as the remaining limb leads to be placed on the subject. Once the ECG was recorded the adhesive electrodes were removed from the subject.

Table 4.4: Detailed 12 lead ECG electrode placements.

Electrode	Location
V1	Fourth intercostal space to the right of the sternum
V2	Fourth intercostal space to the left of the sternum
V3	Midway between electrode position V2 and V4
V4	Fifth intercostal space on the midclavicular line
V5	Anterior axillary line at the same level as V4
V6	Midaxillary line at the same level as V4 and V5

The ECG recordings were collected and delivered to a cardiologist for interpretation. The cardiologist categorised the ECG recordings into three classes: normal ECG, abnormal ECG and variations not necessarily indicating pathology (VNIP). The normal and abnormal ECG records were included in testing the classification algorithm, whereas the lead reconstruction included all three classes. The VNIP subjects are excluded in the classification process as these subjects fall within a spectrum of normal to abnormal ECGs, with additional advanced tests required to confidently establish the subject's ground truths, which fall outside the scope of this clinical study. Each session with the test subjects had a duration of approximately 10 minutes. In order to test medical devices on human subjects, the study was required to adhere to the ethical codes and practices designated by Health Research Ethics Committee (HREC) in order to be granted ethical approval. The test procedure was explained to each subject in which written consent was acquired. The analysis of the data takes place after the recordings have been completed as part of a separate process. All stored data was anonymised to protect the identity of the subjects involved in the study. The ethics reference number for the study is 0579, with proof of ethical clearance presented in Appendix E.2.

4.3 Signal Processing

Once the ECG signals were acquired using the database retrospective study as well as the clinical trial, the signals underwent various processing stages before lead reconstruction and classification could take place (Figure 4.3). Initially, the available ECG records from both the PTB database and the clinical study are filtered. The filtered signals are input directly into the lead reconstruction model, however, further processing including beat detection and feature extraction is required to perform patient classification.

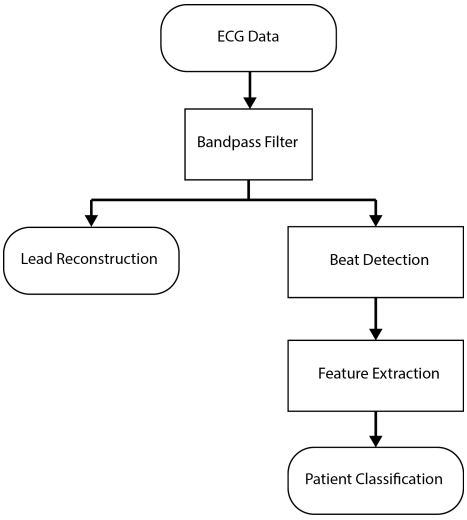

Figure 4.3: Flowchart indicating the data processing procedure from the time the data is collected until the results are collected.

4.3.1 Bandpass Filter

There are various sources of noise that are capable of corrupting ECG data. The most common sources include low frequency muscular activity, motion artefacts, baseline drift and 50 Hz electrical noise. In extreme cases, exposure to noise may result in data being deemed illegible and ultimately discarded. However, it is not always possible to record data in an environment without the presence of noise. Filters are used to remove noise from frequencies outside the ECG frequency bandwidth. Figure 4.4 indicates a fast Fourier transform (FFT) of an ECG signal corrupted by various sources of noise represented in the frequency domain.

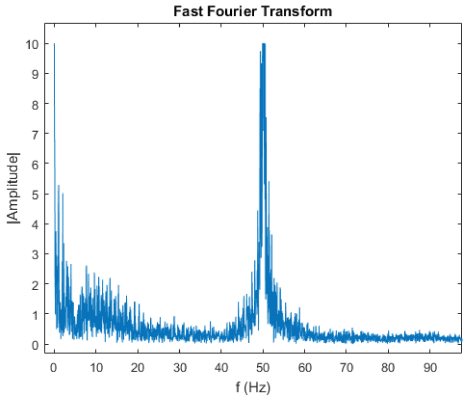

Figure 4.4: Fast Fourier transform of an ECG lead corrupted by 50 Hz noise and low frequency baseline drift, seen by spike at the zero frequency and 50 Hz frequency. This is attributed to baseline drift and electrical mains noise, respectively.

Examples of signals in the time domain, corrupted with baseline wander and 50 Hz mains noise, are compared with the equivalent bandpass filtered signals, in Figure 4.5. When filtering ECG signals, a linear phase filter is recommended in order to negate phase distortion that can affect temporal relationships in the cardiac cycle. This is achieved by the use of a finite impulse response (FIR) filter with coefficients symmetrical around the central coefficient. A linear phase bandpass FIR filter with a bandwidth of 0.05 - 50 Hz was designed, which corresponds to the cardiac monitoring ECG machines used at Tygerberg Hospital. A lower corner frequency of 0.05 Hz is desirable in order to avoid distortion of the ST region (Buendía-Fuentes *et al.*, 2012). The filtered data is directly utilised in the lead reconstruction model, whereas additional signal processing steps is required to identify individual beats and extract features required by the patient classification procedure.

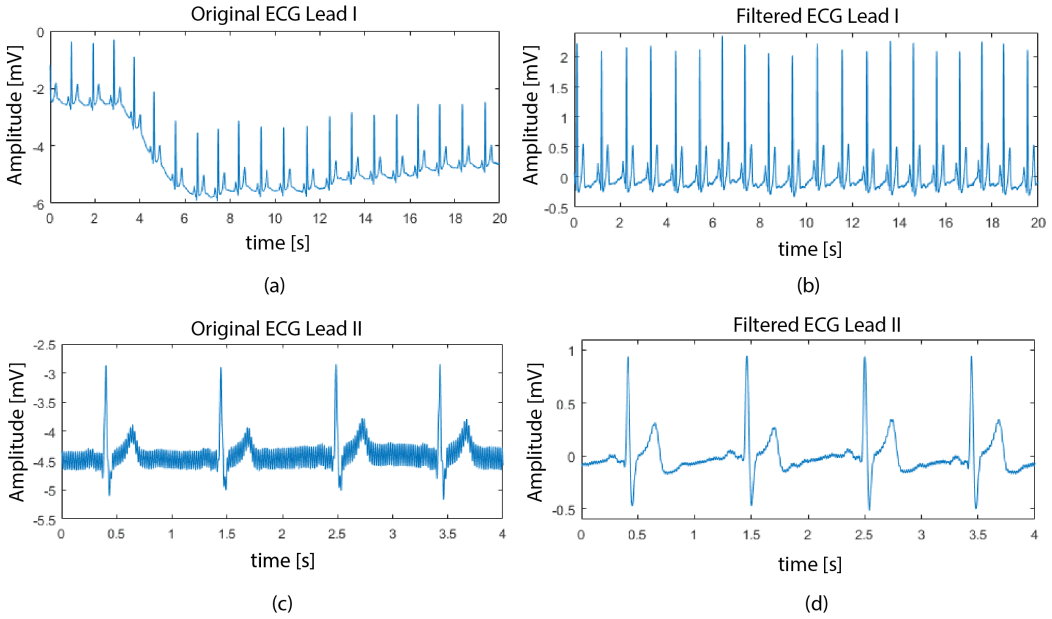

Figure 4.5: Comparison between two ECG recordings affected by different sources of noise, with the corresponding bandpass filtered equivalents: (a) ECG lead affected by baseline drift with the corresponding bandpass filtered ECG signal (b). (c) ECG lead affected by 50Hz mains noise with the corresponding bandpass filtered ECG signal (d).

4.3.2 Beat and Peak Detection

A Wavelet based beat and peak detection method proposed by Martínez *et al.* (2004), was used to identify successive beats within the ECG leads. These beats were isolated in order to extract and generate temporal and morphological features used in ECG classification.

Wavelet analysis converts a continuous time signal into a time-scale representation and is a popular method used in signal processing due to its multi resolution approach. A scale can be interpreted as the inverse of frequency where the signal's high frequency information is represented by the low scales and the low frequency information represented by the high scales. Different frequency ranges can be assigned to each individual scale, which allows the original signal to be analysed at a resolution that corresponds to a specific scale. A wavelet transform, $W_c\, s(b)$, is created by reducing the original signal $s(t)$ into a wavelet representation consisting of dilations, c, and translations, b, of the prototype wavelet, ψ. Therefore, the wavelet transform of a continuous time signal $s(t)$ is:

$$W_c\, s(b) = \frac{1}{\sqrt{c}} \int_{-\infty}^{+\infty} s(t)\, \psi\Big(\frac{t-b}{c}\Big)\, dt, \quad c > 0 \tag{4.1}$$

The wavelet prototype used in this paper is the quadratic spline developed by Mallat and Zhong (1992) and is a popular choice for ECG signals. The Fourier transform of the quadratic spline is defined as:

$$\Psi(\Omega) = j\Omega \left(\frac{\sin\left(\frac{\Omega}{4}\right)}{\frac{\Omega}{4}} \right)^4 \tag{4.2}$$

where j indicates an imaginary number and Ω is the Fourier transform of the sampling frequency ω. The method makes use of the discrete wavelet transform (DWT) in which the wavelets are discretely sampled resulting in a basis function:

$$\psi_{k,l} = 2^{-\frac{k}{2}}\, \psi(2^{-k}t - l); \quad k, l \in Z^+ \tag{4.3}$$

The DWT calculates the coefficients of the wavelet transform on a dyadic scale sequence, in which the coefficients are only calculated for scales of 2^n, where $c = 2^k$ and $b = 2^k l$. Mallat and Zhong (1992) proved that an efficient method to implement a DWT can be achieved by using an octave filter bank represented by a cascade of identical low-pass and high-pass FIR filters. When the signal passes through each stage of the filter bank it is separated into low-frequency approximations and high frequency details. Subsequently, the bandwidth is divided by a factor of two at every stage of the filter. This study implementation of Mallat's algorithm was used without decimation, seen in Figure 4.6. The filters H(z) and G(z) are the respective low-pass filter and high-pass filters, calculated as (Li *et al.*, 1995; Akay, 1996):

$$H(e^{j\omega}) = e^{j\omega/2} \Big(\cos\frac{\omega}{2} \Big)^3 \quad , \quad G(e^{j\omega}) = 4je^{j\omega/2} \Big(\sin\frac{\omega}{2} \Big) \tag{4.4}$$

and correspond to the selection of the quadratic spline wavelet prototype at the sampling rate ω.

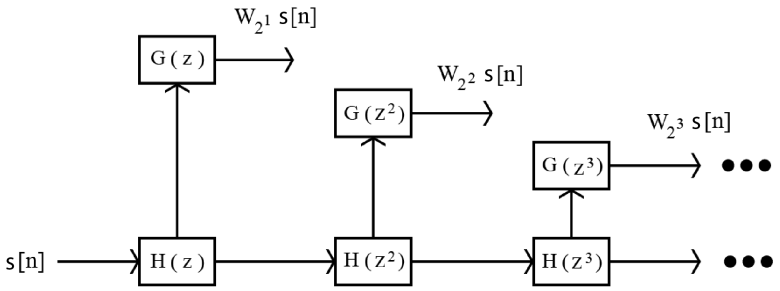

Figure 4.6: Cascade filter bank representation.

The output of five scales of the Wavelet transform is illustrated in Figure 4.7a. The selection of the quadratic spline wavelet prototype results in the zero crossing of the wavelet transforms corresponding to the local maxima or minima of the input signal at various scales (Figure 4.7b). Once the beats were detected using the wavelet QRS detection algorithm, the individual wave peaks as well as the onset and offset of the waves were determined using the same method. The algorithm is capable of identifying any possible normal or abnormal QRS structure that corresponds to two or three waves (QRS, RSR', QS, RS, QR and R complexes). With regards to normal and abnormal P and T waves, the algorithm is capable of identifying morphologies that include positive, negative and biphasic waveforms. This process is described in greater detail in Appendix F.1.

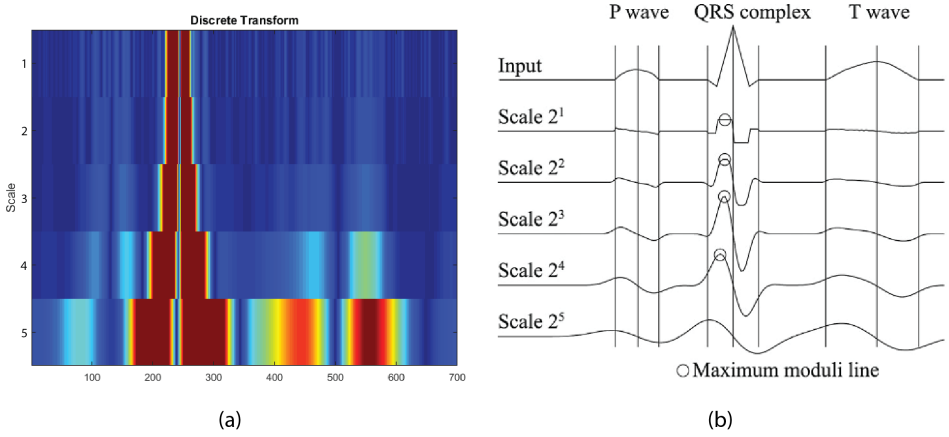

Figure 4.7: ECG wavelet transform (WT): (a) Colour-map of the WT over 5 scales. (b) Five scale WT indicating maximum moduli lines (Rincón *et al.*, 2011).

4.3.3 Feature Extraction

Diagnosing a patient's cardiovascular condition using ECG records requires analysing the waveforms plotted on the 12 lead printout. A normal heart beat

has a sinus rhythm, with consecutive wave peaks or troughs labelled PQRST (Figure 4.8). Natural variations of the PQRST waveform exist across the different ECG leads. Some peaks may be inverted or less prominent depending on which lead is being monitored. During a cardiac cycle the duration of the intervals indicate the heart's rhythmic qualities with the amplitudes of the peaks an indicator of the heart's pumping strength. Deviations in the normal pattern, timing and shape of the PQRST waveform, are identified by cardiologists when diagnosing cardiovascular disease.

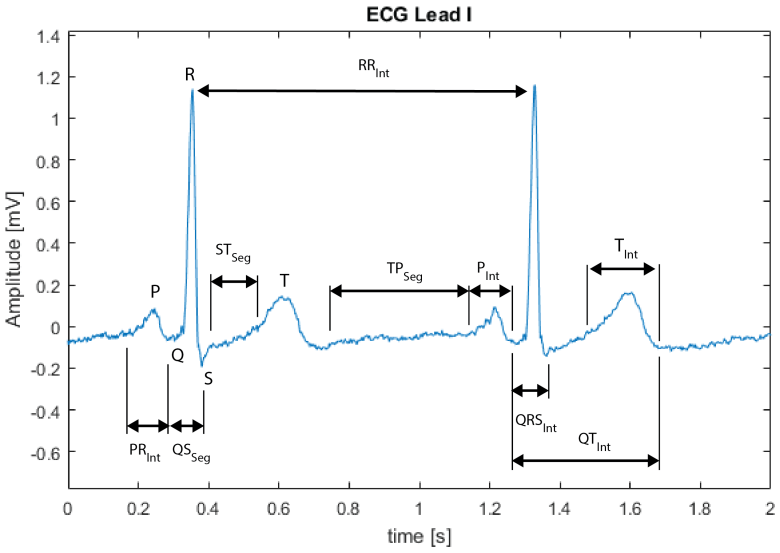

Figure 4.8: Intervals, segments and fiducial points related to the PQRST ECG waveform.

Features are required that accurately describe the heart's current condition in order to classify a patient as having normal or abnormal cardiac function. It was decided to extract features from the ECG leads using both supervised and unsupervised methods. The extracted features from each heartbeat, across the 12 ECG leads, were stored in a feature vector. The feature vector was subsequently fed into the deep pattern recognition neural network (DPRNN) classifier used to determine if cardiovascular disease was present.

4.3.3.1 Supervised Feature Extraction

Features selected with a known, quantifiable response, are referred to as supervised features. Focus was placed on features which cardiologists examine manually during clinical examinations as well as features used in prior literature.

First Order Features:

Once the beat and peak detection was completed, the various amplitudes, intervals and segments of the cardiac cycle were recorded. Initial first order features that were identified are summarised in Table 4.5.

Table 4.5: Extracted amplitude, interval and segment features.

Amplitudes	Intervals	Segments
P	P	QS
Q	T	
R	QRS	
S	RR	
T		

Second Order Features:

Second order features are derived from the ECG leads using advanced methods. The information derived from these methods produce metrics that cannot be directly identified by specialists in a clinical environment. This provides an increase in available data used to describe ECG recordings, resulting in the potential for improved diagnosis and treatment (Umar, 2002; Belle *et al.*, 2013).

The second order features used in this study includes total energy, relative energy and wavelet entropy. These methods are particularly interesting as they produce features that are robust to noise and signal artefacts (Rosso *et al.*, 2001). The wavelet coefficients are calculated as:

$$C_w(k,l) = \sum_{n=1}^{N} s(n)\psi_{k,l}(n) \tag{4.5}$$

where N indicates the length of the signal $s(n)$. The wavelet coefficients $C_w(k,l)$ allow the calculation of the signal's energy at each scale. The Total Energy of an ECG lead is calculated as:

$$E_{Total} = \sum_{k=1}^{S}\sum_{l=1}^{P_k} C_w(k,l)^2 \tag{4.6}$$

which is the summation of the signal's energy over the selected scales, where S and P_k are the selected wavelet decomposition scales (S=5) and the length of the wavelet coefficient $C_w(k,l)$, respectively. The relative energy corresponding to the energy at scale k in relation to the total energy is calculated as:

$$E_k = \frac{\sum_{l=1}^{P_k} C(k,l)^2}{E_{Total}} \tag{4.7}$$

This provides information on which scale contributes the highest proportion of the previously calculated total energy. This is of particular interest as the different portions of the PQRST wave are more prominent at different scales. Using the generalised formula for Shannon's entropy, the wavelet entropy, WE, is determined as:

$$WE = -\sum_{k=1}^{N} E_k \log(E_k) \tag{4.8}$$

which provides valuable dynamic, time-frequency information pertaining to how orderly or chaotic the original signal is. A low WE value close to zero indicates a periodic, orderly signal, with limited relative energy contributions made across the scales. In contrast, a chaotic, disorderly signal will have contributions across the various scales, resulting in a high WE value (Ródenas *et al.*, 2015).

4.3.3.2 Unsupervised Feature Extraction

Supervised learning requires the user to manually identify input features presented to the classification method. The performance of supervised learning techniques hinges on the quality of the features provided by the user. This process in some cases is extremely tedious, time-consuming and labour intensive. Furthermore, these features may not scale well to new problems. It would be preferable to have algorithms that possess the ability to automatically learn unique features from raw data in an unsupervised manner. This study utilised a stacked denoising autoencoder (SDAE), which is one of many available methods to achieve automatic feature generation.

Stacked Denoiseing Autoencoder

A traditional autoencoder (AE) is a special instance of a generic ANN which is trained to reproduce the provided input data, at the output of the network. The process of training an AE is unsupervised, as raw unlabelled data is used as the input. The training process focuses on the optimisation of a cost function which measures the error between the input x and the reconstructed output $\hat{x}$. The AE consists of two parts, namely an encoder stage, which maps the input to a reduced dimension across the hidden layers, and a decoder stage, which maps the reduced dimensional representation back to the original dimension, across the hidden layers. The middle layer, at the bottleneck of the AE, produces the embedded code. The embedded code is a lower dimensional feature representation of the input. With reference to the ECG signal, individual beats are detected and then segmented to include the PQRST waveforms.

The segmented beats are down-sampled and then normalised:

$$x_{norm} = \frac{x - \mu}{\sigma} \tag{4.9}$$

where μ and σ are the signal mean and standard deviations, respectively. This process reduces computational effort and decreases training time by reducing the total number of samples and centring the data around the mean, with a standard deviation of one.

When using AEs in feature extraction the goal is not to produce perfect reconstruction by learning a trivial mapping function from input to output, but to rather learn interesting feature representations of the input. A novel approach implemented by Vincent *et al.* (2010), led to the creation of denoising autoencoders designed to remove noise from partially corrupted input. Before the segmented beat is presented to the autoencoder network, an initial step injects the input signal with random noise. This study made use of masking noise in which a percentage of the input values are forced to zero. The partially corrupted signal is fed into the autoencoder network with the objective of reconstructing the original, uncorrupted signal, at the output. Inital work done by Vincent *et al.* (2010) indicates that optimal performance occurs when 20 % - 35 % of the original signal is corrupted, leading to a corruption level of 30% selected for this study. Individual hidden layers are trained in a greedy layer-wise approach and then stacked together, creating the SDAE (Figure 4.9).

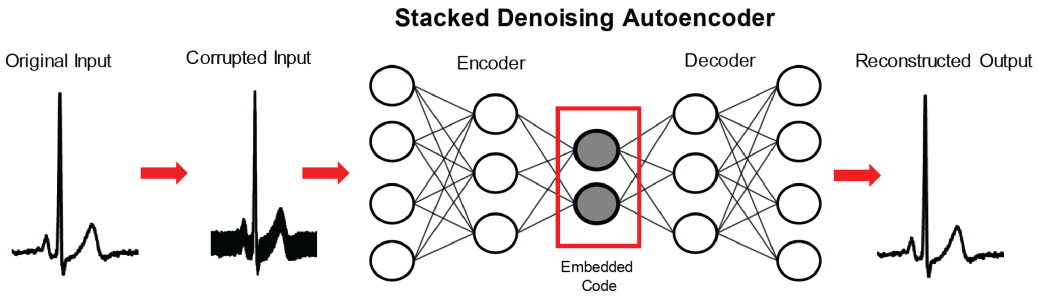

Figure 4.9: Stacked denoising autoencoder.

The use of SDAEs leads to the generation of features with a higher-level representation that is robust to corrupted inputs. Additionally, by performing the denoising task, useful features are extracted that are capable of describing the input distribution. It is important to reiterate that the objective in this case is not the action of removing noise from corrupted data but rather the extraction of useful features that constitute a more robust, higher level representation that is brought about by the use of a denoising autoencoder. These useful features are extracted at the lower-level embedding produced by the bottleneck of the

autoencoder, creating a lower dimensional feature vector representation of the input. This lower level feature representation is referred to as the embedded code and is used as unsupervised features in the classification process.

4.3.4 Feature Selection

The quality of the available features directly influences the classifier's performance. Poor quality, or irrelevant features, are capable of injecting noise into the system which significantly reduces classification accuracy. Noise in a dataset can result from errors made in the measurements of features, or due to natural variation across samples, resulting in misclassification. More features than samples also leads to the curse of dimensionality. This results in the classification model overfitting and not able to generalise well to new data.

Initial features acquired using records obtained from the PTB database were fed into a DPRNN classifier. The classifier using the original feature set produced poor accuracy, sensitivity and specificity results during the initial classification of normal and abnormal heartbeats. Further analysis of the features followed using the t-distributed stochastic neighbour embedding (t-SNE) method which is a data visualisation and dimensionality reduction technique. It was determined that clusters of the lower dimensionality feature representation between the two classes could not be adequately separated. This led to further investigation of the various individual features. It was discovered that the interval onset and offset positions, identified using the wavelet QRS delineation algorithm developed by Martínez *et al.* (2004), was not robust across all the cardiovascular disease categories in the PTB database, and contained high variance. This resulted in many cases in which the two classification classes were indistinguishable, resulting in a low classification performance. Features reliant on the accurate determination of the onset and offset positions are the QRS, P and T interval features. These features were subsequently excluded from the final feature set.

Additionally, the unsupervised features were optimised using the classification performance in a bid to reduce the dimensionality of the embedded code, while preserving sufficient signal information to provide accurate classification. This led to the determination of the dimension of the down-sampled beat segment used as the input to the autoencoder as well as the number of hidden layers, and hidden neurons per hidden layer, in the autoencoder. The initial beat segment consisted of 650 time steps which was down-sampled to 325 time steps, to reduce computational effort while preserving sufficient information from the original signal. The final autoencoder architecture consists of 3 hidden layers with 100 neurons in the first, and third hidden layer, and 30 neurons in the second hidden layer. The number of neurons in the second hidden layer corresponds to the dimension of the generated embedded code,

which is the autoencoder's lower dimensional feature representation of the segmented heartbeat. This embedded code is the unsupervised features extracted and used as classification features. Finally, the classification performance was tested using only supervised or unsupervised feature sets, separately, where the first and second order features made up the supervised feature set. The combined performance using both the combined supervised and unsupervised features was also tested. It was determined that using both the supervised and unsupervised feature sets increases classification accuracy (Appendix G.2 Table G.4). This resulted in the inclusion of both, supervised, and unsupervised features in ECG classification throughout this study (Figure 4.10).

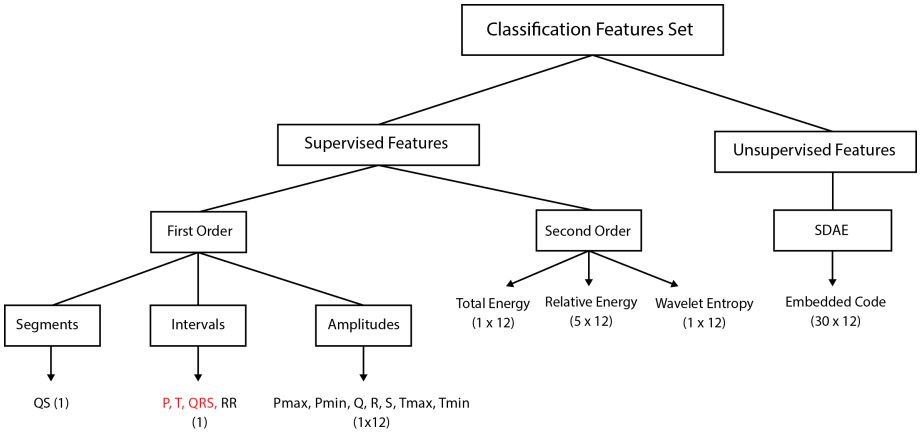

Figure 4.10: Diagram depicting the different features extracted from the ECG leads, where the P, T and QRS interval features (seen in red) are excluded from the final feature vector. The dimensions of the features are represented in brackets.

4.4 Statistical Analysis

The following performance metrics are used to illustrate the performance of the lead reconstruction and patient classification methods used in this project.

4.4.1 Lead Reconstruction

The performance of lead reconstruction techniques are used to compare the interpolated lead with the actual value of the lead. The metrics used to depict the accuracy of these techniques include the root-mean-square error (RMSE), calculated as:

$$RMSE = \sqrt{\frac{1}{N}\sum_{i=1}^{N}(\hat{y} - y)^2} \tag{4.10}$$

in which N represents the number of samples, $\hat{y}$ is the reconstructed lead and y is the actual lead value. Low RMSE values are desirable and indicate accurate lead reconstructions. An additional metric is the Pearson r correlation coefficient represented as:

$$r = \frac{N\sum y\hat{y} - \sum y \sum \hat{y}}{\sqrt{N\sum y^2 - (\sum y)^2}\sqrt{N\sum \hat{y}^2 - (\sum \hat{y})^2}} \tag{4.11}$$

The Pearson r correlation is used to indicate the linear correlation between two variables, where 1 is a complete linear correlation and 0 is no correlation.

4.4.2 Patient Classification

The classification of two classes is referred to as binary classification, in which case the classifier outputs a range of [0, 1]. The output of a classifier can be represented in a confusion matrix, seen in Figure 4.6.

Table 4.6: Confusion matrix for binary classification.

		True Class: Abnormal	True Class: Normal
Predicted Class	Abnormal	True Positives TP	False Positives FP
	Normal	False Negatives FN	True Negatives TN

The confusion matrix represents the true positive (TP), false positive (FP), true negative (TN) and false negative (FN) values, used to calculate accuracy, sensitivity and specificity:

$$Accuracy = \frac{\#TP + \#TN}{\#TP + \#FN + \#TN + \#FP} \tag{4.12}$$

$$Sensitivity = \frac{\#TP}{\#TP + \#FN} \tag{4.13}$$

$$Specificity = \frac{\#TN}{\#TN + \#FP} \tag{4.14}$$

The classifier accuracy indicates the amount of correctly diagnosed normal and abnormal patients out of the total population. The sensitivity refers to the amount of correctly identified abnormal patients with respect to the total amount of abnormal patients and is also referred to as the true positive rate

(TPR). The specificity indicates the number of correctly identified normal patients with respect to the total amount of normal patients, also referred to as the true negative rate (TNR). An additional metric to gauge the performance of a classifier is the use of a receiver operating characteristic (ROC) curve and the corresponding area under the curve (AUC) (Figure 4.11). The ROC curve indicates the TPR vs False Positive Rate (FPR) relationship of the classifier, and is calculated by varying the discrimination threshold of the classifier (Mathworks, 2017). The AUC value indicates the area under the ROC curve and is a measure of accuracy of the classifier with a range of [0, 1]. The perfect classifier produces an ROC plot with a right angle at the top left corner with coordinates (0, 1) and an AUC value corresponding to 1. A classifier that produces a completely random output results in diagonal line with coordinates (1, 1) and the AUC of 0.50. Most classifiers will produce an ROC curve and corresponding AUC values between these two possible extremes.

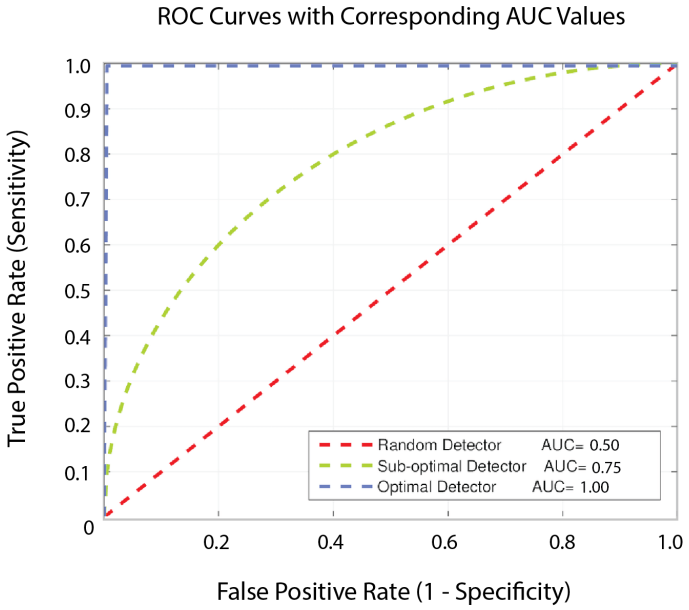

Figure 4.11: ROC curves with corresponding AUC values for three different example classifiers.

Chapter 5

Machine Learning

5.1 Background

The current study makes use of artificial neural networks (ANNs), which were initially introduced in 1943. In recent years there has been a resurgence in the popularity of ANNs. This can be attributed to steep increases in computational performance and processing power, that has become readily available and easily accessible (Jonathan *et al.*, 2010). Artificial neural networks are an artificial intelligence and machine learning technique that was conceptualised from the knowledge of how the human biological neural networks function. This technique is capable of identifying pertinent features from data and establish relationships which are translated to the output of the network. This is achieved by instances of prior learning used to train the ANN. It is widely believed that neural networks can offer a fresh approach to decode complex problems found within nature (Yegnanarayana, 2009).

5.1.1 Biological Representation

Artificial neural networks were initially developed to model the functionality of the biological neural network. The role of the biological neural network is to provide a path of inter-connected neurons that sustains the flow of information, in the form of electrochemical impulses, transmitted from the brain to its target organ. Every biological neuron consists of branches of dendrites responsible for receiving the electrochemical impulses and a cell body containing a nucleus that is connected to an axon. The axon contains terminals responsible for transmitting any impulses to other neurons or organs (Figure 5.1). A neuron is said to "fire" when the collective inputs at the dendrites exceed the firing threshold, resulting in the transmission of the received signal from the dendrites along the axon, to the axon terminal. The continuation of the impulse from the axon terminal of one neuron to the dendrites of a proceeding neuron occurs across junctions known as the synapses (Lewis, 2017). The brain alone is estimated to consist of between 10^{10} - 10^{11} neurons and may

receive stimuli from as many as 10^3 - 10^5 other neurons, resulting in a total amount of synapses in the order of 10^{16} (Nunez and Srinivasan, 2006).

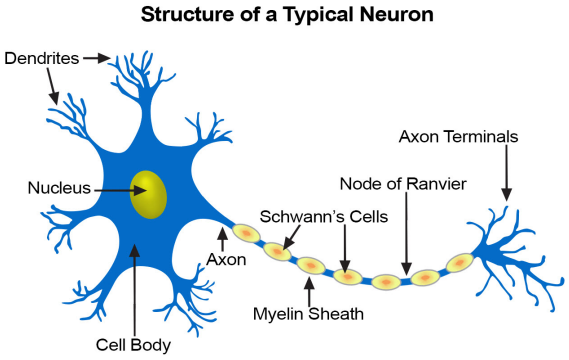

Figure 5.1: Labelled illustration of a biological neuron (SEER Training Modules, 2017).

5.1.2 The Model of a Single Neuron

Artificial neurons are a simplified model of the biological neurons found in the body and are the elementary units used to build neural networks (Figure 5.2).

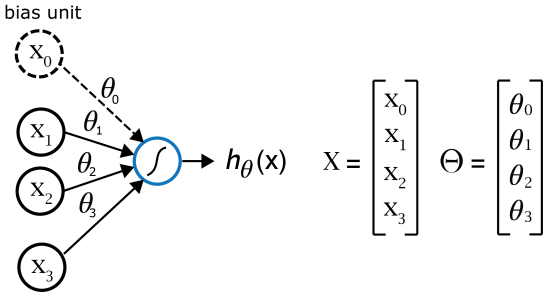

Figure 5.2: The model of a single artificial neuron (Pan, 2016).

The artificial neuron receives one or more input features $(x_1, ..., x_n)$ that represent the dendrites. These input features are multiplied by weighting factors $(\theta_1, ..., \theta_n)$ and the summation of these inputs are passed through an activation function with the result equal to the hypothesis function $h_\theta(x)$ (Pan, 2016). The most common activation functions are the sigmoid activation function,

$$h_\theta(x) = \frac{1}{1 + e^{-\theta^T X}} \tag{5.1}$$

and the hyperbolic tangent function,

$$h_\theta(x) = \tanh(x) = \frac{e^{\theta^T X} - e^{-\theta^T X}}{e^{\theta^T X} + e^{-\theta^T X}} \tag{5.2}$$

where the input features are transformed to within the range of the particular activation function. The only difference between the two mentioned activation functions is the range of the output. The sigmoid function has a range of [0,1], whereas the hyperbolic tangent function has a range of [-1,1], illustrated in Figure 5.3. Input x_0 is referred to as a bias unit. With the aid of θ_0, the bias unit is responsible for shifting the activation function either left and right along the x-axis.

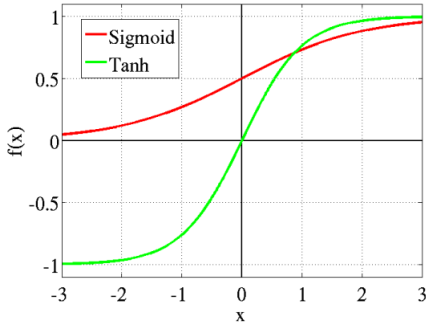

Figure 5.3: A graph representing the sigmoid and hyperbolic tangent activation functions on the same axis (Sharma, 2017).

5.1.3 Neural Networks

The connection of one or more neurons where the output of the initial neuron acts as the input to the proceeding neuron, across two or more layers, constitutes a neural network (Figure 5.4).

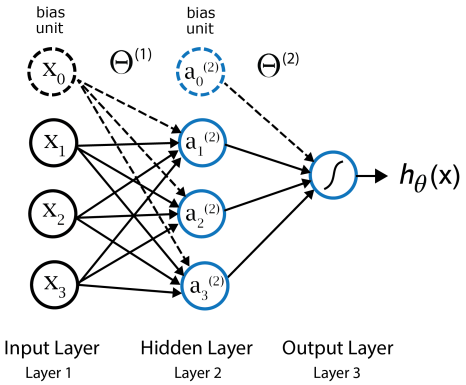

Figure 5.4: Illustration of a multilayer neural network consisting of a single input layer, hidden layer and output layer (Pan, 2016).

The first layer of the neural network, containing the input features, is referred to as the input layers where the last layer, which calculates the final value (hypothesis), is referred to as the output layer. The one or more layers between the input and output layer are referred to as the hidden layers. With reference to Figure 5.4, the neural network consists of an input layer, a single hidden layer containing three neurons and a bias unit each, as well as an output layer with one neuron (Pan, 2016). The activation of the neurons in the hidden layer are calculated as:

$$a_1^{(2)} = g(\Theta_{10}^{(1)}x_0 + \Theta_{11}^{(1)}x_1 + \Theta_{12}^{(1)}x_2 + \Theta_{13}^{(1)}x_3) \tag{5.3}$$

$$a_2^{(2)} = g(\Theta_{20}^{(1)}x_0 + \Theta_{21}^{(1)}x_1 + \Theta_{22}^{(1)}x_2 + \Theta_{23}^{(1)}x_3) \tag{5.4}$$

$$a_3^{(2)} = g(\Theta_{30}^{(1)}x_0 + \Theta_{31}^{(1)}x_1 + \Theta_{32}^{(1)}x_2 + \Theta_{33}^{(1)}x_3) \tag{5.5}$$

where g is the selected activation function, x_0 to x_3 is the input to the network and Θ^1 is the vector containing the weights that are multiplied with the individual inputs across the various hidden neurons. The output of the network is represented as:

$$h_\theta(x) = g(\Theta_{10}^{(2)}a_0 + \Theta_{11}^{(2)}a_1 + \Theta_{12}^{(2)}a_2 + \Theta_{13}^{(2)}a_3) \tag{5.6}$$

in which $h_\theta(x)$ is the hypotheses function and Θ^2 maps the hidden layer activations from the hidden layer to the output of the neural network (Pan, 2016).

5.1.4 Cost Function

The process of training an ANN can occur in either a supervised or unsupervised manner. In the case of supervised learning, the target value is known for each input. The ANN attempts to minimise the error between the calculated output of the network and the known target value which is achieved by minimising a selected cost function. The term cost function refers to any function that derives a relationship between output of the network and the target values. The cost function can be defined as

$$J = \sum_{i=1}^{N} Er(i) \tag{5.7}$$

where N is defined as the number of samples and $Er(i)$ is the selected error function which receives the input and output value pair, $x(i)$ and $y(i)$, for each

sample. Popular examples of the $Er(i)$ error functions include the mean-square error (MSE) function defined as,

$$Er(i) = \frac{1}{N}\sum_{m=1}^{K}(h_\theta^L(x(i)) - y(i))^2 \tag{5.8}$$

and the cross-entropy function described as ,

$$Er(i) = \sum_{m=1}^{K}(y(i)\ln(h_\theta^L(x(i)) + (1 - y(i))\ln(1 - h_\theta^L(x(i)))) \tag{5.9}$$

where $h_\theta^L(x(i))$ is the hypothesis function (or estimated output of the network) for the final layer L of the network for a given true output and input pair, $y(i)$ and $x(i)$, for the sample size, m (Theodoridis and Koutroumbas, 1999). In the case of unsupervised learning no target values are available for training purposes, therefore the weights and biases are updated with reference to the inputs.

5.1.5 Backpropogation

The error between the true output and the output calculated by the neural network is minimised by iteratively adjusting the weights and biases of each neuron in each layer of the neural network. This process of refining the neuron weights and bias values from the last output layer back to the first input layer is referred to as the backpropogation algorithm. The process is repeated until a specified tolerance, or convergence of the cost function, is achieved. The backpropogation algorithm is explained in greater detail in Appendix F.2.

5.2 Patient Classification

Patient classification refers to the automated diagnosis of a patient's current cardiac condition using machine learning techniques. The study makes use of a pattern recognition ANN architecture. Pattern recognition refers to the process of training an ANN to correctly map a set of input patterns to target classes. The network is trained to respond to an input feature vector that closely resembles prior training data and ultimately predict the target class to which the input corresponds. Once the network is successfully trained it may be utilised to classify new, unseen patterns. This study makes use of a deep pattern recognition network (DPRNN) (Figure 5.5), where a deep network refers to any ANN with an architecture consisting of multiple hidden layers.

The extracted features $(x_1, .., x_n)$ are the input to the network where the number of neurons in the input layer is dependant on the dimension of the feature

vector. The number of neurons of the output layer is dependant on the number of classification classes. The classifier is tasked with determining if the input feature vector contains information from a subject with either normal or abnormal cardiac function. This is a traditional binary classification problem with two output neurons.

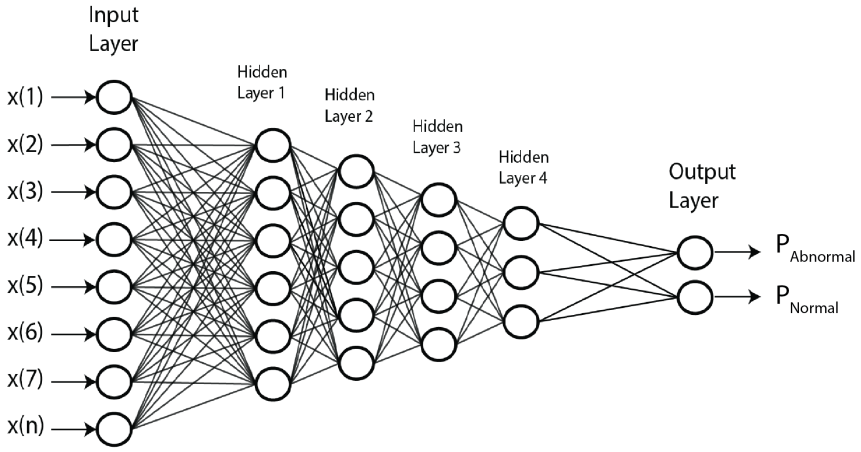

Figure 5.5: Illustration of a deep classification neural network.

The hidden neurons make use of the sigmoid activation function (Equation 5.1), whereas the output layer comprises of a softmax layer. The softmax layer maps the net activation of the final output layer to probabilistic values in the range [0 1], for each output neuron. These probabilistic values indicate the likelihood of the input features representing either classification class, with the sum of both values equal to 1.

The network neuron weights and bias values are updated during training using the scaled conjugate gradient backpropagation algorithm (Møller, 1993). The neuron weights and bias values are updated in proportion to the cost function value calculated using the cross-entropy function (Equation 5.9). Training terminates in the event that the validation performance converges, triggering the early stop condition in order to avoid over-fitting.

5.3 Lead Reconstruction

Lead reconstruction focuses on the interpolation of absent ECG leads, from a reduced lead set. This study focuses on using machine learning techniques such as an ANN to perform lead reconstruction. Pertinent features and relationships amongst the reduced ECG leads are translated to the network output. This is achieved by instances of prior learning used to train the network.

The selected ANN architecture used to perform the ECG lead reconstruction is the focused time-delay neural network (FTDNN). The FTDNN forms part of a general class of dynamic neural network's known as focused networks which are well suited for time series prediction. The FTDNN is a feed-forward network containing tapped delay lines at the input, which results in the output depending on the network's current and past inputs. The task of reconstruction is to formulate a non-linear function, f, that is capable of calculating values for $\hat{y}(t)$ from a reduced lead set of $x(t)$. The model can be characterised as:

$$\hat{y}(t) = f(x(t), x(t-1), ..., x(t-d)) \tag{5.10}$$

where d is the system's input tap delay (Beale *et al.*, 2016). The layout of the neural network can be seen in Figure 5.6.

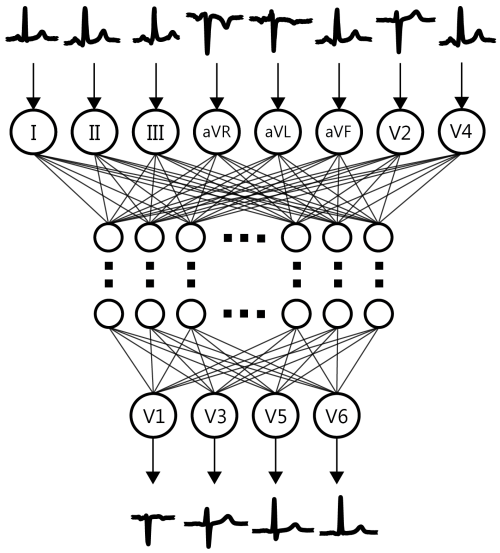

Figure 5.6: Reconstruction of leads V1,V3,V4 and V6 using an ANN.

The network can be described as a feedforward network consisting of 3 hidden layers. The number of neurons used in each of the three hidden layers is 30, 20 and 15. The tapped delay line d is utilised to store prior values of up to two time steps for the input $x(t)$ sequences. The activation function used for the hidden layers is the tan-sigmoid transfer function. The output layer activation function is the linear transfer function. The Levenberg-Marquardt backprorogation algorithm was used to update the neuron weights and bias values during training. Training concluded in the event that the validation performance converged (Beale *et al.*, 2016), thus preventing the model from over-fitting to the training set. The reduced leads input consists of leads I-III, avR, avL, avF and precordial leads V2 and V4. The reconstructed output consists of the remaining precordial leads V1, V3, V5 and V6.

Chapter 6

Results

6.1 Retrospective Study

The retrospective study utilised the PTB online database which consisted of 522 records from 268 patients. The 268 subjects followed an exclusion process whereby individuals with multiple recordings taken on the same day, or following any medical procedure, for example catheterisation, were excluded. This resulted in a total of 247 subjects with 358 records included in the study.

6.1.1 Beat Classification

Each ECG record was segmented into different beats across the multiple ECG leads from which the relevant features were extracted. The selected features from multiple beats were grouped according to patients to ensure no data leaked across the training, validation and test sets. A stratified k-fold cross-validation method was implemented in which the features extracted from the patients were divided across the selected "k" number of folds. Stratification ensured that each fold resembled the total available data by dividing the total data proportionally between the normal and abnormal classification classes, across all the folds. The current study made use of 7 folds consisting of 5 training folds, 1 validation and 1 test fold. The model was trained until the validation performance converged without further improvement at which point the results were recorded for that specific test fold. This process was repeated 7 times, whereby all the folds were rotated to ensure the test fold contained different patients every repetition. Cross-validation prevents over optimistic classification performance and ensures that the resulting classifier accurately represents a population and would potentially generalise well to new data.

The feature set was fed into the deep pattern recognition classification model which was tested using different combinations of leads, resulting in different input neurons, and hidden layer sizes depending on the number of leads selected (Table H.1 in Appendix H.1). Table 6.1 summarises the performance

of the classification models with different lead combinations ranging from the best single lead, to the maximum 12 lead ECG classifier. The performance is measured by taking the mean results of the classifier for accuracy, sensitivity, specificity and AUC, across all 7 folds. The classifier model corresponding to the 12 lead ECG produced the highest accuracy, sensitivity, specificity and AUC values corresponding to 0.90, 0.91, 0.87 and 0.94, respectively. The box-and-whisker diagram and a ROC plot for the full 12 lead ECG classifier are illustrated in Figure 6.1a and Figure 6.1b, respectively.

Table 6.1: Retrospective study mean classification performance across the 7 folds for various ECG lead combinations.

	Performance Metrics			
Classifier	Accuracy (%)	Sensitivity (%)	Specificity (%)	AUC
Single Lead II	85	87	79	0.90
All Limb Leads	86	86	86	0.92
All Limb Leads + V2	87	88	85	0.93
All Limb Leads + V2,V4	87	88	88	0.93
Full 12 Lead ECG	90	91	87	0.94

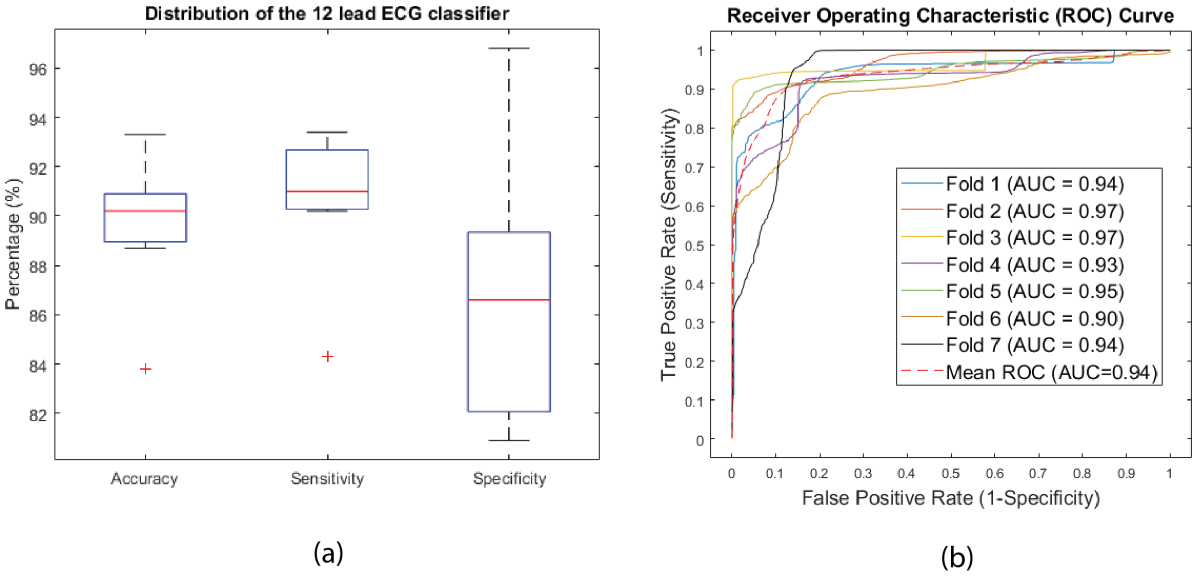

Figure 6.1: Classification performance for the full 12 lead ECG model in the retrospective study: (a) A box-and-whisker diagram illustrating the accuracy, sensitivity and specificity distribution of the classifier across the 7 folds. (b) The ROC curve for the classifier across the 7 folds as well as the resulting mean ROC curve with corresponding AUC values.

The results of all individual single lead classifiers (of which lead II produced the highest performance) is represented in Appendix H, Table H.3, with the corresponding box-and-whisker distribution and ROC curve plotted in Figure H.3 and H.4, respectively. The results of the all limb lead classifier as well as the limb lead classifier with various combinations of precordial leads are represented in Figures H.5 and H.6 as well as Table G.3 and Figure G.1, in Appendix G.1.

6.1.2 Lead Reconstruction

The 12 lead ECG records were used to train, validate and test the FTDNN lead reconstruction model, using a 3-Fold cross validation method. The limb leads (I, II and III), augmented leads (avR, avL and avF) as well as two precordial leads V2 and V4 were input into the network, which reconstructed the remaining precordial leads (V1, V3, V5 and V6). The mean and standard deviations of the RMSE values of the different disease subgroups across the various derived ECG leads are displayed in Table 6.2. The mean RMSE values and corresponding 95% confidence interval (CI) for the reconstructed leads are illustrated in Figure 6.2. The distribution of the lead reconstruction RMSE results is represented as a box-and-whisker diagram in Appendix H.1, Figure H.1.

Table 6.2: Retrospective study mean RMSE (μV) for the reconstructed precordial leads.

	Reconstructed Leads (μV)			
Classification	V1	V3	V5	V6
Normal	85 ± 27	97 ± 82	100 ± 51	101 ± 48
Abnormal	123 ± 81	102 ± 71	134 ± 106	117 ± 97
Bundle Branch Block	168 ± 70	120 ± 55	170 ± 66	149 ± 58
Cardiomyopathy	185 ± 99	174 ± 133	349 ± 277	182 ± 93
Dysrhythmia	69 ± 6	87 ± 65	196 ± 98	174 ± 69
Myocarditis	47 ± 1	88 ± 9	160 ± 1	67 ± 3
Myocardial Hypertrophy	63 ± 5	75 ± 7	127 ± 48	106 ± 49
Myocardial Infarction	120 ± 79	97 ± 64	114 ±64	111 ± 98
Valvular Heart Disease	57 ± 8	48 ± 11	144 ± 27	98 ± 10
All Cases	118 ± 78	101 ± 72	128 ± 101	115 ± 92

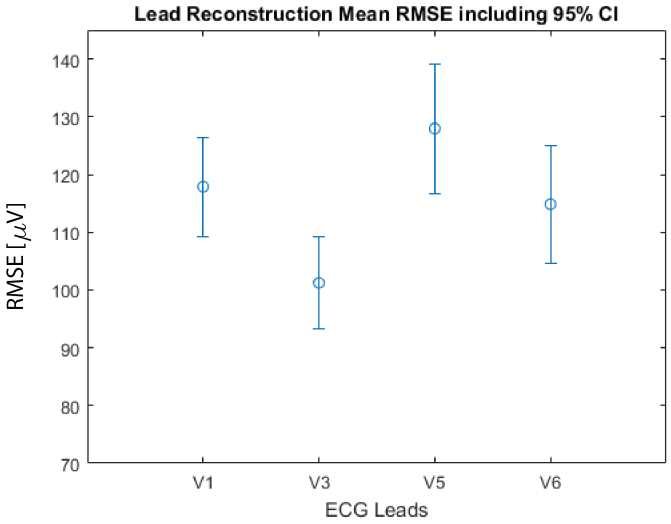

Figure 6.2: Retrospective study lead reconstruction RMSE mean values and corresponding 95% CI.

The average Pearson r correlation values are summarised in Table 6.3. The leads used as inputs to the FTDNN were omitted as they are used to derive the remaining leads and therefore exhibit a RMSE value of zero and perfect correlation ($r = 1.00$). The results across the reconstructed leads for all classes indicate RMSE values of between 101 and 128 μV and correlation values ranging from 0.87 to 0.98. All correlation values were statistically significant at $p \ll 0.01$, calculated using a 95% CI.

Table 6.3: Retrospective study mean Pearson r correlation values for the reconstructed precordial leads.

	Reconstructed Leads (r)			
Classification	V1	V3	V5	V6
Normal	0.90	0.97	0.94	0.96
Abnormal	0.91	0.98	0.90	0.85
Bundle Branch Block	0.80	0.98	0.94	0.92
Cardiomyopathy	0.94	0.98	0.81	0.85
Dysrhythmia	0.96	0.95	0.78	0.96
Myocarditis	0.98	0.99	0.96	0.98
Myocardial Hypertrophy	0.97	0.99	0.97	0.95
Myocardial Infarction	0.91	0.98	0.90	0.84
Valvular Heart Disease	0.97	0.99	0.86	0.94
All Cases	0.91	0.98	0.90	0.87

6.2 Clinical Study

The clinical study recorded 70 patients at Tygerberg Hospital. After examination of the recordings it was discovered that 3 records contained missing information and one recording was corrupted by motion artefacts, and were ultimately excluded. The remaining 66 subjects included 23 normal, 35 abnormal and 8 VNIP recordings, of which 29 were male and 37 female, with a mean age of 54 years old.

6.2.1 Patient Classification

The patient classification for the clinical study consists of features extracted from 58 patients, corresponding to the normal and abnormal classification classes recorded using the prototype device. Each record consisted of 10 seconds of data, segmented into different beats whereby the extracted features were fed into the classification models previously trained using the PTB database records. In order to classify the patient as having abnormal or normal cardiac function, the classifier probability values produced by the last two neurons in the output layer are averaged across each patient's segmented heartbeats. An example of this procedure is illustrated in Appendix H.1, Table H.2. The perfect classification of abnormal cardiac function produces a probability of [1, 0] with a probability of [0, 1] indicating a perfect classification of a subject with normal cardiac function. The classification results for the best performing lead combinations using data obtained from the clinical study is summarised in Table 6.4.

Table 6.4: Clinical study classification performance for various ECG lead combinations.

	Classification Performance			
Classifier	Accuracy (%)	Sensitivity (%)	Specificity (%)	AUC
Single Lead I	81	77	87	0.82
All Limb Leads	81	83	78	0.82
All Limb Leads + V2	81	83	78	0.82
All Limb Leads + V4	85	83	87	0.85
All Limb Leads + V2,V4	85	83	87	0.85

The classification performance of the models using precordial lead V4 and the model using both precordial leads V2 and V4 produced the highest scores for accuracy, sensitivity, specificity and AUC corresponding to 0.85, 0.83, 0.87 and 0.85, respectively. The confusion matrix and ROC plot are illustrated in Table 6.5 and Figure 6.3, respectively. From the confusion matrix it is possible to see that the classifier misdiagnosed 6 abnormal patients, from a

total of 35, as having normal cardiac function leading to a sensitivity of 83%. Additionally, 3 abnormal patients were misdiagnosed as having normal cardiac function, leading to a specificity of 87%. The classifier correctly diagnosed 29 abnormal patients and 20 normal patients, resulting in a total classification accuracy of 85%.

Table 6.5: Clinical study classifier confusion matrix using the full lead set of the prototype device.

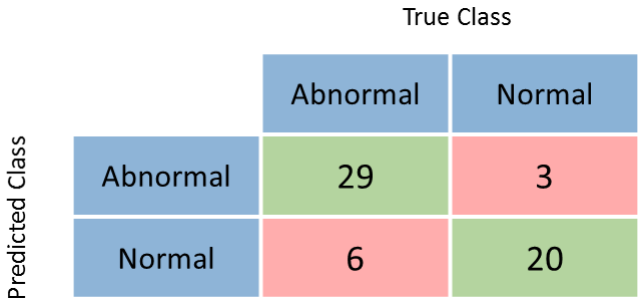

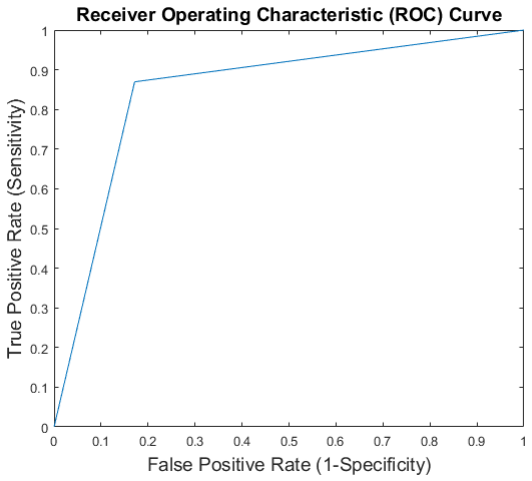

Figure 6.3: Clinical study ROC curve using the full lead set of the prototype device.

6.2.2 Lead Reconstruction

Initially, the FTDNN was trained using records solely obtained from the PTB database and subsequently tested using the 68 subjects from the normal, abnormal and VNIP classes, acquired during the clinical trial using the control device. However, the lead reconstruction model produced weak performance with high RMSE values and low Pearson r correlation values. The FTDNN was retrained using a 3-Fold cross validation approach, where data from the clinical study was rotated between the training, validation and test folds and data from

the PTB database was appended to the training fold. The mean and standard deviations of the RMSE values of the different disease subgroups across the various derived ECG leads are displayed in Table 6.6. The mean RMSE values and corresponding 95% CI is illustrated in Figure 6.4. The distribution of the lead reconstruction RMSE results is represented as a box-and-whisker diagram in Appendix H.2, Figure H.2.

Table 6.6: Clinical study mean RMSE (μV) for the reconstructed precordial leads.

	Reconstructed Leads (μV)			
Classification	V1	V3	V5	V6
Normal	158 ± 94	196 ± 108	161 ± 58	149 ± 45
Abnormal	207 ± 186	321 ± 263	233 ± 250	200 ± 141
VNIP	120 ± 64	197 ± 91	115 ± 18	108 ± 21
All Cases	181 ± 152	266 ± 215	197 ± 216	192 ± 112

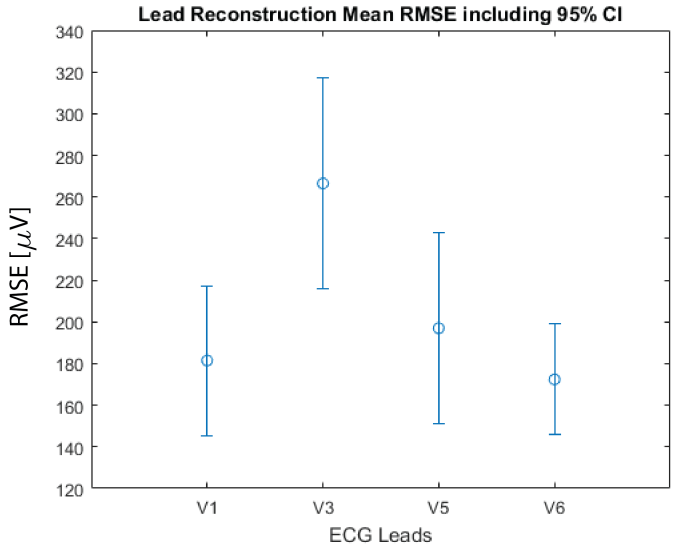

Figure 6.4: Clinical study lead reconstruction RMSE mean values and corresponding 95% CI.

The average Pearson r correlation values are summarised in Table 6.7. The leads used as inputs to the FTDNN were omitted as they are used to derive the remaining leads and therefore exhibit a RMSE value of zero and perfect correlation ($r = 1.00$). The results across the reconstructed leads for all classes indicate RMSE values of between 181 and 266 μV, and correlation values ranging from 0.91 to 0.95. All correlation values were statistically significant at $p \ll 0.01$, calculated using a 95% CI.

Table 6.7: Clinical study mean Pearson r correlation values for the reconstructed precordial leads.

	Reconstructed Leads (r)			
Classification	V1	V3	V5	V6
Normal	0.95	0.93	0.95	0.94
Abnormal	0.94	0.90	0.94	0.92
VNIP	0.93	0.88	0.97	0.96
All Cases	0.94	0.91	0.95	0.93

6.2.3 Electronic Stethoscope

In addition to the reduced lead ECG, the electronic stethoscope was tested to provide additional information not required in the automatic diagnostic process. An example of a recording from a healthy test subject taken using the electronic stethoscope is illustrated in Figure 6.5, with the S1 and S2 heart sounds seen clearly. The recorded data was post-processed using a digital bandpass filter with corner frequencies at 25 Hz and 700 Hz.

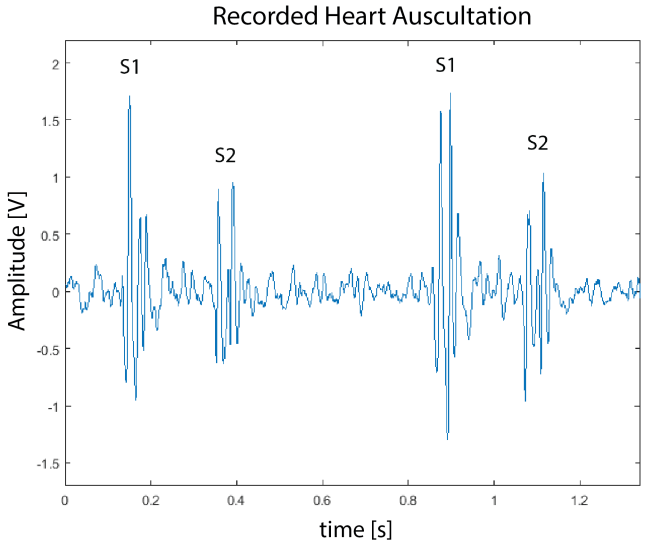

Figure 6.5: Recorded phonocardiogram using the electronic stethoscope prototype with labelled heart sounds S1 and S2.

Chapter 7

Discussion

7.1 Cost Analysis

The available hardware was researched and selected such as to reduce the total production cost of the device. Table B.2 (Appendix B.2) lists all the hardware required to develop the device with the corresponding purchase prices. The total price of the current device came to R6059 and is compared with similar devices in Table 7.1 using the dollar denomination.

Table 7.1: Cost comparison of various CVD diagnostic devices (Botha, 2010).

Device	**Description**	**Price**[†]
Littmann 3200	Electronic Stethoscope	$400
Contec CMS9000	3/5 Lead ECG	$700
GE MAC 1200	12 Lead ECG	$1190
Philips Zymed	Holter Monitor	$400
Eko Duo[*]	Hybrid: 1 lead ECG and Electronic Stethoscope	$349
CardioSleeve[*]	Hybrid: 3 lead ECG and Electronic Stethscope	$600
Current Device	8 Lead ECG and Electronic Stethoscope	$446

[†] $1 = R13.59 at the current exchange rate (05-10-2017)
[*] Requires a smart phone for operation

The current device costs significantly less than both a gold standard 12 lead ECG and a reduced 3/5 lead ECG, but is slightly more expensive than an electronic stethoscope. The price is comparable with similar hybrid ECG and electronic stethoscope devices such as the Eko Duo and CardioSleeve. However, it should be noted that these devices require a smartphone to operate and the CardioSleeve does not come with a stethoscope attachment which would ultimately increase the total cost in excess of the current device. This option of implementing the device using a smartphone was not a possibility for the current project as it cannot be expected for primary care givers in rural locations to have access to the latest smartphones. This lead to the imple-

mentation of the LCD touchscreen. Bulk purchases of components and parts as well as a possible in-house design of a stethoscope chestpiece, rather than purchasing an already existing stethoscope, are potential methods to reduce the total price of the device. Additional factors that would raise the selling price of the developed device would include labour and shipping costs as well as a selected profit margin.

7.2 Safety Analysis

Various methods have been used to ensure the device is developed safely without compromising on recording accuracy, device performance and total cost. The device makes use of ESD protection by virtue of a diode array provided by the SP720 component. This ensures that voltage spikes across the ECG lead wires due to misuse of the device or in the case of defibrillation purposes, will not damage the electronics of the device. Electrical isolation is provided by the ADUM6403 and ADUM4400 in the event that the RPi is connected to peripheral devices powered through the electrical mains. An insulation barrier provides the clearance required for protection against creepage current that may occur across the PCB. The safety standards adhered to by the current device, as well as the components responsible for ensuring those standards were met, are summarised in Table B.1 (Appendix B.1.2).

7.3 Patient Classification

7.3.1 Retrospective Study

The performance of the retrospective study is compared to prior studies conducted in the field (Table 7.2) that focuses on multi-lead beat classification methods that utilised the PTB database. The current study produced a classifier performance similar to that of Tripathy *et al.* (2014) and comparable with that of Yan *et al.* (2010) and Arif *et al.* (2012). The prior studies exhibit strengths in that they are able to classify abnormal subjects into specific cardiovascular disease categories, with high accuracies. However, all three prior studies discard various disease classes and only include a small percentage of the total available beats of the included diseases. This could potentially lead to falsely high classification performances, with classifcation models untested against the full database. Tripathy *et al.* (2014) and Yan *et al.* (2010) make use of hold-out validation methods in which beats are randomly assigned to the training and test data sets. This leads to the potential for the overlap of patient data expressed in both the training and testing validation set resulting in a classification model that produces a classification performance that is over optimistic. The use of k-fold cross-validation perfomed in the current study as well as by Tripathy *et al.* (2014), ensures decreased bias and variance.

Table 7.2: Comparison of beat classification performance for studies done using the PTB database.

Authors	Features	Validation Method	Classifier Type	Performance Measures
Tripathy *et al.* (2014)[a]	Unsupervised Second Order	5-fold cross-validation	LS-SVM	Acc. = 90
Yan *et al.* (2010)[b]	Second Order	Hold-out: 75% training 25% test	SVM	Sens. = 96% Spec. = 99%
Arif *et al.* (2012)[c]	First Order	Hold-out: 50% training 50% test	KNN	Acc. = 99.9% Sens. = 99.9% Spec. = 99.9%
Present Work[d]	First Order Second Order Unsupervised	7-fold stratified cross-validation	ANN	Acc. = 90% Sens. = 91% Spec. = 87% AUC = 0.94

[a] Classification classes: HC, CM, MI, HT, DR.
[b] Classification classes: HC, CM, MI, HT, BBB, VHD
[c] Classification classes: HC, MI
[d] Classification classes: Normal (HC), Abnormal (CM, MI, HT, DR, BBB, VHD, HF, MC)

7.3.2 Clinical Study

Analysis of the results represented in Table 6.4 indicates the clinical study performance, for the different lead subsets, gradually increases as leads are added as inputs to the classifier. This trend was also observed in the retrospective study and is to be expected, as more available information should yield an equal or improved classification performance. Using the maximum available ECG leads of the prototype for classification produced high accuracy, sensitivity and specificity percentages. The 0.85 AUC indicates a great classifier capable of distinguishing between normal and abnormal patients.

The clinical study classifier incorrectly classified 6 patients with heart abnormalities as having normal cardiac function. The diseases belonging to the 6 misclassified abnormal patients are listed in Table I.1 (Appendix I). Of the 6 total misclassified subjects, only 1 subject exhibited pathology included in the training set from the PTB database. The lack of available training data could result in the incorrect classification due to the classifier not being sensitive enough with respect to the features exhibited by the specific pathology. Although the misdiagnosed patients with Bradycardia and Tachycardia did not form part of the training data, the classifier was robust enough to correctly classify 7 additional cases of Bradycardia and 3 cases of Tachycardia, as having abnormal cardiac function. One of the incorrectly diagnosed abnormal patients was declared to exhibit borderline left atrial enlargement, indicating

uncertainty in the subject's ground truth which could also have potentially lead to the incorrect classification.

The performance of the patient classification model used in the clinical study is compared with prior studies done in the field. Literature compared in the study (Table 7.3) focused on multi-lead patient classification methods that utilised data acquired from a clinical study or PTB database. Huang and Zhou (2015) classified normal and abnormal cardiac function, whereas Sun *et al.* (2012) distinguished between normal cardiac function and MI, using the PTB database. Haraldsson *et al.* (2004) classified normal and MI subjects in a clinical study. The current study used data from the PTB database to train a classifier that was tested using a clinical study to distinguish between normal and abnormal patients. Therefore, the hold-out validation method is used to determine the performance of only the clinical data, as opposed to the previously used cross-validation method in the retrospective study. This is acceptable due to the large amount of available data gathered by including additional records from the clinical trial. The current study produces a classification performance that is comparable to the prior studies performed by Huang and Zhou (2015), Sun *et al.* (2012) and Haraldsson *et al.* (2004).

Table 7.3: Comparison of patient classification performance for studies done using the PTB database and clinical studies.

Authors	**Features**	**Validation Method**	**Classifier Type**	**Performance Measures**
Huang and Zhou (2015)[a]	First Order	Hold-out: 50% Training 50% Test	S-DA	Acc. = 89% Sens. = 90% Spec. = 85%
Sun *et al.* (2012)[b]	First Order	10-fold cross-validation	LTMIL	Sens. = 92% Spec. = 88%
Haraldsson *et al.* (2004)[c]	First Order Second Order	Hold-out: 67% Training 33% Test	ANN	AUC = 0.83
Present Work[d]	First Order Second Order Unsupervised	Hold-out: 55% Training 22% Validation 23% Test	ANN	Acc. = 85% Sens. = 83% Spec. = 87% AUC = 0.85

[a] Classification classes: Normal, Abnormal
[b] Classification classes: HC, MI
[c] Classification classes: HC, MI
[d] Classification classes: Normal, Abnormal

A comparison between prior research projects performed within the research group is presented in Table 7.4, where the "auscultation jacket" (Visagie, 2007) and the PCG device (Botha, 2010) diagnosed CVD using heartsounds. The current device compares favourably with the results obtained in previous studies which performed clinical trails.

Table 7.4: Classification performance in comparison with past CVD diagnostic devices (Botha, 2010).

Diagnostic Device	Accuracy	Sensitivity	Specificity
Auscultation Jacket	85%	76%	90%
PCG Device	86%	82%	88%
Current Device	85%	83%	87%

7.4 Lead Reconstruction

The current lead reconstruction retrospective and clinical study is the first study to make use of an ANN, more specifically a FTDNN, to reconstruct missing leads. The retrospective study resulted in the reconstruction of the full 12 lead ECG with mean Pearson r correlations between 0.87 and 0.98, and a mean RMSE range of between 101 and 128 μV. The clinical study presented an increase in mean RMSE with values between 181 and 266 μV, although maintained an excellent Pearson r correlations of between 0.91 and 0.95. All leads were statistically significant at $p \ll 0.01$, with a CI of 95%. The mean performance of RMSE and Pearson r correlation values of the retrospective and clinical study are compared to prior literature in Table 7.5.

Table 7.5: Lead reconstruction performance in comparison with prior studies.

Authors	Method	RMSE (μV)	Correlation
Schreck and Fishberg (2013)	NLO Universal Transform	40 - 95	0.71 - 0.90†
Nelwan *et al.* (2008)	EASI Lead Transform	75 - 140	-
Drew *et al.* (2004)	Mason-Likar (ML) Transform	90 - 169	-
Tsouri and Ostertag (2014)	ICA Patient Specific Transform	-	93% - 96%*
Present Work: Retrospective Study	FTDNN	101 - 128	0.87 - 0.98†
Present Work: Clinical Study	FTDNN	181 - 266	0.91 - 0.95†

† Pearson r correlation
* Percentage correlation

A comparison of the RMSE for the various studies is seen in Figure 7.1 which was adapted from Schreck and Fishberg (2013). The distributions of various ECGs measures are often skewed, multi-modal, or heavy-tailed. It is therefore preferred to compare the distributions as quartiles, which outperform the sample mean and standard deviation (Huang and Zhou, 2015). The slight increase in RMSE with maintained high performance of correlation in the clinical study, indicates that the results of the clinical study proved to have great morpholog-

ical shape but was not able to reach the same peak magnitudes as the original waves, resulting in an increase in RMSE. This decrease in RMSE performance obtained in the clinical trial could be attributed to various factors. The use of both data obtained from the PTB online database, as well as data recorded in the clinical study, to train the reconstruction model introduces the potential for variability. This could be due to the differences in the 12 lead devices used to take the recordings, as well as the different professionals who placed the leads. A potential solution would be to record a larger training population using a single control device placed by the same professional, to ensure consistency. This would reduce variability of lead placement between professionals and devices, ultimately improving the trained lead reconstruction model and RMSE.

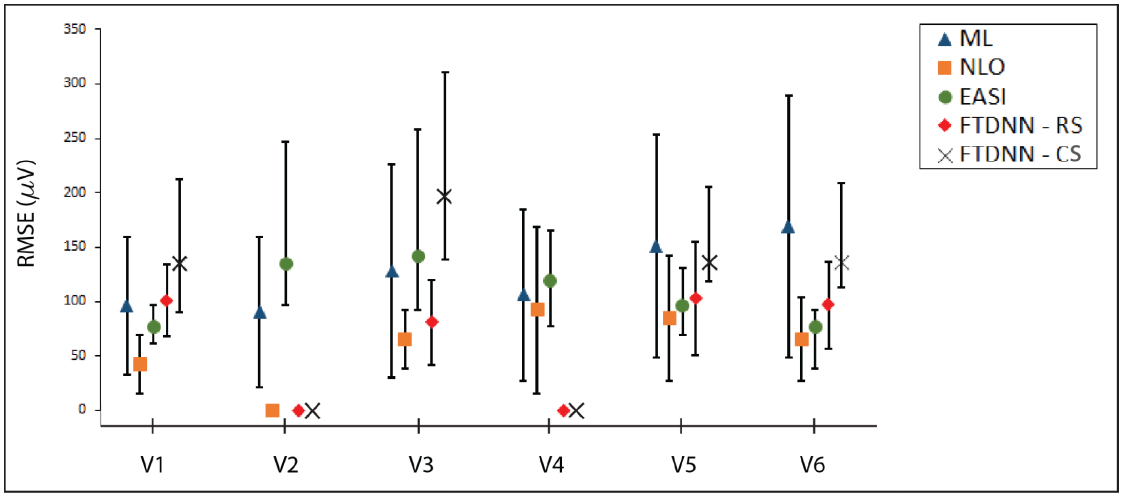

Figure 7.1: Illustration of the central tendency of the various lead reconstruction methods. The NLO and ML methods are represented using the mean RMSE bounded by standard deviation, whereas the EASI method, FTDNN retrospective study (FTDNN-RS) and FTDNN clinical study (FTDNN-CS) are represented using the median and quartile values.

The non-linear optimisation (NLO) method, produced by Schreck and Fishberg (2013), made use of the PTB database as well as one additional database. The current study made use of the same input leads, with the addition of V4. The NLO correlation values for leads V1, V3-V6 for all cases was 0.71 - 0.90, which exhibits slightly weaker correlation in comparison with the current study. However, the RMSE values of the NLO method were lower and compared favourably to that of the EASI leads, Mason Likar (ML) and the current study FTDNN reconstruction methods, on the same set of axes seen in Figure 7.1.

The EASI lead study performed by Nelwan *et al.* (2008) made use of non-standard lead placements based on the Frank leads to derive all 12 lead ECG. The FTDNN method performed better with respect to correlation results with slightly less favourable RMSE values. However, the EASI study consisted of only 44 male subjects all of which required a percutaneous coronary intervention (PCI) procedure. This limited the range of tested cardiovascular disease to men with acute coronary syndromes. The clinical value of vectorcardiography and the Frank lead system was an alternative lead placement system to the current traditional 12 lead ECG, however, since its inception 50 years ago, the method has become obsolete. This is due to the lack of existing education on the technology, placement and equipment. In contrast, the current study as well as Schreck and Fishberg (2013) made use of conventional 12-lead ECG placements.

Drew *et al.* (2004) performed the ML study which also made use of unconventional lead placements for two leads located in the vicinity of the traditional lead V3 and V4. The FTDNN retrospective study produced lower RMSE and higher correlation values with the FTDNN clinical study performing similar to the ML method with slightly higher central tenancy RMSE values and greater variance across the leads. The ML validation study reconstructed leads for pre-hospital ST segment monitoring, limiting the focus of the study to cardiac rhythm, prior infarction, ST/T wave changes and acute myocardial ischemia.

Tsouri and Ostertag (2014) made use of the same PTB database and exhibited high correlation between the reconstructed leads and the actual leads. The current FTDNN study displays the Pearson r correlation values which are closely related to the percentage correlation. In terms of correlation it can be deduced that the current study compares less favourably to that of Tsouri and Ostertag (2014). However, it is important to note that the FTDNN does not require past values of all the 12-leads for each patient, where Tsouri and Ostertag (2014) requires a calibration period in which data from all the leads are required, for a specific patient, before missing leads may be reconstructed. This would not be appropriate in situations in which only reduced lead ECGs are available. Specialists trained in placing the full 12 lead ECG would also be required to place the initial leads before they are removed, which is not desirable.

Chapter 8

Conclusion

8.1 Overview

This project aimed to achieve the research and development of a low-cost portable device capable of screening patients with potential cardiovascular disease in rural areas. The prototype device consisted of a six lead wire ECG and electronic stethoscope, operated using a LCD touchscreen. The ECG recorded the limb leads, augmented leads, and precordial leads V2 and V4 using the ADAS1000 ECG front-end. An electronic stethoscope recorded signals by virtue of the Panasonic WM-61A electret condenser microphone placed in close proximity to a standard stethoscope chestpiece. The signals were amplified using operational amplifier circuit and transmitted to the Raspberry Pi from the ADS1015. Ethical clearance was acquired to conduct the clinical study which took place at the Cardiology Department at Tygerberg Hospital. The test population included 66 subjects, 23 normal, 35 abnormal and 8 VNIP. The current cardiac condition of subjects was verified by a cardiologist using a 12 lead ECG recording, before being placed into the respective diagnostic class. Recordings were taken using both the developed hand-held device, as well as a full 12 lead control device. The machine learning classification and lead reconstruction algorithms were trained using ECG records obtained from the PTB online database and tested using data from the clinical trial. The recorded ECG signals were filtered and passed through a beat detection algorithm to extract first order, second order as well as unsupervised features from a SDAE. The feature set was classified using a DPRNN. The retrospective study produced a 12 lead ECG classification accuracy, sensitivity, specificity and AUC of 90%, 91%, 87% and 0.94, respectively. The clinical trial made use of all available six lead wires during the classification process and produced an accuracy, sensitivity, specificity and AUC of 85%, 83%, 87% and 0.85, respectively. The lead reconstruction was achieved using a FTDNN. Filtered signals were passed directly into the lead FTDNN in which leads V1,V3,V5 and V6 were reconstructed. The retrospective study produced a mean RMSE

range of between 101 and 128 μV and mean Pearson r correlation of 0.87 to 0.98. The clinical study produced a slightly higher mean RMSE of between 181 and 266 μV, and a mean Pearson r correlation of between 0.91 and 0.95. All reconstructed leads for both studies were statistically significant ($p \ll 0.01$) at a CI of 95%.

8.2 Objectives

The project objectives are summarised in Table 8.1. The only objective partially achieved was objective number three, due to the manufacturing cost of the developed portable device being slightly more expensive than the Echo Duo. However, it should be noted that the Echo Duo would require the use of a smartphone in order to operate, which would significantly increase the price in excess of the developed device. Bulk purchases of components and parts would further reduce the total price of the device, however, additional costs would include labour and shipment costs, as well as a selected profit margin.

Table 8.1: Objectives summary.

Objective	**Status**	**Description**
1. Develop a prototype that can record the heart's electrical signals and heart sounds.	Completed	The developed device accurately recorded the heart's electrical activity using a 6 lead-wire system as well as heart sounds using a stethoscope embedded with an electret condensor microphone.
2. The device should be portable and able to be used in rural locations.	Completed	The developed device is compact, battery powered and operated using a touch screen without the need for external peripherals.
3. The cost of the device should be cheaper than currently existing technology.	Partially Completed	The device total cost is significantly cheaper than ECG machines used at Tygerberg Hospital and the Cardio-Sleeve, but more expensive than the Echo Duo, at the current exchange rate.
4. Recorded signals should be plotted graphically and stored locally on the device.	Completed	Signals were stored locally on a Micro SD card and plotted in real-time on the LCD touchscreen.
5. The device should contain wireless data sharing capabilities.	Completed	The device is capable of sharing data using either Bluetooth or Wifi.
6. Record data and measurements during the testing of the prototype on test subjects.	Completed	Ethical clearance was granted in which 66 subjects consisting of 23 normal, 35 abnormal and 8 VNIP recordings.
7. The development of machine learning algorithms in patient diagnosis and ECG lead reconstruction.	Completed	A DPRNN classification, and FTDNN lead reconstruction algorithm, was trained using an online database and tested in the clinical trial.

8.3 Limitations

Due to the study requiring data from human subjects, ethical clearance was required in order to run the clinical trail. This placed additional time constraints on-top of the standard duration of the MEng degree. This influenced the amount of time available to gather samples and the overall population size. In order to accurately gather data both the developed device and the control device required the electrodes to be placed by a trained ECG technician or medical doctor. This study relied on electrode placements performed by trained ECG technicians and Dr. Titus at Tygerberg hospital. By using different personnel to place the electrodes, variability of electrode placement between experts is possible. The diagnosis of the patients used to test the classification algorithm required the experience of Dr. Weich, a trained cardiologist. However, the cardiologist relied solely on ECG recordings to determine the patient's current cardiac condition. In rare cases, cardiac abnormalities may not be immediately obvious in ECG recordings and may acquire additional tests such as auscultation, echocardiography and physical examinations. Albeit extremely rare, this could potentially lead to an incomplete diagnosis of patients used as the ground truths in the study. Due to the developed prototype being a reduced lead device, the lead reconstruction FTDNN had to be tested using the data acquired from the 12 lead control in order to generate RMSE and correlation values between the reconstructed leads and the actual leads. The use of machine learning algorithms such as neural networks for the classification and lead reconstruction presents a black-box approach, whereby functional relationships generated from input to output, within the neural networks, do not provide any insights into the structure of the relationship being approximated.

8.4 Future Recommendations

8.4.1 Prototpye Hardware and Software Design

An additional ADAS1000 module would allow the user to expand the available lead set to the full 12 lead ECG. This would allow the device to be operated as a gold standard 12 lead ECG in a clinical setting or a reduced lead portable device in rural settings. The addition of a DB15 female port would enable the use of a detachable ECG lead wires as well as a shielded cable which aids in the improvement of noise rejection. A more elegant, space saving method to power the prototype would be to use a single 3.7 V lithium iron battery with a DC boost module to increase the voltage to meet the 5 V requirement. This approach was explored during the development of the device, however, the recently released RPi model 3B required more current than previous models, with no appropriate boost modules available at the time. Recently an

updated DC boost module ("Powerboost 1000C" by Adafruit) was released for the latest RPi model. The use of a condenser microphone in the electronic stethoscope could be improved by active noise cancellation in which an additional external microphone record the ambient noise and subtracts this from the actual stethoscope recording. An additional potential design improvement would be the incorporation of the stethoscope in the base of the device case similar to the Eko Duo.

An additional software mode can be added to the GUI, allowing the simultaneous recording of both ECG and heartsounds. This could facilitate the previous work done by Botha (2010) and Visagie (2007) in which a combination of ECG and heart sounds features are used in the automated patient classification procedure. The use of cloud based computing could be introduced to centralise the signal processing and machine learning process, negating the reliance on available computers installed with the correct software being present during rural applications. The recorded ECG data could be programmed to display on the standard block grid paper, allowing the leads to be printed and analysed in the conventional manner most cardiologists are accustomed to.

8.4.2 ECG Classification and Lead Reconstruction

Improved interval classification features that were originally excluded, due to poor accuracy in the feature extraction process, have the potential to improve classification performance. Additionally, non-ECG related features, such as body weight, height, blood pressure, BMI, age and ethnicity could also be included as features in the classification process. The trade-off between RMSE and Pearson r correlation provides only a partial description of ECG lead reconstruction performance. Future studies conducted at Tygerberg Hospital will include the generation of reconstructed 12 lead ECG printouts using the FTDNN method, which will be assessed in a blind classification study performed by cardiologists, in order to test the feasibility of lead reconstruction.

8.5 Conclusion

A portable device was developed capable of recording the ECG and heart sounds. The developed device is cheaper than available products and capable of operation in a rural environment while maintaining a high quality of ECG recordings, comparable to that of established ECG devices. The device was successfully tested using a clinical study where the results obtained compare favourably with the initial retrospective study as well as prior research done in the field. The study successfully met the required aims and objectives as set out in the first chapter. This evidence supports the possibility of deploying a low-cost portable device in rural locations capable of referring patients with

potential cardiac abnormalities to hospitals for further examination. The use of a portable device with simple lead wire placement capable of autonomous diagnosis has the potential of transforming cardiovascular care for patients in rural locations.

Appendices

Appendix A

ECG Printed Circuit Board (PCB)

A.1 ADAS1000

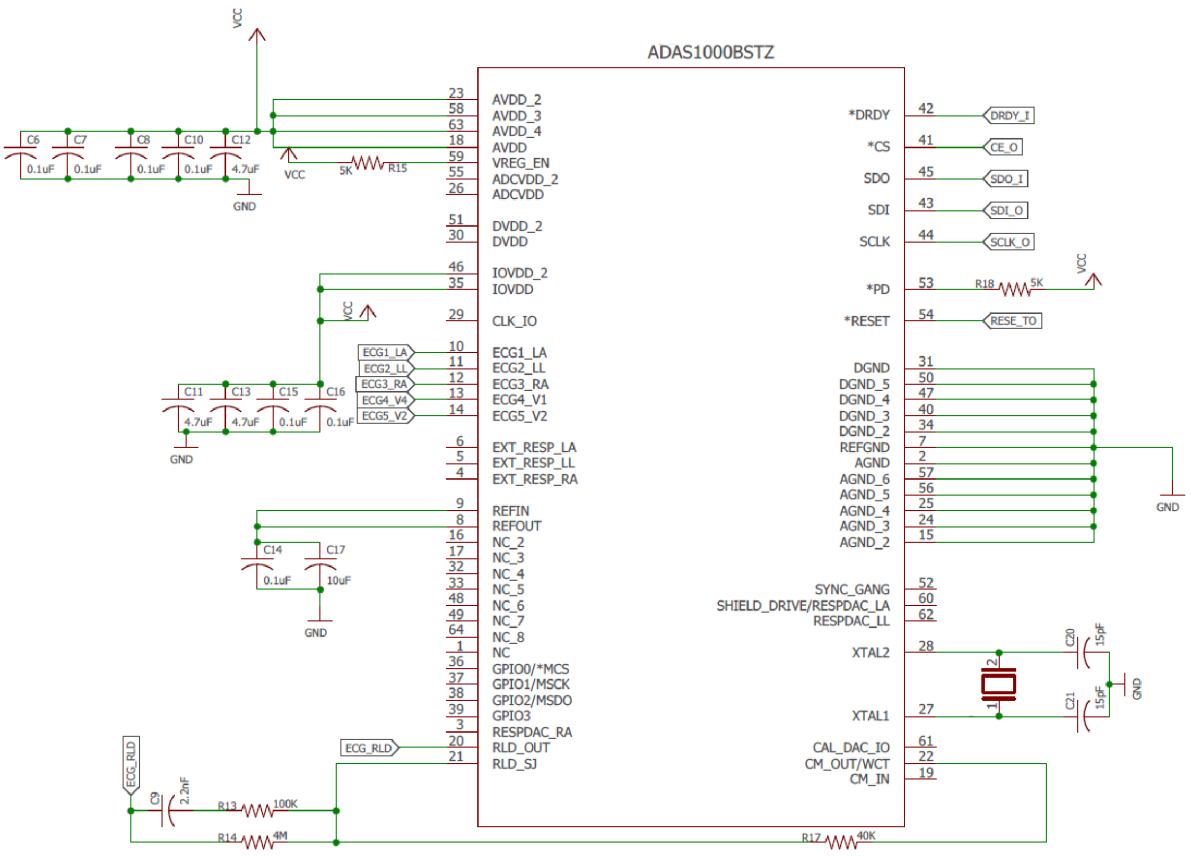

Figure A.1: Schematic for the ADAS1000 ECG front-end component (Abtahi *et al.*, 2014).

A.2 SP720

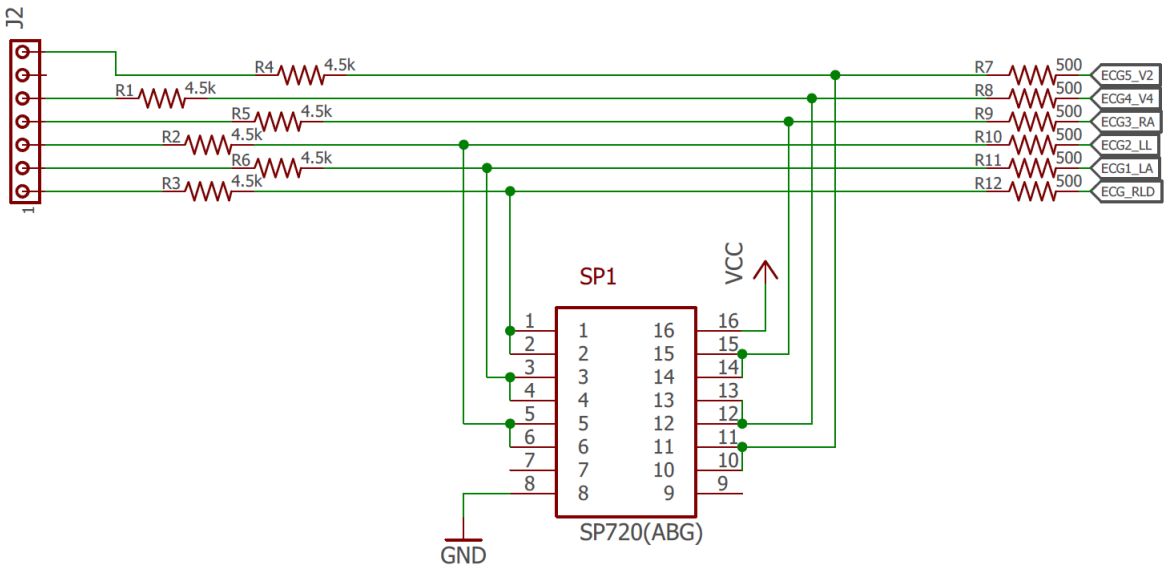

Figure A.2: Schematic for component SP720.

A.3 ADUM6400

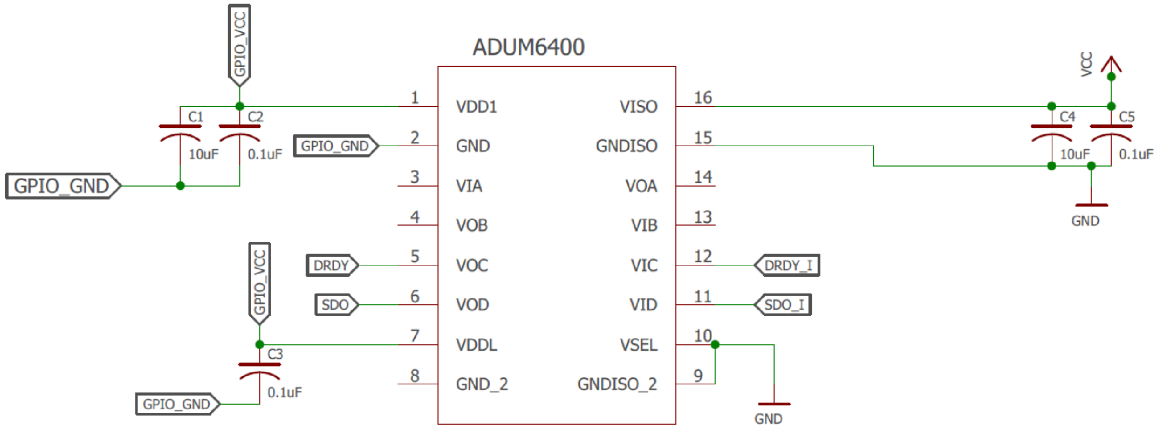

Figure A.3: Schematic for the ADUM6400 opto-coupler component (Abtahi *et al.*, 2014).

A.4 ADUM4400

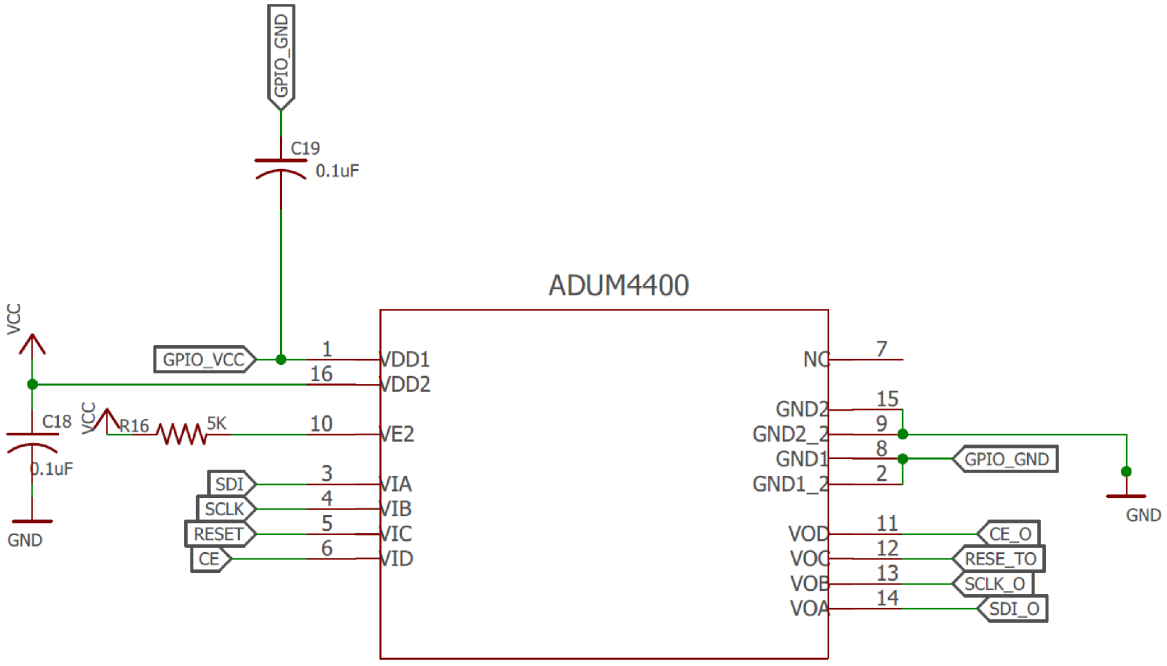

Figure A.4: Schematic for the ADUM4400 opto-coupler component (Abtahi *et al.*, 2014).

A.5 Raspberry Pi 3 Model B Pinout

Stethoscope VCC	01	3.3v DC Power		DC Power 5v	02	LCD VCC
Stethoscope SDA	03	GPIO02 (SDA1 , I²C)		DC Power 5v	04	ADAS GPIO_VCC
Stethoscope SCL	05	GPIO03 (SCL1 , I²C)		Ground	06	ADAS GPIO_GND
	07	GPIO04 (GPIO_GCLK)		(TXD0) GPIO14	08	
LCD GND	09	Ground		(RXD0) GPIO15	10	
	11	GPIO17 (GPIO_GEN0)		(GPIO_GEN1) GPIO18	12	
	13	GPIO27 (GPIO_GEN2)		Ground	14	Stethoscope GND
	15	GPIO22 (GPIO_GEN3)		(GPIO_GEN4) GPIO23	16	ADAS DRDY
	17	3.3v DC Power		(GPIO_GEN5) GPIO24	18	ADAS RESET
ADAS SDI	19	GPIO10 (SPI_MOSI)		Ground	20	
ADAS SDO	21	GPIO09 (SPI_MISO)		(GPIO_GEN6) GPIO25	22	
ADAS SCLK	23	GPIO11 (SPI_CLK)		(SPI_CE0_N) GPIO08	24	ADAS CE
	25	Ground		(SPI_CE1_N) GPIO07	26	
	27	ID_SD (I²C ID EEPROM)		(I²C ID EEPROM) ID_SC	28	
	29	GPIO05		Ground	30	
	31	GPIO06		GPIO12	32	
	33	GPIO13		Ground	34	
	35	GPIO19		GPIO16	36	
	37	GPIO26		GPIO20	38	
	39	Ground		GPIO21	40	

Figure A.5: Raspberry Pi model 3B pinout indicating the GPIO pins assigned to the ECG front-end, electronic stethoscope and the LCD touchscreen.

Appendix B

Design Analysis

B.1 Safety Analysis

B.1.1 Electrical Isolation and Insulation Layer

The current device is designed to be battery operated, however, there may be occasions where the RPi is to be connected to additional peripherals, such as monitors or printers, which require a mains power supply. It is therefore recommended that the device adheres to relevant electrical safety measures. Electrical safety of medical equipment is regulated by the International Electrotechnical Commission (IEC) 60601-1 and 60950, which defines necessary conditions to ensure the safety of patients, device operators, as well as the surrounding environment (Been *et al.*, 2007). This is achieved by means of proper electrical isolation and the use of opto-couplers.

Opto-couplers isolate sections of the PCB that are exposed to a high-voltage power supply while simultaneously allowing the transfer of signals to and from the isolated region. This allows for electrical separation (isolation) between the leads attached to patients and high voltage peripherals that may be attached to the RPi. The ADUM4400 and ADUM6403 were used in the optocoupler circuit (Figure B.1) (Abtahi *et al.*, 2014).

In addition to the optocoupler circuit, the PCB was manufactured with an insulated region, without copper, which runs under the optocouplers to the boundary of the PCB (Abtahi *et al.*, 2014). This separates the isolated region from the remainder of the PCB (Figure B.2) which prevents creepage current as advised by IEC 60601.

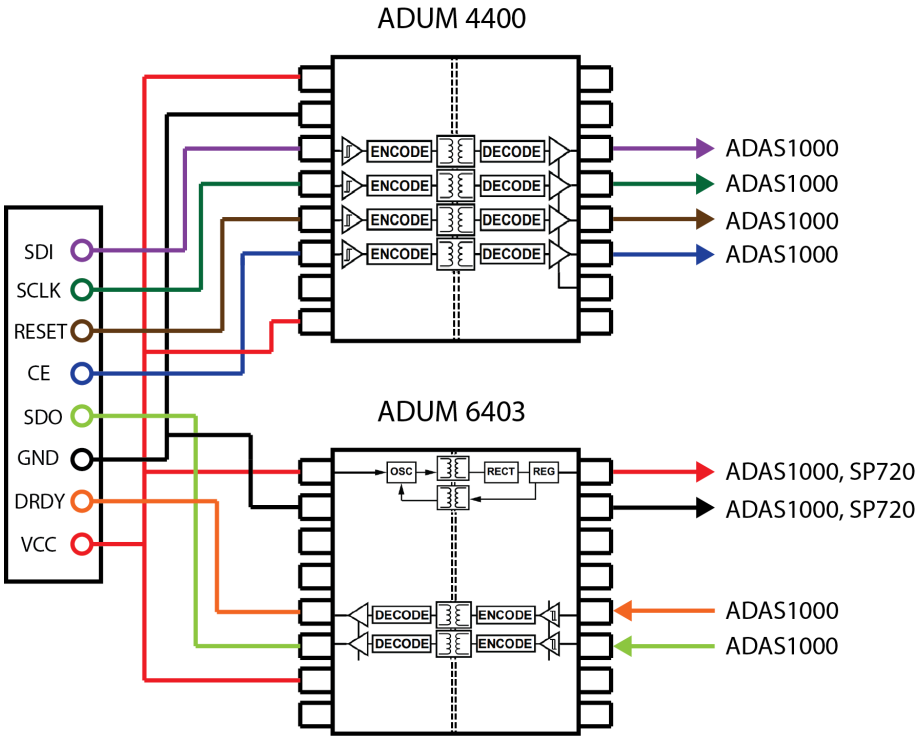

Figure B.1: Schematic indicating the signals to and from the RPi that cross the opto-couplers (ADUM4400 and ADUM6403) to the ADAS1000 and SP720.

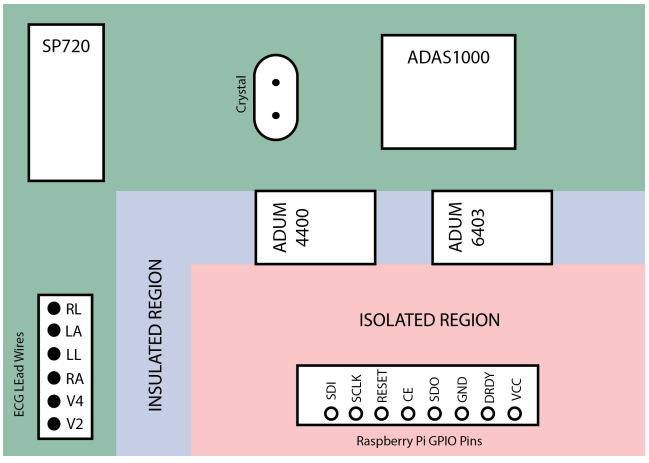

Figure B.2: Illustration of the PCB layout indicating the isolated region created by the opto-couplers as well as the manufactured insulated region (Abtahi *et al.*, 2014).

B.1.2 ECG Medical Devices Safety Standards

Table B.1: ECG medical device safety standards that were successfully adhered to by the prototype device (Abtahi *et al.*, 2014).

Standard	**Description**	**Provided by**
AAMI EC11	Diagnostic electrocardiographic devices	ADAS1000
AAMI EC38	Particular requirements for the safety, including essential performance, of ambulatory electrocardiographic systems	ADAS1000
AAMI EC13	Cardiac monitors, heart rate meters, and alarms	ADAS1000
IEC60601-1-1	General requirements for safety	ADAS1000 ADUM6403/6600
IEC60601-1-2	General requirements for basic safety and essential performance	PCB Design
IEC60601-2-25 IEC60601-2-27	Particular requirements for the basic safety and essential performance of electrocardiographic monitoring equipment.	ADAS1000
IEC60601-2-51	Particular requirements for safety, including essential performance, of recording and analysing single channel and multichannel electrocardiographs	ADAS1000
IEC61000	Protection against ESD and over-voltage	SP720 Insulation Barrier

B.2 Cost Analysis

Table B.2: Final cost for the hardware required to develop the prototype device.

Item	**Price**
ECG snap-on leads	R289.00
SP720 Diode protection	R31.15
ADAS1000 ECG Frontend	R547.54
ADUM4400 Optocoupler	R128.00
ADUM6400 Optocoupler	R282.00
Raspberry Pi 3 Model B	R567.00
LCD Touchscreen	R883.00
Protective Case	R318.00
Stethoscope	R2098.00
MCP6002 Operational amplifier	R5.32
Panasonic WM-61A Microphone	R30.00
ADS11015 A/D converter I2C module	R285.00
PCB Manufacturing	R118.33
Battery Pack	R424.00
Crystal Oscillator	R2.70
Resistors and Capacitors	R50.00
Total	**R6059.04**

Appendix C

Electronic Stethoscope Calculations

The necessary parameters required for the design of the microphone pre-amplifier circuit are represented in Table C.1. The design procedure follows steps laid out by Caldwell (2015).

Table C.1: Technical specifications of the Panasonic WM-61A microphone.

Parameter	Value
Sensitivity	35 ± 4 dBV
Standard Operating Voltage	2V
Maximum Current Consumption	0.5 mA
Maximum Impedance	2.2 kΩ
Minimum Signal to Noise Ratio	62 dB

The microphone sensitivity value is provided as a decibel value relative to a unit volt (1 V), measured at 1 Pascal, or 94 dB sound pressure level (SPL). This value is converted to a linear value in volts per Pascal of air pressure

$$10^{\frac{-35dB}{20}} = 17,78 \text{ mV/Pa} \tag{C.1}$$

This value is converted to current per Pascal of air pressure using the maximum impedance value in Table C.1, as it can be assumed that this value was used to measure the microphone sensitivity.

$$\frac{17,78\ mv/Pa}{2,2\ k\Omega} = 8,08\ \mu\text{A/Pa} \tag{C.2}$$

The calculated microphone gain is influenced by the maximum expected sound pressure level recorded by the microphone. It is assumed that the maximum sound pressure level is 100 dB SPL, which is 2 Pa of air pressure, providing an output current of

$$\frac{8.083\mu A}{Pa} \times 2Pa = 16,17\ \mu\text{A} \tag{C.3}$$

This allows the value of R2 to be calculated as

$$R2 = \frac{V_{Out}}{I_{Out}} = \frac{1,228\ V}{16,17\ \mu A} = 75,96\ \text{k}\Omega \tag{C.4}$$

where V_{Out} is selected as 1.228 VRMS which is a typical value for line level audio levels. The capacitor C2 provides stability against parasitic capacitance produced by the inverting operational amplifier. The capacitor also creates a pole with resistor R2 in which the frequency value of the pole is required to be large enough to avoid interference with the microphone's audible bandwidth. A response deviation of -0,1 dB at 20 kHz was selected as an acceptable value resulting in the calculation of the pole as

$$f_p = \frac{f}{\sqrt{(\frac{G_0}{G_f})^2 - 1}} = \frac{20\ kHz}{\sqrt{(\frac{1}{0,989})^2 - 1}} = 133,73\ \text{kHz} \tag{C.5}$$

where G_0 and G_f represent the gains at low frequency and at frequency f, respectively. Selecting 20 kHz for f, and 0,989 (-0,1 dB) for G_f, results in a pole at 133,73 kHz. The value for C2 is calculated as

$$C2 = \frac{1}{2\pi f_p R_2} = \frac{1}{2\pi(133,73\ kHz)(75\ k\Omega)} = 15,87\ \text{pF} \tag{C.6}$$

The microphone is biased using resistor R1 which can be calculated using the supply voltage (V_{CC}), the maximum operating voltage (V_{OP}) and the maximum current consumption (I_c), provided by Table C.1

$$R1 = \frac{V_{CC} - V_{OP}}{I_c} = \frac{3,3\ V - 2\ V}{0,5\ mA} = 14\ \text{k}\Omega \tag{C.7}$$

The capacitor C1 creates a high pass filter with R1 in which the corner frequency must avoid attenuating low frequency sound waves. A 5 Hz corner frequency is selected and the value of C1 is calculated as

$$C1 = \frac{1}{2\pi f_c R_1} = \frac{1}{2\pi(5\ Hz)(14\ k\Omega)} = 2,32\ \mu\text{F} \tag{C.8}$$

The resistor pair, R_3 and R_4, center the output voltage at the midpoint between V_{CC} and ground to provide the largest possible output signal swing. Large resistor values of 100 kΩ, where $R_3 = R_4$, were selected to limit the

current resulting in $V_B = V_{CC}/2$ (1,65 V). The capacitor C3 is provided to eliminate thermal noise created by the resistors as well as noise created from the power supply. A value of 2.2 μF for capacitor C3 is sufficient to provide a low pass filter with the corner frequency of

$$f_c = \frac{1}{2\pi(R_3 \parallel R_4)C_3} = \frac{1}{2\pi(100\ k\Omega \parallel 100\ k\Omega)2.2\mu F} = 1,48\ \text{Hz} \tag{C.9}$$

The gain of the pre-amplifier circuit is calculated as

$$A_N = 1 + \frac{R_2}{R_1} = 1 + \frac{75,96\ k\Omega}{14\ k\Omega} = 6,43 \tag{C.10}$$

The calculated gain was too large for the low supply voltage resulting in the operational amplifier saturating when the signal approached V_{CC} and ground. Therefore, a lower value of R2 was selected to reduce the gain. The final values of the components can be seen in Table C.2.

Table C.2: Final values of the components used in the pre-amplifier circuit.

Components	**Value**
R1	15 kΩ
R2	56 kΩ
R3	100 kΩ
R4	100 kΩ
C1	2.2 μF
C2	15 μF
C3	2.2 μF

Appendix D

Serial Communication

D.1 Serial Peripheral Communication Protocol

D.1.1 Introduction to SPI

Serial Peripheral Communication (SPI) is a serial interface bus commonly used to digitally transfer data between microcontrollers and various peripheral devices, such as sensors (Grusin, 2017). The SPI protocol consists of a master-slave architecture, in which one master device controls communication with one or more slave devices, by initiating read and write commands (Bai, 2016). With regards to the hand-held portable device, the Rapberry Pi is the master and the ADAS1000 ECG frontend is the slave (Figure D.1).

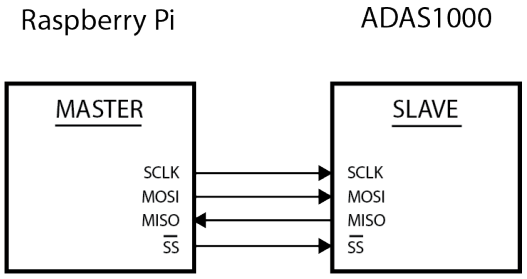

Figure D.1: SPI communication between the Raspberry Pi (master) and the ADAS1000 (slave).

The SPI protocol makes use of 4 signal lines, a clock signal (SCLK), "Master Out - Slave In" (MOSI), "Master In - Slave Out" (MISO) and "Slave Select" (SS). The SPI protocol is a synchronous data bus where information is transmitted continuously at a constant rate using separate data and clock lines (Cowley, 2012). The oscillating clock signal ensures that transmission and reception is kept in-sync, with bits on the data line being sampled at either the rising or falling clock edge (Grusin, 2017). In the event that a master

communicates with multiple slaves, the master will identify the specific slave it wishes to communicate with by setting the SS line low. This disconnects the slave from the serial bus, ultimately activating the slave which is now expecting to receive data. The SS line makes use of "active low" logic in which it is enabled by setting the signal low. To initiate a read or write command, the master device sets the SS line low, triggering the SCLK line to oscillate, allowing the transmission of data from the master to the slave on the MOSI line. In the event that data is read from the slave, the master device sends the "read command" on the MOSI line, while simultaneously sampling the received signal from the slave on the MISO line. When communication with the specific slave is complete, the SS line is set high again (Figure D.2).

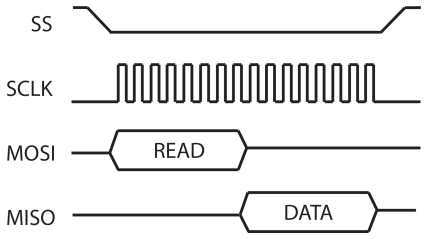

Figure D.2: SPI signal and data transmission diagram.

D.1.2 ADAS1000 SPI Registers

Table D.1: Writing to a ADAS1000 register.

Write command	R/W	Register Address	Data
0X85E0000A	1	0000101	11100000000000000001010

Table D.2: ADAS1000 register addresses and header bytes.

Register	Header	Lead I	Lead II	Lead III	V2	V4
Address	0x40	0x11	0x12	0x13	0x14	0x15

D.2 Inter-Intergrated Circuit Protocol

D.2.1 Introduction to I2C

The I2C protocol consists of a master-slave architecture, similar to that of SPI, in which the RPI initiates read and write commands with the ADS1015 of the electronic stethoscope. The key difference between SPI and I2C communication, is the latter only requires two signal lines, a serial clock (SCL)

and a serial data (SDA) line, which are connected to "VCC" through pull-up resistors (Figure D.3).

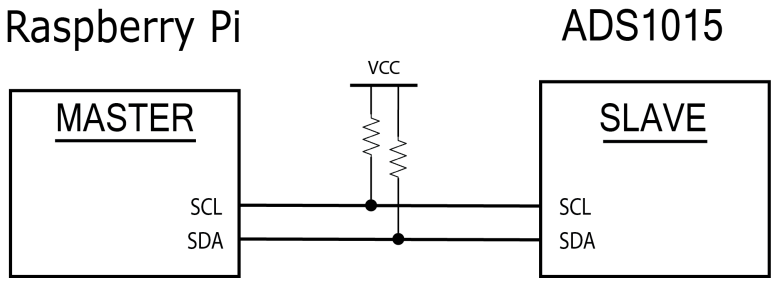

Figure D.3: I2C communication between the Raspberry Pi (master) and the ADS1015 (slave).

Communication between the master and the slave is initiated and completed by the master, which triggers a start or stop condition. Initially the bus is in an idle state, characterised by both the SDA and SCL lines floating high. The start condition is initiated by the master pulling the SDA line low, after which data is transmitted. Communication is terminated when the master brings the SDA line high. A single data bit is transmitted on the SDA line during each clock pulse on the SCL line, where one byte consists of eight bits in which the Most Significant Bit (MSB) is sent first. A byte may correspond to a device address, register address, or data that is written to or read from a slave device. After the transmission of each byte, an acknowledge (ACK) bit, or not acknowledge (NACK) bit, is transmitted from the slave to the master to indicate whether the byte was successfully received. This is achieved by the slave pulling the SDA line low during the 9th clock cycle, which represents a successful transmission (ACK) of a byte. In the event that the ACK/NACK bit is high during the 9th clock cycle, this indicates that the byte failed to be transmitted successfully resulting in a NACK occurring (Figure D.4). A NACK could be due to many factors such as the slave receiving data or commands that it does not understand or the slave is unable to receive additional bytes (Valdez and Becker, 2015).

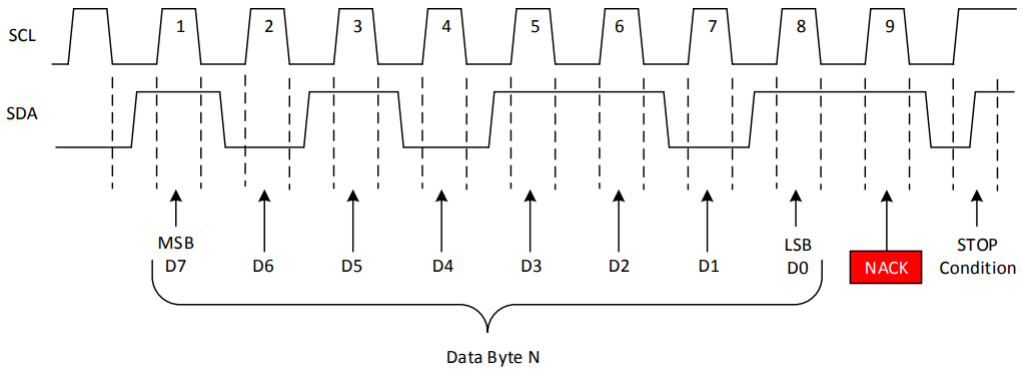

Figure D.4: I2C master transmission procedure (Valdez and Becker, 2015).

In order to send or receive data, the master must initiate a read or write command to, or from, registers in the slave device. The term register refers to locations in the slave's memory which contains the required sampled data that is sent to the master. The master is required to write commands to the slave register address in order to instruct the slave to perform required tasks. The master triggers the start condition, followed by the slave's address and R/W bit, set to 0, to indicate a write command. The slave sends the acknowledge bit to indicate the data was sent successfully. The master responds by sending the data of the register to the slave device that it wishes to communicate with. This is followed by the ACK bit, sent from the slave device, indicating that the slave is ready for transmission. The master responds by sending data to be written to the slave's register, followed by the ACK bit from the slave. The stop condition from the master terminates the transmission (Valdez and Becker, 2015). This process is illustrated in Figure D.5.

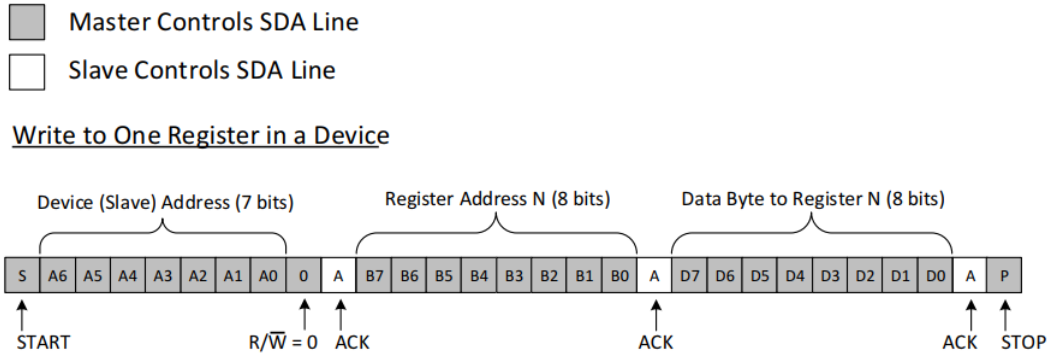

Figure D.5: I2C communication procedure with slave registers (Valdez and Becker, 2015).

Reading from the slave occurs in a similar manner to the writing process. The master informs the slave which register it intends to read from by issuing a

standard write command. Once the master has sent the slave and register address, the master triggers a repeated start condition followed by the slaves register, with the R/W bit set to 1, indicating a read command. The slave sends the ACK bit indicating it is ready to transmit data to the master. The master responds by releasing the SDA line which the slave uses to transmit data to the master. The master transmits the ACK bit to the slave after each byte, indicating it is ready for more data. Once the master has received all the expected data it issues a NACK, followed by the stop condition, in order to terminate the transmission (Valdez and Becker, 2015). This process is illustrated in Figure D.6.

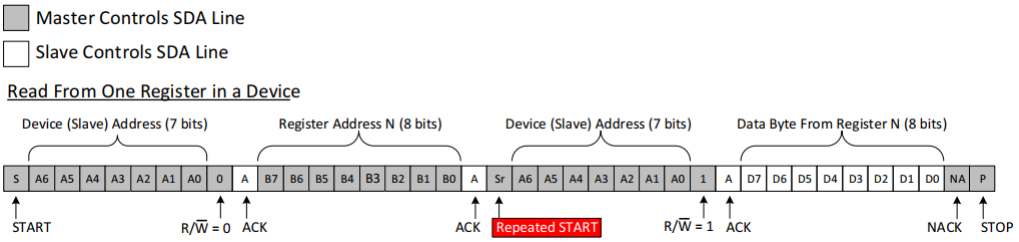

Figure D.6: I2C read procedure from slave registers (Valdez and Becker, 2015).

D.2.2 ADS1015 I2C Registers

Table D.3: The I2C specification for interfacing with the ADS1015.

ADS1015 I2C Specifications	
Slave Address	0X48
CONFIG Register	0X01C3C3

Appendix E

Clinical Study

E.1 Sample Size Calculation

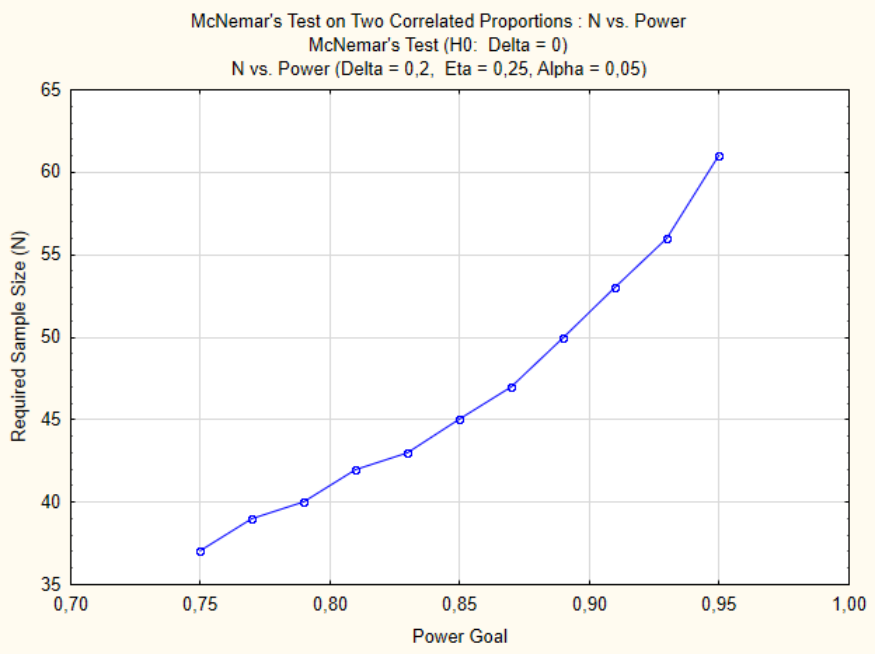

Figure E.1: McNemar's test indicating the relationship between the required sample size and the desired power.

E.2 Ethical Clearance Documentation

UNIVERSITEIT
STELLENBOSCH
UNIVERSITY

Approved

New Application

Ethics Reference #: 0579

Title: Assessing the diagnostic outcomes of the 5 cable ECG prototype

Dear Gideon Titus

The **New Application** received on 12/07/2017 07:36 , was reviewed by members of the **Undergraduate Research Ethics Committee** via Minimal Risk Review procedures on 12 September 2017 and was approved.

Please note the following information about your approved research protocol:

Protocol approval period: This project has been approved for a period of one year from the date of this approval letter.

Please remember to use your **protocol number** (0579) on any documents or correspondence with the HREC concerning your research protocol.

Please note that this decision will be ratified at the next HREC full committee meeting. HREC reserves the right to suspend UREC approval and to request changes or clarifications from student applicants. The UREC coordinator will notify the applicant (and if applicable, the supervisor) of the changes or suspension within 1 day of receiving the notice of suspension from HREC. HREC has the prerogative and authority to ask further questions, seek additional information, require further modifications, or monitor the conduct of your research and the consent process.

After Ethical Review:

Please note a template of the progress report is obtainable on https://applyethics.sun.ac.za/Project/Index/641 and should be submitted to the Committee before the year has expired. The Committee will then consider the continuation of the project for a further year (if necessary). Annually a number of projects may be selected randomly for an external audit.

Translation of the consent document to the language applicable to the study participants should be submitted.

Federal Wide Assurance Number: 00001372

Institutional Review Board (IRB) Number: IRB0005239

The Health Research Ethics Committee complies with the SA National Health Act No.61 2003 as it pertains to health research and the United States Code of Federal Regulations Title 45 Part 46. This committee abides by the ethical norms and principles for research, established by the Declaration of Helsinki, the South African Medical Research Council Guidelines as well as the Guidelines for Ethical Research: Principles Structures and Processes 2015 (Department of Health).

Provincial and City of Cape Town Approval

Please note that for research at a primary or secondary healthcare facility permission must still be obtained from the relevant authorities (Western Cape Department of Health and/or City Health) to conduct the research as stated in the protocol. Contact persons are Ms Claudette Abrahams at Western Cape Department of Health (healthres@pgwc.gov.za Tel: +27 21 483 9907) and Dr Helene Visser at City Health (Helene.Visser@capetown.gov.za Tel:+27 21 400 3981). Research that will be conducted at any tertiary academic institution requires approval from the relevant hospital manager. Ethics approval is required BEFORE approval can be obtained from these health authorities.

We wish you the best as you conduct your research.

For standard HREC forms and documents please visit: https://applyethics.sun.ac.za/Project/Index/641

If you have any questions or need further assistance, please contact the HREC office at 0219389207.

Sincerely,

Debbie Marais

UREC Coordinator

Undergraduate Research Ethics Committee

INVESTIGATOR RESPONSIBILITIES

Protection of Human Research Participants

Some of the responsibilities investigators have when conducting research involving human participants are listed below:

1. Conducting the Research: You are responsible for making sure that the research is conducted according to the HREC approved research protocol. You are also responsible for the actions of all your co-investigators and research staff involved with this research.

- Participant Enrolment: You may not recruit or enrol participants prior to the HREC approval date or after the expiration date of HREC approval. All recruitment materials for any form of media must be approved by the HREC prior to their use. If you need to recruit more participants than was noted in your HREC approval letter, you must submit an amendment requesting an increase in the number of participants.
- Informed Consent:You are responsible for obtaining and documenting effective informed consent using **only** the HREC approved consent documents, and for ensuring that no human participants are involved in research prior to obtaining their informed consent. Please give all participants copies of the signed consent documents. Keep the originals in your secured research files for at least fifteen (15) years.
- Continuing Review:The HREC must review and approve all HREC approved research protocols at intervals appropriate to the degree of risk but not less than once per year. There is **no grace period**. Prior to the date on which the HREC approval of the research expires, **it is your responsibility to submit the continuing review report in a timely fashion to ensure a lapse in HREC approval does not occur.** If HREC approval of your research lapses, you must stop new participant enrolment, and contact the HREC Office immediately.
- Amendments and Changes:If you wish to amend or change any aspect of your research (such as research design, interventions or procedures, number of participants, participant population, informed consent document, instruments, surveys or recruiting material), you must submit the amendment to the HREC for review using the current Amendment Form. You **may not initiate** any amendments or changes to your research without first obtaining written HREC review and approval. The **only exception** is when it is necessary to eliminate apparent immediate hazards to participants and the HREC should be immediately informed of this necessity.
- Adverse or Unanticipated Events:Any serious adverse events, participant complaints, and all unanticipated problems that involve risks to participants or others, as well as any research-related injuries, occurring at this institution or at other performance sites must be reported to the HREC within **five (5) days** of discovery of the incident. You must also report any instances of serious or continuing problems, or non-compliance with the HREC's requirements for protecting human research participants. The only exception to this policy is that the death of a research participant must be reported in accordance with the Stellenbosch University Health Research Ethics Committee Standard Operating
Procedures www.sun25.sun.ac.za/portal/page/portal/Health_Sciences/English/Centres%20and%20Institutions/Research_Development_Support/Ethics/Application_package. All reportable events should be submitted to the HREC using the Serious Adverse Event Report Form.
- Research Record Keeping: You must keep the following research-related records, at a minimum, in a secure location for a minimum of fifteen years; the HREC approved research protocol and all amendments; all informed consent documents; recruiting materials; continuing review reports; adverse or unanticipated events; and all correspondence from the HREC.
- Reports to the MCC and Sponsor: When you submit the required annual report to the MCC or you submit a required report to your Sponsor, you must provide a copy of that report to the HREC. You may submit the report at the time of continuing HREC review.
- Provisions of Emergency Medical Care: When a physician provides emergency medical care to a participant without prior HREC review and approval, to the extent permitted by law, such activities will not be recognized as research nor will the data obtained by any of such activities be used in support of research.
- Final Reports: When you have completed (no further participant enrolment, interactions, interventions or data analysis) or stopped work on your research, you must submit a Final Report to the HREC.
- On-Site Evaluations, MCC Inspections, or Audits: If you are notified that your research will be reviewed or audited by the MCC, the Sponsor, any other external agency or any internal group, you must inform the HREC immediately of the impending audit/evaluation.

Appendix F

Algorithms

F.1 Wavelet Beat and Peak Detection

The wavelet delineation algorithm developed by Martínez *et al.* (2004) works in 5 phases:

1. QRS complex detection
2. Identification of the individual Q, R and S waves within the QRS complex
3. Determination of the onset and offset of the QRS complex
4. P wave detection and onset and offset delineation
5. P wave detection and onset and offset delineation

The algorithm pseudo-code implementation can be described using the following procedure:

(i) The maximum moduli are identified across the scales when the magnitude of the wavelet transform exceeds the thresholds

$$\varepsilon^i_{QRS} = \mathrm{RMS}(W^i_2 s[n]), \quad i = 1, 2, 3 \tag{F.1}$$

$$\varepsilon^4_{QRS} = 0.5\,\mathrm{RMS}(W^4_2 s[n]), \quad i = 1, 2, 3 \tag{F.2}$$

for scales 2^1 to 2^4.

(ii) All identified maximum moduli are analysed, rejecting any isolated or redundant moduli.

(iii) The QRS complex is identified as the zero crossing between either a maximum - minimum, or minimum - maximum pair at scale 2^1.

(iv) If a QRS complex has not been successfully identified after an extended period of time, reduce threshold values and return to step (i).

(v) The algorithm identifies significant slopes within the QRS complex that exceed the thresholds

$$\gamma_{QRS\_pre} = 0.06 \max(|W_2^2 s[n]|), \quad n \in SW_{QRS} \tag{F.3}$$

$$\gamma_{QRS\_post} = 0.09 \max(|W_2^2 s[n]|), \quad n \in SW_{QRS} \tag{F.4}$$

for previous and subsequent waves, where SW refers to a search window. The significant waves crossing at scale 2^1 are wave peaks and are labelled (Q, R or S) according to the sign and sequence of the maximum moduli.

(vi) The QRS wave onset and offset is identified as the first and last significant slope of the QRS, respectively, located with respect to the positions of the first (n_{first}) and last significant QRS wave (n_{last}). The onset and offset positions are identified as either the position in which $W_2^2 s[n_n]$ is below the thresholds ξ_{QRSon} or ξ_{QRSend}, or the local minimum for $W_2^2 s[n_n]$ before n_{first} or after n_{last}, with closest point to the QRS identified as the QRS onset and offset respectively.

$$\xi_{QRSon} = \begin{cases} 0.05\, W_2^2 s[n_{first}], & \text{if } W_2^2 s[n_{first}] > 0 \\ 0.07\, W_2^2 s[n_{first}], & \text{if } W_2^2 s[n_{first}] < 0 \end{cases} \tag{F.5}$$

$$\xi_{QRSend} = \begin{cases} 0.125\, W_2^2 s[n_{last}], & \text{if } W_2^2 s[n_{last}] > 0 \\ 0.71\, W_2^2 s[n_{last}], & \text{if } W_2^2 s[n_{last}] < 0 \end{cases} \tag{F.6}$$

(vii) A search window for the P wave is located before the onset of the QRS and is calculated using the RR interval. Within the window a local maximum is identified for $W_2^4 s[n_n]$. If two significant waves exceeds threshold

$$\varepsilon_P = 0.02\, \mathrm{RMS}(W_2^4 s[n]) \tag{F.7}$$

then a P wave is present where the peak is identified as the zero crossing between the two waves at scale 2^3. A wave is considered to be significant if it exceeds the threshold

$$\gamma_P = 0.125 \max(|W_2^4 s[n]|), \quad n \in SW_P \tag{F.8}$$

(viii) In the event that a P wave is not successfully identified in step (vii), repeat the step at scale 5 ($|W_2^5 s[n]|$).

(ix) The onset and offset follows the same procedure with the thresholds identified as

$$\xi_{Pon} = 0.5\, W_2^4 s[n_{first}] \tag{F.9}$$

$$\xi_{Pend} = 0.9\, W_2^4 s[n_{last}] \tag{F.10}$$

which are applied at the scale in which the P wave is detected.

(x) Steps (vii)-(ix) are repeated when identifying the T wave in which the search window occurs after the QRS offset, and the corresponding thresholds are used

$$\varepsilon_T = 0.25\, \mathrm{RMS}(W_2^4 s[n]) \tag{F.11}$$

$$\gamma_T = 0.125 \max(|W_2^4 s[n]|), \quad n \in SW_T \tag{F.12}$$

$$\xi_{Ton} = 0.25\, W_2^4 s[n_{first}] \tag{F.13}$$

$$\xi_{Tend} = 0.4\, W_2^4 s[n_{last}] \tag{F.14}$$

F.2 Backpropogation

The conventional backpropagation algorithm is a gradient descent algorithm where the neuron weights are adjusted with the negative value of the calculated gradient of the cost function. Initially, all the neuron and bias weights are pre-initialised to random values. The input values, $x(i)$, are propagated forward through the layers of the network until the cost function, J, is calculated for the output layer using the hypothesis function, $h_\theta(x)$, and the actual output, $y(i)$. The value of the cost function is then propagated backwards, updating the values of the individual weights corresponding to each neuron in each layer.

The weight between the corresponding neuron p in the previous layer, h-1, and neuron j in the layer q is represented as θ_q^h (Theodoridis and Koutroumbas, 1999). The vector containing all the individual weights at neuron q in layer h are represented as $\Theta_q^h = [\theta_{q0}^h, \theta_{q1}^h, \theta_{q2}^h ... \theta_{qn_{h-1}}^h]^T$ where n_{h-1} is the total number of neurons in the previous layer $h-1$. During each iteration the weight vector containing the individual neuron weights is updated by

$$\Theta_q^h = \Theta_q^h - \Delta\Theta_q^h \tag{F.15}$$

where $\Delta\Theta_q^h$ is the correction term used to update the values of the weights calculated as

$$\Delta\Theta_h^q = \sum_{i=1}^{N} \delta_q^h(i) y^{h-1}(i) \tag{F.16}$$

In order to compute the correction term, the individual correction terms δ_q^{h-1} for layers $h = L, L-1, L-2, ...2$ (excluding the input layer h=1) and neurons $q = 1, 2, 3, ...n_h$ are calculated using the equation:

$$\delta_q^{h-1} = e_j^{h-1}(i) h_\theta'^{h-1}(x(i)) \tag{F.17}$$

where, $h_\theta'^{L}(x(i))$, is the derivative of the transfer function, $h_\theta^L(x(i))$, and $er_j^{h-1}(i)$ is calculated as

$$er_q^{h-1}(i) = \sum_{p=1}^{nr} \delta_p^{h-1}(i) \theta_p^{h-1}(i) \tag{F.18}$$

Appendix G

Additional Methods

G.1 Precordial Lead Selection

Table G.1: Mean RMSE μV using a different single individual precordial leads as input to the FTDNN lead reconstruction method

		Reconstructed leads				
Input Lead	V1	V2	V3	V4	V5	V6
V1	-	227	306	292	195	134
V2	137	-	164	215	187	138
V3	185	185	-	159	188	132
V4	234	350	225	-	159	131
V5	315	546	461	257	-	90
V6	335	592	531	344	129	-

Table G.2: Mean Pearson r correlation using a different single individual precordial leads as input to the FTDNN lead reconstruction method

		Reconstructed leads				
Input Lead	V1	V2	V3	V4	V5	V6
V1	-	0.93	0.81	0.76	0.90	0.93
V2	0.97	-	0.95	0.87	0.91	0.92
V3	0.93	0.90	-	0.95	0.91	0.92
V4	0.84	0.78	0.86	-	0.94	0.93
V5	0.70	0.43	0.42	0.79	-	0.96
V6	0.66	0.36	0.20	0.60	0.93	-

Table G.3: The average classifier results for all the limbs leads including one precordial leads across the 7 folds.

	K-Fold Mean Results		
Single Precordial Lead	Accuracy (%)	Sensitivity (%)	Specificity (%)
V1	86	87	85
V2	87	88	85
V3	86	87	84
V4	85	85	87
V5	87	87	87
V6	86	86	85

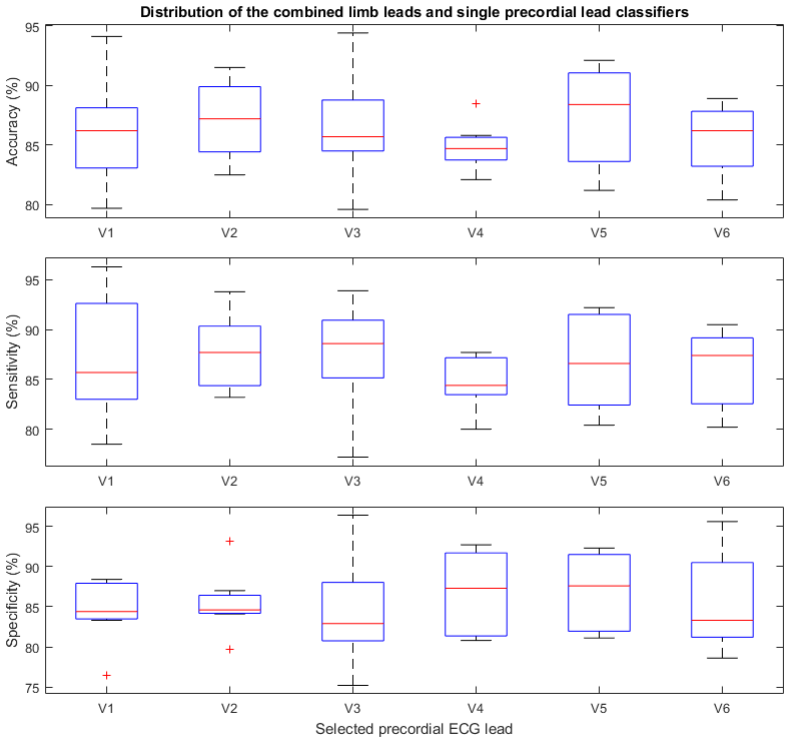

Figure G.1: Box and whisker diagram indicating the classification accuracy, sensitivity and specificity of the combined limb leads and single precordial ECG lead classifier.

G.2 Classifier feature selection

Table G.4: Initial classifier accuracy, sensitivity and specificity for supervised, unsupervised and combined feature sets.

	Supervised			Unsupervised			Combined		
Leads	Acc.	Sens.	Spec.	Acc.	Sens.	Spec.	Acc.	Sens.	Spec.
I	76%	78%	70%	77%	79%	75%	85%	84%	88%
II	72%	75%	63%	76%	79%	67%	85%	87%	79%
III	73%	74%	65%	71%	73%	65%	76%	78%	69%
avR	79%	82%	70%	77%	79%	72%	85%	86%	84%
avL	77%	81%	63%	78%	80%	70%	82%	81%	83%
avF	72%	76%	61%	74%	76%	70%	79%	81%	71%
V1	72%	74%	68%	76%	79%	65%	80%	81%	74%
V2	73%	75%	67%	72%	74%	63%	78%	79%	75%
V3	72%	73%	67%	70%	71%	67%	75%	77%	71%
V4	75%	76%	72%	76%	76%	73%	81%	82%	79%
V5	74%	78%	75%	76%	76%	73%	85%	85%	86%
V6	77%	78%	74%	75%	75%	78%	85%	84%	89%

Appendix H

Additional Results

H.1 Classification Network Architecture

The various neural network architectures discussed in Section 6.1.1 is represented in Table H.1. The values in brackets represent the number of neurons pertaining to the specific layer. The input and output layer are a single layer each, whereas the hidden layer sizes vary in dimension from between 3 and 5 across the different number of input leads presented to the classifier. The number of input neurons corresponds to the dimension of the input features and the output layer corresponds to the number of classification classes.

Table H.1: DPRNN classifier architecture for the various input leads.

Classifier	**Input Layer**	**Hidden Layers**	**Output Layer**
Single Lead	[45]	[40-20-10]	[2]
All Limb Leads	[296]	[250-100-50-20]	[2]
All limb Leads + Single Precordial Lead	[303]	[250-100-50-20]	[2]
All limb Leads + Two Precordial Leads	[346]	[280-150-50-20]	[2]
Full 12 Lead ECG	[518]	[500-300-200-100-10]	[2]

Table H.2: The classification outputted probability scores of a single test subject classified as exhibiting abnormal cardiac function.

Beats	**Probability**
1	[0.95, 0.05]
2	[0.93, 0.07]
3	[0.94, 0.06]
4	[0.93, 0.07]
5	[0.93, 0.07]
6	[0.90, 0.10]
7	[0.93, 0.07]
8	[0.92, 0.08]
9	[0.91, 0.09]
10	[0.90, 0.10]
11	[0.91, 0.09]
12	[0.93, 0.07]
Average	[0.92, 0.08]

H.2 Lead Reconstruction

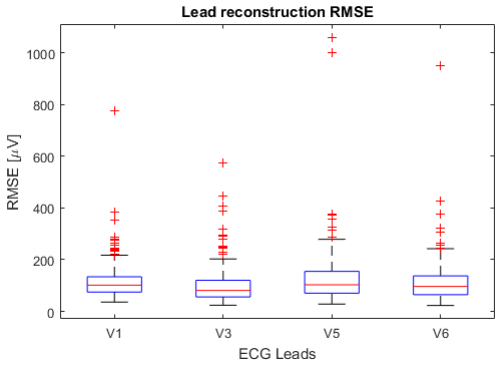

Figure H.1: Retrospective study box and whisker diagram indicating the RMSE error for the reconstructed leads.

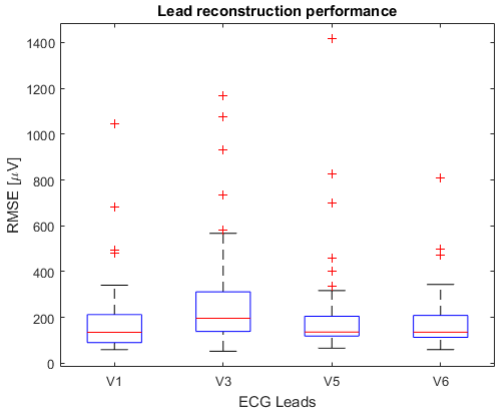

Figure H.2: Clinical study box and whisker diagram indicating the RMSE error for the reconstructed leads.

H.3 Classification

H.3.1 Single Leads

Table H.3: The retrospective study average classifier results for the individual ECG leads across the 7 folds.

	K-Fold Mean Results		
Leads	Accuracy (%)	Sensitivity (%)	Specificity (%)
I	85	84	88
II	85	87	79
III	76	78	69
avR	85	86	84
avL	82	81	83
avF	79	81	71
V1	80	81	74
V2	78	79	75
V3	75	77	71
V4	81	82	79
V5	85	85	86
V6	85	84	89

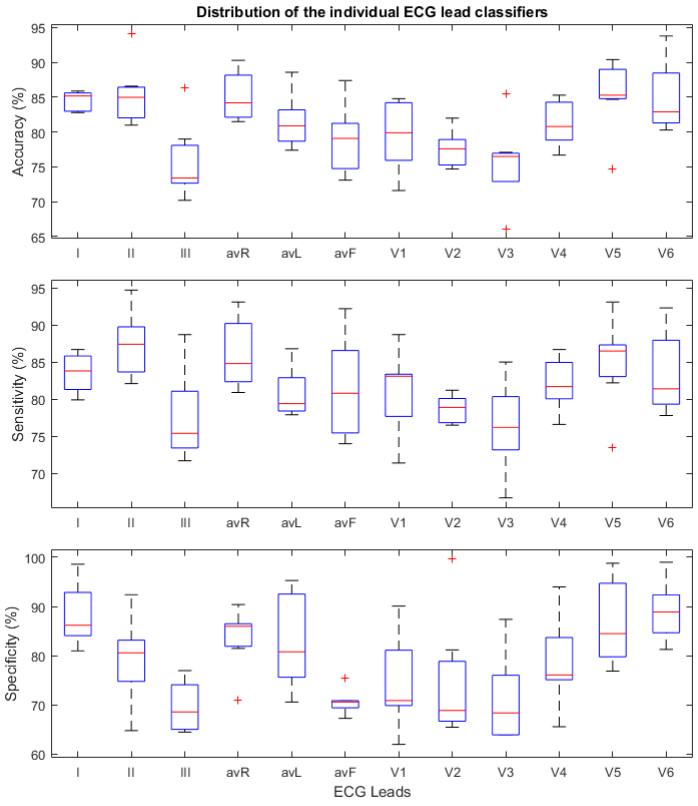

Figure H.3: Box and whisker diagram indicating the classification accuracy, sensitivity and specificity of the individual ECG leads corresponding to the retrospective study.

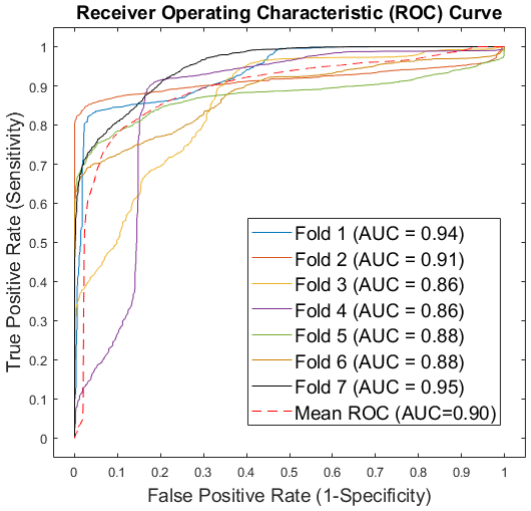

Figure H.4: ROC curve for lead II

H.3.2 All Limb Leads

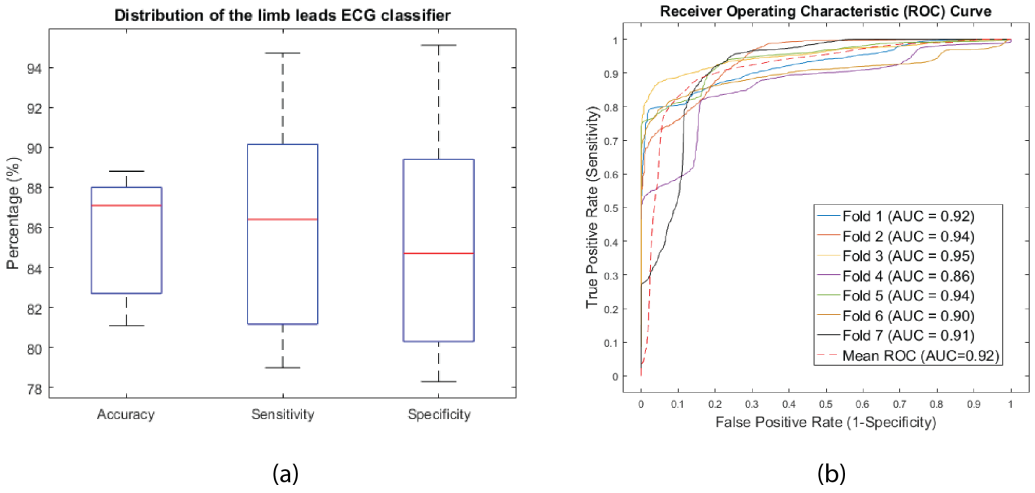

Figure H.5: The classification performance for the retrospective study corresponding to all the limb leads: (a) The classifier distribution for accuracy, sensitivity and specificity. (b) The ROC curves and corresponding AUC values across the 7 folds, as well as the resulting mean ROC and AUC value is plotted.

H.3.3 All Limb Leads and Precordial Leads V2 and V4

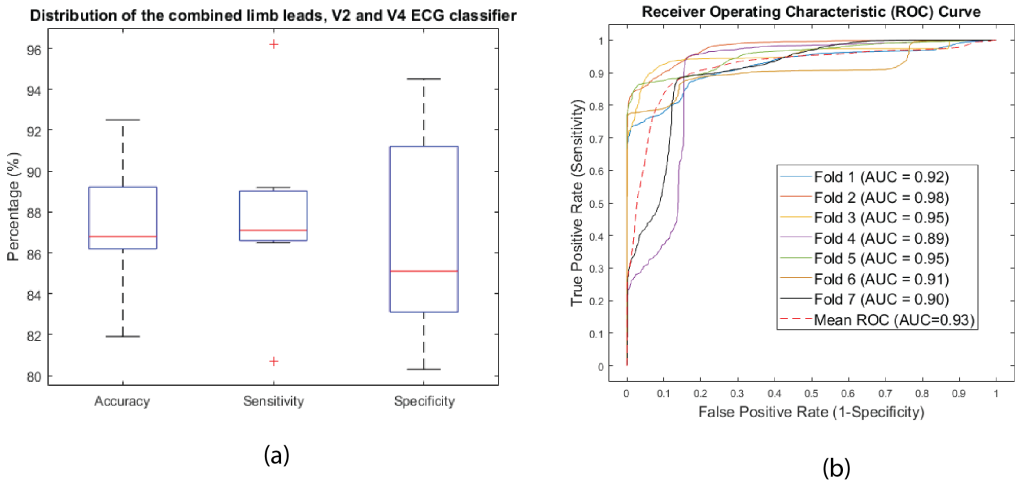

Figure H.6: The classification performance for the retrospective study corresponding to all the limb leads and precordial leads V2 and V4: (a) The classifier distribution for accuracy, sensitivity and specificity. (b) The ROC curves and corresponding AUC values across the 7 folds, as well as the resulting mean ROC and AUC value is plotted.

Appendix I

Additional Discussion

Table I.1: Clinical trial cardiovascular disease incorrectly classified as normal.

#	**Incorrectly classified abnormal patients**
1	Tachycardia
2	Bradycardia
3	Ventricular and Atrial Extrastimulation
4	Left Ventricular Hypertrophy
5	Borderline Left Atrial Enlargement
6	First-Degree Atrioventricular Block

List of References

Abboud, S. and Barnea, O. (1995). Errors due to sampling frequency of the electrocardiogram in spectral analysis of heart rate signals with low variability. In: *Computers in Cardiology 1995*, pp. 461–463. IEEE.

Abtahi, F., Snäll, J., Aslamy, B., Abtahi, S., Seoane, F. and Lindecrantz, K. (2014). Biosignal pi, an affordable open-source ecg and respiration measurement system. *Sensors*, vol. 15, no. 1, pp. 93–109.

Akay, M. (1996). *Detection and estimation methods for biomedical signals*. Academic Press, Inc.

Analog Devices (2014). ADAS1000. Tech. Rep., ADAS1000-1/ADAS1000-2–Low Power, Five Electrode Electrocardiogram (ECG) Analog Front End–Datasheet.

Anuradha, B. and Reddy, V.V. (2008). Ann for classification of cardiac arrhythmias. *ARPN Journal of Engineering and Applied Sciences*, vol. 3, no. 3, pp. 1–6.

Arif, M., Malagore, I.A. and Afsar, F.A. (2012). Detection and localization of myocardial infarction using k-nearest neighbor classifier. *Journal of medical systems*, vol. 36, no. 1, pp. 279–289.

Asl, B.M., Setarehdan, S.K. and Mohebbi, M. (2008). Support vector machine-based arrhythmia classification using reduced features of heart rate variability signal. *Artificial intelligence in medicine*, vol. 44, no. 1, pp. 51–64.

Assous, S., Gunn, D., Hopper, C., Jackson, P.D., Linnett, L. and Lovell, M. (2007). *An approach for correcting magnitude and phase distortion in wideband piezoelectric transducer systems*. IEEE.

Bai, Y. (2016). *Microcontroller Engineering with MSP432: Fundamentals and Applications*. Crc Press.

Barill, T. and Inc, S.L. (2012). *The Six Second ECG: A Practical Guide to Basic and 12 Lead ECG Interpretation*. SkillStat Learning Incorporated. ISBN 9780986472305.
Available at: `https://books.google.co.za/books?id=yh2AoAEACAAJ`

Barret, K.E., Barman, S.M., Boitano, S. and Brooks, H.L. (2012). *Ganong's Review of Medical Physiology*. ISBN 9780071780049.

Beaglehole, R. and Bonita, R. (2008). Global public health: a scorecard. *The Lancet*, vol. 372, no. 9654, pp. 1988–1996.

Beale, M., Hagan, M. and Demuth, H. (2016). Neural network toolbox getting started guide. in r2016b.

Been, Y.S., Khan, J.N., Hui, D.C.P. *et al.* (2007). Designing medical devices for isolation and safety. *EDN (Electronic Design, Strategy, News)*, pp. 75–78.

Belle, A., Kon, M.A. and Najarian, K. (2013). Biomedical informatics for computer-aided decision support systems: a survey. *The Scientific World Journal*, vol. 2013.

Bond, R.R., Finlay, D., Nugent, C., Breen, C., Guldenring, D. and Daly, M. (2012). The effects of electrode misplacement on clinicians interpretation of the standard 12-lead electrocardiogram. *European journal of internal medicine*, vol. 23, no. 7, pp. 610–615.

Botha, J. (2010). *Autonomous auscultation of the human heart*. Ph.D. thesis, Stellenbosch: University of Stellenbosch.

Buendía-Fuentes, F., Arnau-Vives, M., Arnau-Vives, A., Jiménez-Jiménez, Y., Rueda-Soriano, J., Zorio-Grima, E., Osa-Sáez, A., Martínez-Dolz, L., Almenar-Bonet, L. and Palencia-Pérez, M. (2012). High-bandpass filters in electrocardiography: source of error in the interpretation of the st segment. *ISRN cardiology*, vol. 2012.

Cables and Sensors (2011). 12-Lead ECG Placement Guide with Illustrations. [Online] Available at: `https://www.cablesandsensors.com/pages/12-lead-ecg-placement-guide-with-illustrations`, [Accessed 30 July 2017].

Caldwell, J. (2015). *Single-Supply, Electret Microphone Pre-Amplifier Reference Design*. Texas Instruments.

Chen, M.A. (2016). Holter monitor (24h). [Online] Available at: `https://medlineplus.gov/ency/article/003877.htm`, [Accessed 30 July 2017].

Chengwei, L., Shoubin, W., Aijun, X. and Hui, P. (2007). Clinical diagnosis of cardiac disease based on support vector machine. In: *World Congress on Medical Physics and Biomedical Engineering 2006*, pp. 1273–1276. Springer.

Cowley, J. (2012). *Communications and Networking: An Introduction*. Springer Science & Business Media.

Daniels, R., Partridge, A., Kekana, D. and Musundwa, S. (2013). Rural livelihoods in South Africa. working paper series no. 122. *Cape Town: Southern Africa Labour and Development Research Unit, University of Cape Town*.

Dawson, D., Yang, H., Malshe, M., Bukkapatnam, S.T., Benjamin, B. and Komanduri, R. (2009). Linear affine transformations between 3-lead (frank xyz leads) vectorcardiogram and 12-lead electrocardiogram signals. *Journal of electrocardiology*, vol. 42, no. 6, pp. 622–630.

Dokur, Z. and Ölmez, T. (2001). Ecg beat classification by a novel hybrid neural network. *Computer methods and programs in biomedicine*, vol. 66, no. 2, pp. 167–181.

Dower, G.E., Machado, H.B. and Osborne, J. (1980). On deriving the electrocardiogram from vectoradiographic leads. *Clinical cardiology*, vol. 3, no. 2, pp. 87–95.

Drew, B.J., Dempsey, E.D., Joo, T.H., Sommargren, C.E., Glancy, J.P., Benedict, K. and Krucoff, M.W. (2004). Pre-hospital synthesized 12-lead ecg ischemia monitoring with trans-telephonic transmission in acute coronary syndromes: pilot study results of the st smart trial. *Journal of Electrocardiology*, vol. 37, pp. 214–221.

Eko (2017). Duo. [Online] Available at: `https://ekodevices.com/duo/`, [Accessed 30 July 2017].

Feild, D.Q., Feldman, C.L., Hor, B.M. *et al.* (2002). Improved easi coefficients: their derivation, values, and performance. *Journal of electrocardiology*, vol. 35, no. 4, pp. 23–33.

Feild, D.Q., Zhou, S.H., Helfenbein, E.D., Gregg, R.E. and Lindauer, J.M. (2008). Technical challenges and future directions in lead reconstruction for reduced-lead systems. *Journal of electrocardiology*, vol. 41, no. 6, pp. 466–473.

Geselowitz, D.B. (2015). Electrocardiography. [Online] Available at: `http://ethw.org/Electrocardiography`, [Accessed 30 July 2017].

Goldberger, A., Amaral, L., Glass, L., Hausdorff, J., Ivanov, P.C., Mark, R., Mietus, J., Moody, G., Peng, C. and Stanley, H. (2000). Physiobank, physiotoolkit, and physionet: Components of a new research resource for complex physiologic signals. circulation [online]. 101 (23), pp. e215–e220.

Grusin, M. (2017). Serial peripheral interface (spi). [Online] Available at: `https://learn.sparkfun.com/tutorials/serial-peripheral-interface-spi`, [Accessed 10 September 2017].

Güler, İ. and Übeylı, E.D. (2005). Ecg beat classifier designed by combined neural network model. *Pattern recognition*, vol. 38, no. 2, pp. 199–208.

Haraldsson, H., Edenbrandt, L. and Ohlsson, M. (2004). Detecting acute myocardial infarction in the 12-lead ecg using hermite expansions and neural networks. *Artificial Intelligence in Medicine*, vol. 32, no. 2, pp. 127–136.

Herman, M., Ingram, D., Levy, J., Cook, J. and Athans, R. (1991). Variability of electrocardiographic precordial lead placement: a method to improve accuracy and reliability. *Clinical cardiology*, vol. 14, no. 6, pp. 469–476.

Huang, R. and Zhou, Y. (2015). Disease classification and biomarker discovery using ecg data. *BioMed research international*, vol. 2015.

Jonathan, R.S., Peter, N., Ernest, D., Jonathan, R.S. and Jonathan, R.S. (2010). Artificial intelligence: A modern approach. vol. 2.

Kania, M., Rix, H., Fereniec, M., Zavala-Fernandez, H., Janusek, D., Mroczka, T., Stix, G. and Maniewski, R. (2014). The effect of precordial lead displacement on ecg morphology. *Medical & biological engineering & computing*, vol. 52, no. 2, pp. 109–119.

Kerwin, A., McLean, R. and Tegelaar, H. (1960). A method for the accurate placement of chest electrodes in the taking of serial electrocardiographic tracings. *Canadian Medical Association Journal*, vol. 82, no. 5, p. 258.

Kligfield, P., Gettes, L.S., Bailey, J.J., Childers, R., Deal, B.J., Hancock, E.W., van Herpen, G., Kors, J.A., Macfarlane, P., Mirvis, D.M. *et al.* (2007). Recommendations for the standardization and interpretation of the electrocardiogram. *Circulation*, vol. 115, no. 10, pp. 1306–1324.

Koekemoer, H. and Scheffer, C. (2008). Heart sound and electrocardiogram recording devices for telemedicine environments. In: *2008 30th Annual International Conference of the IEEE Engineering in Medicine and Biology Society*, pp. 4867–4870. IEEE.

Lei, W.K., Li, B.N., Dong, M.C. and Vai, M.I. (2007). Afc-ecg: an adaptive fuzzy ecg classifier. In: *Soft Computing in Industrial Applications*, pp. 189–199. Springer.

Leng, S., San Tan, R., Chai, K.T.C., Wang, C., Ghista, D. and Zhong, L. (2015). The electronic stethoscope. *Biomedical engineering online*, vol. 14, no. 1, p. 66.

Lewis, P. (2017). Analogy between human and artificial neural nets. [Online] Available at: `http://users.ecs.soton.ac.uk/phl/ctit/nn/node2.html`, [Accessed 23 August 2017].

Li, C., Zheng, C. and Tai, C. (1995). Detection of ecg characteristic points using wavelet transforms. *IEEE Transactions on biomedical Engineering*, vol. 42, no. 1, pp. 21–28.

Littelfuse (2017). TVS Diode Arrays (SPA Diodes) General Purpose ESD Protection - SP720 Series. Tech. Rep., Littelfuse.

Littmann, M. (2017). 3M Littmann Electronic Stethoscope Model 3200. [Online] Available at: `http://www.littmann.com/3M/en_US/littmann-stethoscopes/products/~/3M-Littmann-Electronic-Stethoscope-Model-3200?N=5932256+8711017+3293188392&rt=rud`, [Accessed 30 July 2017].

Mallat, S. and Zhong, S. (1992). Characterization of signals from multiscale edges. *IEEE Transactions on pattern analysis and machine intelligence*, vol. 14, no. 7, pp. 710–732.

Marieb, E.N. (2015). *Essentials of Human Anatomy & Physiology*. Eleventh edn. San Francisco, CA, Pearson/Benjamin Cummings. ISBN 9780321919007.

Martínez, J.P., Almeida, R., Olmos, S., Rocha, A.P. and Laguna, P. (2004). A wavelet-based ecg delineator: evaluation on standard databases. *IEEE Transactions on biomedical engineering*, vol. 51, no. 4, pp. 570–581.

Mathworks (2017). Detector performance analysis using roc curves. [Online] Available at: `http://www.mathworks.com/help/phased/examples/detector-performance-analysis-using-roc-curves.html`, [Accessed 4 November 2016].

McCann, K., Holdgate, A., Mahammad, R. and Waddington, A. (2007). Accuracy of ecg electrode placement by emergency department clinicians. *Emergency Medicine Australasia*, vol. 19, no. 5, pp. 442–448.

Meghriche, S., Draa, A. and Boulemden, M. (2008). On the analysis of a compound neural network for detecting atrio-ventricular heart block (avb) in an ecg signal. *International Journal of Biological and Medical Sciences*, vol. 1, no. 1, pp. 1–11.

Møller, M.F. (1993). A scaled conjugate gradient algorithm for fast supervised learning. *Neural networks*, vol. 6, no. 4, pp. 525–533.

Munro, J.F. and Edwards, C.R.W. (1990). *Macleod's clinical examination*. Churchill Livingstone.

Nelwan, S.P., Kors, J.A., Crater, S.W., Meij, S.H., van Dam, T.B., Simoons, M.L. and Krucoff, M.W. (2008). Simultaneous comparison of 3 derived 12-lead electrocardiograms with standard electrocardiogram at rest and during percutaneous coronary occlusion. *Journal of electrocardiology*, vol. 41, no. 3, pp. 230–237.

Nelwan, S.P., Kors, J.A., Meij, S.H., van Bemmel, J.H. and Simoons, M.L. (2004). Reconstruction of the 12-lead electrocardiogram from reduced lead sets. *Journal of electrocardiology*, vol. 37, no. 1, pp. 11–18.

Nunez, P.L. and Srinivasan, R. (2006). *Electric fields of the brain: the neurophysics of EEG*. Oxford University Press, USA.

Ostertag, M.H. (2014). *Reconstructing electrocardiogram leads from a reduced lead set through the use of patient-specific transforms and independent component analysis*. Rochester Institute of Technology.

Ouyang, N., Ikeda, M. and Yamauchi, K. (1997). Use of an artificial neural network to analyse an ecg with qs complex in v 1–2 leads. *Medical and Biological Engineering and Computing*, vol. 35, no. 5, pp. 556–560.

Pan, Y. (2016). Neural Networks: Representation. [Online] Available at: `http://www.yuthon.com/2016/08/15/Coursera-Machine-Learning-Week-4/`, [Accessed 23 August 2017].

Pillay-van Wyk, V., Msemburi, W., Laubscher, R., Dorrington, R.E., Groenewald, P., Matzopoulos, R., Prinsloo, M., Nojilana, B., Nannan, N., Gwebushe, N. *et al.* (2013). Second national burden of disease study south africa: national and subnational mortality trends, 1997–2009. *The Lancet*, vol. 381, p. S113.

Prasad, G.K. and Sahambi, J. (2003). Classification of ecg arrhythmias using multiresolution analysis and neural networks. In: *TENCON 2003. Conference on Convergent Technologies for the Asia-Pacific Region*, vol. 1, pp. 227–231. IEEE.

Rajaganeshan, R., Ludlam, C., Francis, D., Parasramka, S. and Sutton, R. (2008). Accuracy in ecg lead placement among technicians, nurses, general physicians and cardiologists. *International journal of clinical practice*, vol. 62, no. 1, pp. 65–70.

Rangayyan, R.M. and Reddy, N.P. (2002). Biomedical signal analysis: a case-study approach. *Annals of Biomedical Engineering*, vol. 30, no. 7, pp. 983–983.

Reed, T.R., Reed, N.E. and Fritzson, P. (2004). Heart sound analysis for symptom detection and computer-aided diagnosis. *Simulation Modelling Practice and Theory*, vol. 12, no. 2, pp. 129–146.

Rijuven (2016). i2Dtx CardioSleeve. [Online] Available at: `https://rijuven.com/medicaldevices/cardiosleeve`, [Accessed 30 July 2017].

Rincón, F., Recas, J., Khaled, N. and Atienza, D. (2011). Development and evaluation of multilead wavelet-based ecg delineation algorithms for embedded wireless sensor nodes. *IEEE Transactions on Information Technology in Biomedicine*, vol. 15, no. 6, pp. 854–863.

Ródenas, J., García, M., Alcaraz, R. and Rieta, J.J. (2015). Wavelet entropy automatically detects episodes of atrial fibrillation from single-lead electrocardiograms. *Entropy*, vol. 17, no. 9, pp. 6179–6199.

Rosso, O.A., Blanco, S., Yordanova, J., Kolev, V., Figliola, A., Schürmann, M. and Başar, E. (2001). Wavelet entropy: a new tool for analysis of short duration brain electrical signals. *Journal of neuroscience methods*, vol. 105, no. 1, pp. 65–75.

Rudiger, A., Hellermann, J.P., Mukherjee, R., Follath, F. and Turina, J. (2007). Electrocardiographic artifacts due to electrode misplacement and their frequency in different clinical settings. *The American journal of emergency medicine*, vol. 25, no. 2, pp. 174–178.

Sa-ngasoongsong, A., Kunthong, J., Sarangan, V., Cai, X. and Bukkapatnam, S.T. (2012). A low-cost, portable, high-throughput wireless sensor system for phonocardiography applications. *Sensors*, vol. 12, no. 8, pp. 10851–10870.

Schijvenaars, B. (2000). *Intra-individual Variability of the Electrocardiogram: Assessment and exploitation in computerized ECG analysis.*

Schijvenaars, B.J., Kors, J.A., van Herpen, G., Kornreich, F. and van Bemmel, J.H. (1997). Effect of electrode positioning on ecg interpretation by computer. *Journal of electrocardiology*, vol. 30, no. 3, pp. 247–256.

Schreck, D., Brotea, C. and Shah, S. (2002). Derivation of the 12-lead electrocardiogram using abstract factor analysis and simplex optimization. *Int J Bioelectromagn*, vol. 4, pp. 337–338.

Schreck, D.M. and Fishberg, R.D. (2013). Derivation of the 12-lead electrocardiogram and 3-lead vectorcardiogram. *The American journal of emergency medicine*, vol. 31, no. 8, pp. 1183–1190.

SEER Training Modules (2017). Nerve Tissue national institutes of health, national cancer institute. [Online] Available at: `https://training.seer.cancer.gov/`, [Accessed 23 August 2017].

Sejersten, M., Pahlm, O., Pettersson, J., Clemmensen, P.M., Rautaharju, F., Zhou, S., Maynard, C., Feldman, C.L. and Wagner, G.S. (2003). The relative accuracies of ecg precordial lead waveforms derived from easi leads and those acquired from paramedic applied standard leads. *Journal of electrocardiology*, vol. 36, no. 3, pp. 179–185.

Sengur, A. and Turkoglu, I. (2008). A hybrid method based on artificial immune system and fuzzy k-nn algorithm for diagnosis of heart valve diseases. *Expert Systems with Applications*, vol. 35, no. 3, pp. 1011–1020.

Sharma, S. (2017). Activation Functions: Neural Networks. [Online] Available at: `https://medium.com/towards-data-science/activation-functions-neural-networks-1cbd9f8d91d6`, [Accessed 4 November 2016].

Stethographics (2007). Auscultatory sites. [Online] Available at: `http://www.stethographics.com/heart/main/sites.htm`, [Accessed 27 July 2016].

Sun, L., Lu, Y., Yang, K. and Li, S. (2012). Ecg analysis using multiple instance learning for myocardial infarction detection. *IEEE transactions on biomedical engineering*, vol. 59, no. 12, pp. 3348–3356.

Sunway (2017). Electrocardiography (ecg). [Online] Available at: `http://sunwaymedical.com/medical-technology-facilities/special-diagnostics/electrocardiography-ecg/`, [Accessed 14 November 2017].

The World Bank (2017). Rural population (% of total population). [Online] Available at: `https://data.worldbank.org/indicator/SP.RUR.TOTL.ZS?locations=ZA`, [Accessed 4 November 2016].

Theodoridis, S. and Koutroumbas, K. (1999). *Pattern Recognition*. Academic Press, San Diego.

Thinklabs (2003). Thinklabs One Digital Stethoscope. [Online] Available at: `http://www.thinklabs.com/`, [Accessed 30 July 2017].

Tripathy, R., Sharma, L. and Dandapat, S. (2014). A new way of quantifying diagnostic information from multilead electrocardiogram for cardiac disease classification. *Healthcare technology letters*, vol. 1, no. 4, pp. 98–103.

Tsouri, G.R. and Ostertag, M.H. (2014). Patient-specific 12-lead ecg reconstruction from sparse electrodes using independent component analysis. *IEEE journal of biomedical and health informatics*, vol. 18, no. 2, pp. 476–482.

Übeyli, E.D. (2007). Ecg beats classification using multiclass support vector machines with error correcting output codes. *Digital Signal Processing*, vol. 17, no. 3, pp. 675–684.

Umar, H. (2002). Clinical decision-making using computers: opportunities and limitations. *Dental Clinics of North America*, vol. 46, no. 3, pp. 521–538.

Valdez, J. and Becker, J. (2015). *Understanding the I2C Bus*. Texas Instruments.

Van Oosterom, A., Hoekema, R. and Uijen, G. (2000). Geometrical factors affecting the interindividual variability of the ecg and the vcg. *Journal of electrocardiology*, vol. 33, pp. 219–227.

Vincent, P., Larochelle, H., Lajoie, I., Bengio, Y. and Manzagol, P.-A. (2010). Stacked denoising autoencoders: Learning useful representations in a deep network with a local denoising criterion. *Journal of Machine Learning Research*, vol. 11, no. Dec, pp. 3371–3408.

Visagie, C. (2007). *Screening for abnormal heart sounds and murmurs by implementing neural networks*. Ph.D. thesis, Stellenbosch: University of Stellenbosch.

Wilson, F.N., Johnston, F.D., Macleod, A.G. and Barker, P.S. (1934). Electrocardiograms that represent the potential variations of a single electrode. *American Heart Journal*, vol. 9, no. 4, pp. 447–458.

Winter, B.B. and Webster, J.G. (1983). Driven-right-leg circuit design. *IEEE Transactions on Biomedical Engineering*, , no. 1, pp. 62–66.

World Health Organisation (2017). Cardiovascular diseases (CVDs). [Online] Available at: `http://www.who.int/mediacentre/factsheets/fs317/en/`, [Accessed 16 October 2017].

Yan, J., Lu, Y., Xu, Y., Liu, J. and Wu, X. (2010). Intelligent diagnosis of cardiovascular diseases utilizing ecg signals. *International Journal of Information Acquisition*, vol. 7, no. 02, pp. 81–97.

Yegnanarayana, B. (2009). *Artificial neural networks*. PHI Learning Pvt. Ltd.

Yu, S.-N. and Chen, Y.-H. (2007). Electrocardiogram beat classification based on wavelet transformation and probabilistic neural network. *Pattern Recognition Letters*, vol. 28, no. 10, pp. 1142–1150.

Zinke-Allmang, M. (2008). *Physics for the Life Sciences*. Nelson Education. ISBN 9780176442590.